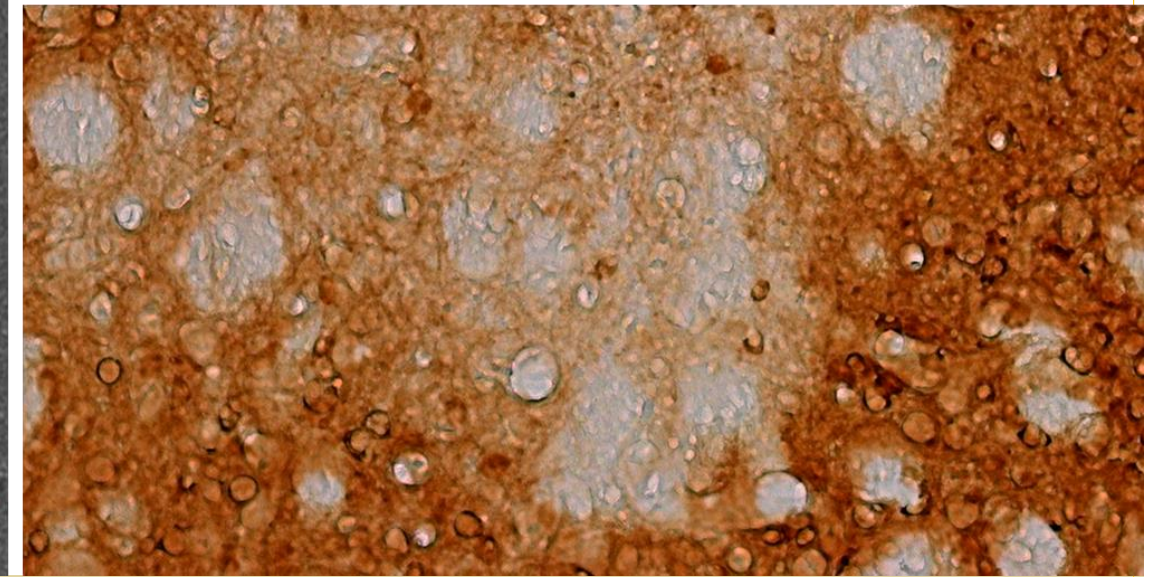
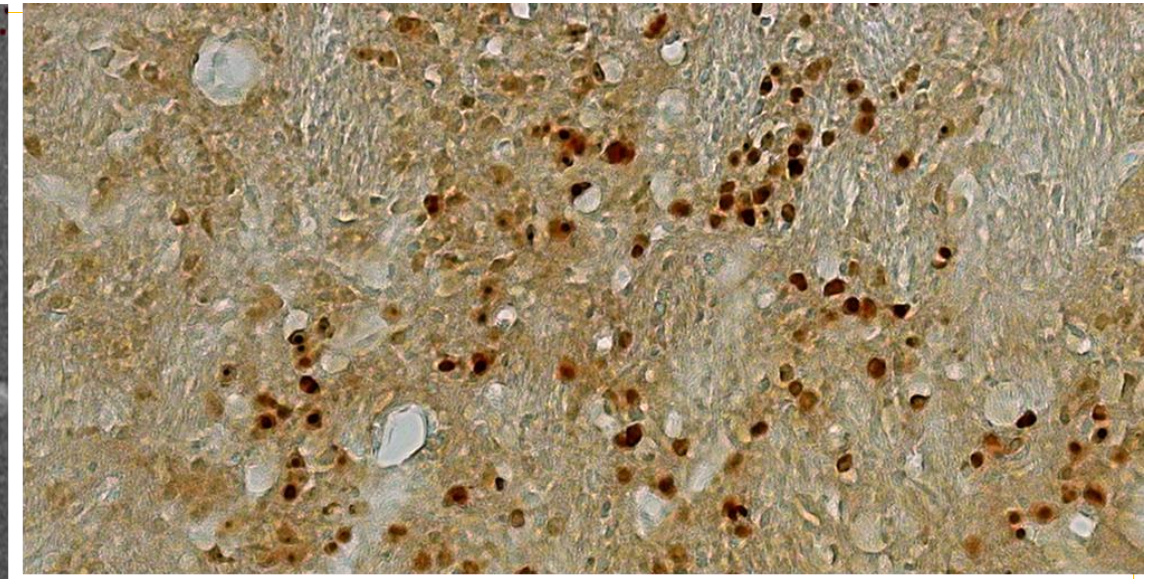


Mariana Oliveira Conceição

NON-VIRAL SILENCING OF MACHADO-JOSEPH DISEASE THROUGH THE SYSTEMIC ROUTE

UNIVERSIDADE DE COIMBRA



Mariana Oliveira Conceição

NON-VIRAL SILENCING OF MACHADO-JOSEPH DISEASE THROUGH THE SYSTEMIC ROUTE

Tese de doutoramento em Ciências Farmacêuticas, na área de especialização de Biotecnologia Farmacêutica, orientada pelo Professor Doutor Luis Pereira de Almeida e pela Professora Doutora Conceição Pedroso de Lima e apresentada à Faculdade de Farmácia da Universidade de Coimbra

Setembro 2015



UNIVERSIDADE DE COIMBRA

Non-viral silencing of Machado-Joseph disease through the systemic route

Mariana Oliveira Conceição

Setembro de 2015



UNIVERSIDADE DE COIMBRA

Non-viral silencing of Machado-Joseph disease through the systemic route

Silenciamento não viral da doença de Machado-Joseph através da via sistémica

Mariana Oliveira Conceição

Thesis submitted to the Faculty of Pharmacy of the University of Coimbra for the attribution of the Doctor degree in Pharmaceutical Sciences, in the specialty field of Pharmaceutical Biotechnology.

Tese apresentada à Faculdade de Farmácia da Universidade de Coimbra para prestação de provas de doutoramento em Ciências Farmacêuticas, na área de especialização de Biotecnologia Farmacêutica.

Setembro de 2015



UNIVERSIDADE DE COIMBRA

Non-viral silencing of Machado-Joseph disease through the systemic route

The research work presented in this thesis was performed at the Center for Neuroscience and Cell Biology of the University of Coimbra under the supervision of Prof. Luís Pereira de Almeida and Prof. Conceição Pedroso de Lima. Part of this work was performed at Paul L. Foster School of Medicine, Texas Tech University, USA, under the supervision of Prof. Manjunath Swamy.

This work was supported by FEDER funds through the Operational Program Competitiveness Factors – COMPETE, by national funds through the Portuguese Foundation for Science and Technology (FCT), PTDC/SAU-FAR/116535/2010, ERA-Net for Research Programmes on Rare Diseases: E-Rare4/0003/2012, Programa Mais Centro (CENTRO-07-ST24-FEDER-002002, 002006, 002008), by the strategic project UID/NEU/04539/2013 and by the Richard Chin and Lily Lock Machado-Joseph Research Fund. Mariana Conceição was supported by a PhD fellowship of the Portuguese Foundation for Science and Technology, reference SFRH/BD/68780/2010.

O trabalho experimental apresentado nesta tese foi elaborado no Centro de Neurociências e Biologia Celular da Universidade de Coimbra sob a supervisão do Professor Luís Pereira de Almeida e da Professora Conceição Pedroso de Lima. Parte deste trabalho foi realizado na Faculdade de Medicina Paul L. Foster, Universidade Técnica do Texas, USA, sob a supervisão do Professor Manjunath Swamy.

Este trabalho foi financiado por fundos FEDER através do Programa Operacional Factores de Competitividade – COMPETE, por fundos nacionais, através da Fundação Portuguesa para a Ciência e Tecnologia (FCT), PTDC/SAU-FAR/116535/2010, *ERA-Net for Research Programmes on Rare Diseases: E-Rare4/0003/2012*, Programa Mais Centro (CENTRO-07-ST24-FEDER-002002, 002006, 002008), pelo projecto estratégico UID/NEU/04539/2013 e pelo *Richard Chin and Lily Lock Machado-Joseph Research Fund*. Mariana Conceição foi suportada por uma bolsa de doutoramento da Fundação Portuguesa para a Ciência e Tecnologia (FCT), referência SFRH/BD/68780/2010.



Front Cover:

Left: *in vivo* imaging of a C57/Bl6 mouse injected with brain-targeted liposomes encapsulating a near infrared dye. The image was acquired using an IVIS Lumina equipment. **Right:** Microscope images of striatal neuropathology induced by mutant ataxin-3 expression. **Top right:** Ubiquitin-positive inclusions. **Bottom right:** DARPP-32 staining.

Acknowledgements/ Agradecimentos

Ao Professor Doutor Luís Pereira de Almeida, o meu sincero agradecimento por me ter dado a oportunidade de fazer o doutoramento no seu grupo e por toda a confiança, total apoio e disponibilidade demonstrados, desde o primeiro dia. Agradeço também todos os ensinamentos, que tanto me fizeram crescer ao longo deste percurso. É para mim um grande exemplo de que, com esforço e perseverança, podemos atingir todos os nossos objetivos.

To Professor Manjunath Swamy I would like to acknowledge for receiving me in his laboratory in El Paso, Texas, USA. It was a pleasure to be part of his team. Even though it was a short time, it was a great experience both personally and professionally.

À Professora Doutora Conceição Pedroso de Lima agradeço por me ter aceitado como sua aluna, e por todo o apoio, encorajamento e toda a sua simpatia ao longo deste percurso.

À Doutora Célia Gomes agradeço toda a ajuda e disponibilidade essenciais para a realização da experiência envolvendo a obtenção de imagens no equipamento IVIS Lumina XR.

To all my colleagues from El Paso laboratory, especially to Harendra Chahar, Jang Gi Choi, Chunting Ye, Preeti Bharaj and Sojan Abraham I would like to express my gratitude for welcoming me and making me feel at home. Because of your support and friendship, time flew fast while I was there.

Aos meus colegas e amigos do grupo de Vetores e Terapia Génica do Centro de Neurociências e Biologia Celular da Universidade de Coimbra, agradeço por toda a amizade, palavras de encorajamento e momentos de boa disposição. Particularmente, gostaria de expressar a minha gratidão à Liliana, ao Clévio e ao Pedro por toda a ajuda prestada na realização deste trabalho. Um obrigada especial à Sara, por todos os momentos de boa disposição, bem como pela amizade incondicional, a qualquer hora, em

qualquer dia. À Ana Cristina, Dina, Geetha e Patrícia agradeço também a amizade, palavras de encorajamento e todos os momentos partilhados ao longo destes últimos anos.

Por fim, um agradecimento especial aos meus amigos e familiares que, estando fora do ambiente de laboratório, sempre compreenderam os momentos de ausência e me incentivaram neste percurso. Agradeço em especial aos meus pais, ao meu irmão e ao Hugo por todo o amor e carinho sempre presentes no decorrer desta caminhada, mesmo nos momentos mais difíceis. Sei que vocês serão sempre o meu porto seguro! À Bárbara e à Margarida, amigas de longa data, agradeço por toda a amizade demonstrada e por me darem muita força com palavras de encorajamento em várias circunstâncias.

Porque todos contribuíram, de uma forma ou de outra, para a realização deste trabalho, esta tese é-vos dedicada!

TABLE OF CONTENTS

Abbreviations	I
Summary	V
Resumo	VII

CHAPTER 1

General Introduction.....	1
1.1. Machado-Joseph disease	3
1.1.1. Machado-Joseph disease and associated clinical symptoms	3
1.1.2. Molecular genetics of Machado-Joseph disease and the ataxin-3 protein.....	4
1.1.3. Neuropathology of Machado-Joseph disease	5
1.1.4. Neuronal intranuclear inclusions.....	6
1.1.5. Pathogenesis of Machado-Joseph disease	7
1.1.6. Promising therapeutic strategies for Machado-Joseph disease.....	8
1.2. RNA interference.....	10
1.2.1. RNA interference and its mechanism.....	10
1.2.2. Clinical trials using RNAi to treat human diseases	13
1.2.3. RNAi and neurodegenerative diseases.....	16
1.2.4. RNAi and Machado-Joseph disease.....	17
1.2.4.1. Non-allele <i>versus</i> allele-specific silencing of ataxin-3	18
1.3. Non-viral vectors for gene silencing in the Central Nervous System upon systemic administration	19
1.3.1. Obstacles to the delivery of siRNAs to the brain upon intravenous administration.....	19
1.3.1.1. The BBB and how to overcome the BBB.....	20
1.3.2. Non-viral strategies with proven brain distribution of gene-therapy molecules upon intravenous administration	22
1.3.2.1. Cell-targeting peptides	25
1.3.2.2. Polymer-derived nanoparticles	26
1.3.2.3. Exosomes.....	27
1.3.2.4. Lipid-based nanoparticles.....	28
1.3.3. Formulating an ideal non-viral vector for the delivery of nucleic acids to the brain.....	29
1.3.4. Stable Nucleic Acid Lipid Particles	30
1.3.4.1. SNALPs in clinical trials	31
1.3.4.2. Brain-targeting of SNALPs.....	32
1.3.4.2.1. Rabies virus glycoprotein derived peptide	33
1.3.4.2.1.1. Rabies Virus	33
1.3.4.2.1.2. Studies with RVG peptide.....	34
1.4. Objectives	37

CHAPTER 2

A targeted lipid-based strategy to deliver silencing sequences to the brain by intravenous administration 39

2.1. Abstract 41

2.2. Introduction 42

2.3. Materials and Methods..... 44

2.3.1. Materials 44

2.3.2. Cell lines and culturing conditions 45

2.3.3. Mice..... 45

2.3.4. Synthesis and characterization of stable nucleic acid lipid particles..... 45

2.3.4.1. Preparation of ligand-coupled micelles 45

2.3.4.2. Encapsulation of siRNAs or NIR dye into liposomes and subsequent postinsertion of ligand-coupled micelles 46

2.3.4.3. Liposomes characterization 47

2.3.5. Assessment of cellular uptake by flow cytometry 47

2.3.6. Assessment of cellular internalization by confocal microscopy 48

2.3.7. Production of lentiviral vectors encoding for the human mutant ataxin-3..... 48

2.3.8. Evaluation of mutant ataxin-3 mRNA and protein levels by quantitative real-time PCR (qRT-PCR) and Western Blot (WB), respectively..... 49

2.3.9. Analysis of the biodistribution properties of targeted-liposomes using an *in vivo* imaging technology platform..... 50

2.3.9.1. *in vivo* NIR fluorescence images of the brain after intravenous administration of targeted-liposomes..... 50

2.3.9.2. *ex vivo* NIR fluorescence images of brain and major organs after intravenous administration of targeted-liposomes 51

2.3.10. Statistical analysis 51

2.3. Results..... 52

2.3.1. Generation of brain-targeted SNALPs..... 52

2.3.2. Characterization of brain-targeted SNALPs 53

2.3.3. RVG-9r promotes robust association of liposomes to neuronal cells..... 55

2.3.4. RVG-9r-targeted liposomes encapsulating siRNAs targeting mutant ataxin-3 efficiently reduce mutant ataxin-3 levels 57

2.3.5. Intravenous administration of RVG-9r-targeted liposomes promotes accumulation in the brain..... 59

2.4. Discussion..... 61

CHAPTER 3

Non-invasive silencing of mutant ataxin-3 decreases striatal neuropathology in a lentiviral mouse model of Machado-Joseph disease..... 65

3.1. Abstract 67

3.2. Introduction 68

3.3. Materials and Methods	70
3.3.1. Materials.....	70
3.3.2. Mice	70
3.3.3. Synthesis and characterization of brain-targeted stable nucleic acid lipid particles	70
3.3.4. Production of lentiviral vectors encoding human mutant ataxin-3	70
3.3.5. Injection of lentiviral vectors encoding mutant ataxin-3 into the striatum	70
3.3.6. Striatal distribution experiment	71
3.3.7. Mutant ataxin-3 silencing experiment	71
3.3.8. Mutant ataxin-3 mRNA silencing in the mouse striatum by qRT-PCR.....	71
3.3.9. Immunohistochemical procedure	72
3.3.10. Quantification of ubiquitin-positive inclusions and DARPP-32 depleted volume...	73
3.3.11. Quantification of condensed pycnotic nuclei volume.....	73
3.3.12. Quantification of GFAP and Iba-1 immunoreactivity	74
3.3.13. Statistical analysis.....	74
3.4. Results	75
3.4.1. RVG-9r-targeted SNALPs deliver siRNAs and decrease mutant ataxin-3 mRNA levels in the striatum of a lentiviral mouse model of Machado-Joseph disease	75
3.4.2. RVG-9r-targeted SNALPs decrease the number of ubiquitin-positive inclusions and mediate striatal neuroprotection in a lentiviral mouse model of Machado-Joseph disease	77
3.4.3. RVG-9r-targeted SNALPs reduce neuroinflammation in a lentiviral mouse model of Machado-Joseph disease.....	81
3.5. Discussion	83

CHAPTER 4

Non-invasive silencing of mutant ataxin-3 attenuates behavioral deficits and neuropathology in a cerebellar transgenic mouse model of Machado-Joseph disease	87
--	-----------

4.1. Abstract	89
4.2. Introduction	90
4.3. Materials and Methods	92
4.3.1. Materials.....	92
4.3.2. Mice	92
4.3.3. Synthesis and characterization of stable nucleic acid lipid particles	92
4.3.4. Analysis of siRNA delivery to the cerebellum by flow cytometry	92
4.3.5. Evaluation of the silencing efficiency of mutant ataxin-3 levels in the cerebellum of a MJD transgenic mouse model	93
4.3.6. Motor behavioural assessment	94
4.3.6.1. Experimental design	94
4.3.6.2. Beam walking analysis	94
4.3.6.3. Swimming performance	95
4.3.6.4. Footprint pattern analysis	95
4.3.6.5. RotaRod Performance	96
4.3.7. Neuropathology evaluation.....	96

4.3.7.1. Tissue preparation	96
4.3.7.2. Fluorescence immunohistochemical procedure.....	96
4.3.7.3. Cresyl Violet staining.....	97
4.3.7.4. Quantification of Purkinje cell number, mutant ataxin-3 aggregates and thickness of the cerebellar layers.....	97
4.3.8. Quantification of IL-6 serum levels by ELISA.....	97
4.3.9. Statistical analysis	98
4.4. Results	99
4.4.1. RVG-9r-targeted SNALPs deliver siRNAs and suppress mutant ataxin-3 in the cerebellum of a Machado-Joseph disease transgenic mouse model	99
4.4.2. Intravenous administration of RVG-9r-targeted SNALPs does not stimulate the production of pro-inflammatory cytokines or a microglia-related gene in the cerebellum	102
4.4.3. Non-invasive silencing of mutant ataxin-3 alleviates motor disabilities	103
4.4.4. Non-invasive silencing of mutant ataxin-3 attenuates cerebellar-associated neuropathology.....	108
4.4.5. Intravenous administration of RVG-9r-targeted SNALPs stimulates IL-6 acute secretion	110
4.4.6. Repeated intravenous administration of RVG-9r-targeted SNALPs is well tolerated	110
4.5. Discussion	112
 CHAPTER 5	
Final conclusions and future perspectives	115
 References	121

Abbreviations

AAV	Adeno-associated virus
AD	Alzheimer's disease
ATX-3 72Q	Mutant ataxin-3 with 72 glutamines
BACE1	β -secretase 1
BBB	Blood-brain barrier
BCECs	Brain capillary endothelial cells
CAG	Cytosine-adenine-guanine
CD	Cyclodextrin
Cebpb	CCAAT/Enhancer Binding Protein (C/EBP) β
Chol	Cholesterol
CNS	Central nervous system
CPPs	Cell-penetrating peptides
C₁₂E₈	Octaethylene glycol monododecyl ether
C16 PEG2000 Ceramide	N-palmitoyl-sphingosine-1-[succinyl(methoxypolyethylene glycol) 2000]
DARRP-32	Dopamine- and cyclic AMP-regulated phosphoprotein of 32 kDa
DGLs	Dendrigraft poly-L-lysines
DODAP	1,2-dioleoyl-3-dimethylammonium-propane
DRPLA	Dentatorubropallidolusian atrophy
DSPC	1,2-distearoyl-snglycero-3-phosphocholine
DSPE-PEG-MAL	1,2-distearoyl-sn-glycero-3-phosphatidylethanolamine-N-[maleimide (polyethylene glycol)-2000] ammonium salt
dsRNAs	Double-stranded RNAs
EGFP	Enhanced green fluorescent protein
EUS	Endoscopic ultrasound
FAM	5-carboxyfluorescein
FDA	U.S. Food and Drug Administration
GFAP	Glial fibrillary acidic protein
GUSB	β -glucuronidase
HBS	HEPES-buffered saline solution
HD	Huntington's disease
HPRT	Hypoxanthine guanine phosphoribosyl transferase

Iba-1	Ionized calcium-binding adapter molecule 1
ICG	Indocyanine green
ICV	Intracerebroventricular
IL-1β	Interleukin-1 β
IL-6	Interleukin-6
IN	Intranasal
IR	Insulin receptor
IV	Intravenous
IVT	Intravitreal
LNP	Lipid-based nanoparticle
LPS	Lipopolysaccharides
Luc	Firefly luciferase
LV	Lentivirus
miRNAs	microRNAs
MJD	Machado-Joseph disease
mRNA	Messenger RNA
MutAtax3	Mutant ataxin-3
nAChRs	Nicotinic acetylcholine receptors
NCAM	Neuronal cell adhesion molecule
NII	Neuronal intranuclear inclusions
NIR	Near infrared dye
NP	Nanoparticle
PAMAM	Polyamidoamine
PBS	Phosphate-buffered saline
PCR	Polymerase chain reaction
PD	Parkinson's disease
pDNA	Plasmid DNA
PEG	Polyethylene glycol
PEI	Polyethyleneimine
PFA	Paraformaldehyde
PILs	Polyethylene glycol grafted immunoliposomes
PolyQ	Polyglutamine
Pre-miRNAs	Precursor-microRNAs
Pri-miRNAs	Primary-microRNAs

p75NTR	Low-affinity nerve growth factor receptor
qRT-PCR	Quantitative real-time PCR
RES	Reticuloendothelial system
Rho-PE	l- α -phosphoethanolamine-N-(lissamine rhodamine B sulfonyl) ammonium salt
RISC	RNA-induced silencing complex
RNAi	RNA interference
RS	Receptor saturation
RVG	Rabies virus glycoprotein
RVG29	Short peptide derived from RVG, with 29 amino acids
RVG-9r	RVG-29 with nine-arginine residues
RV-MAT	Rabies viral matrix protein
RV-MAT-9r	Rabies viral matrix protein with nine-arginine residues
SBMA	Spinobulbar muscular atrophy
SC	Subcutaneous
SCA	Spinocerebellar ataxia
SCA3	Spinocerebellar ataxia type 3
shRNAs	Short hairpin RNAs
siCTR	Control siRNA
siMutAtax3	siRNA targeting mutant ataxin-3
siRNAs	Small interfering RNAs
SNALPs	Stable nucleic acid lipid particles
SNP	Single nucleotide polymorphism
SSPEI	Branched PEI with a disulfide linkage (-S-S-)
TNF-α	Tumor necrosis factor- α
TfR	Transferrin receptor
TTR	Transthyretin
TTRA	Transthyretin-mediated amyloidosis
3'UTR	3'Untranslated region

Summary

Machado-Joseph disease (MJD), also known as spinocerebellar ataxia type 3 (SCA3), is a neurodegenerative disorder and the most common autosomal dominantly-inherited ataxia worldwide. Genetically, this disorder is caused by the over-repetition of a CAG tract in the coding region of the *ATXN3/MJD1* gene, which confers a toxic gain-of-function to the ataxin-3 protein leading to neuronal dysfunction and degeneration in multiple brain regions. No effective disease-modifying treatment was developed for MJD so far, consequently it remains a fatal and incurable disease for which the only available options consist in the use of physiotherapy and pharmacological compounds to alleviate some specific symptoms.

Gene silencing by RNA interference (RNAi) mechanism represents one of the most straightforward approaches for MJD treatment enabling to block the production of the disease-causing protein, in an attempt to stop disease progression. Studies exploring the RNAi potential for the treatment of MJD showed its efficacy in different animal models. However, successful experiments involved intracranial administration of viral vectors, and there is a need for a safer and less invasive procedure. Therefore, the aim of this project was to develop a non-viral strategy to deliver small interfering RNAs (siRNAs) to the brain by a non-invasive administration, and the evaluation of its therapeutic potential in two genetically-modified mouse models of MJD.

In the first part of this project, described in chapter 2, we successfully generated brain-targeted stable nucleic acid lipid particles (SNALPs) through the incorporation of a short peptide derived from rabies virus glycoprotein (RVG-9r). Brain-targeted SNALPs exhibited important characteristics for systemic delivery: high encapsulation efficiency of siRNAs, ability to protect the encapsulated siRNAs, appropriate and homogeneous particle size distribution. Flow cytometry and confocal microscopy studies revealed specific *in vitro* delivery of siRNAs to neuronal cells. Moreover, brain-targeted SNALPs efficiently decreased mutant ataxin-3 levels, the MJD-causing protein, in a neuronal cell line. Importantly, *in vivo* experiments demonstrated that the RVG-9r peptide increased the accumulation of the nanoparticles in the mouse brain, upon intravenous administration.

In chapter 3, we evaluated the therapeutic potential of intravenous administration of RVG-9r-targeted SNALPs in a lentiviral-based mouse model of MJD. Notably, our studies provided evidences that non-invasive administration of brain-targeted SNALPs decreased the number of ubiquitin-positive inclusions and mediated neuroprotection in a striatal lentiviral-based mouse model of MJD.

Lastly, in chapter 4, as cerebellum is one of the mostly affected brain-regions in MJD patients, we evaluated the efficacy and outcomes of mutant ataxin-3 silencing using RVG-9r-targeted SNALPs in a cerebellar-transgenic mouse model of MJD, when implemented after disease onset. Importantly, brain-targeted SNALPs internalized in the cerebellar parenchyma, where the carried siRNAs reduced mutant ataxin-3 levels, alleviated motor performance defects, rescued neuropathology and did not induce a strong immune response, constituting a promising therapy for MJD.

In summary, the present thesis provides evidence that a clinically-relevant nanoparticle-based formulation is a promising therapeutic strategy for MJD patients. Our data strengthen other studies that revealed the benefits of RNAi for MJD therapy, disclosing a new strategy that has a high potential to be used in the clinic for the treatment of several neurodegenerative diseases known to be linked to the production of pathogenic proteins.

Resumo

A doença de Machado-Joseph (DMJ), também conhecida como ataxia espinocerebelosa do tipo 3, é uma doença neurodegenerativa e a ataxia autossômica dominante mais comum a nível mundial. Geneticamente, esta doença é causada por uma expansão do trinucleótido CAG na região codificante do gene *ATXN3/MJD1*, o que confere à proteína ataxina-3 propriedades tóxicas que resultam em morte e disfunção neuronal em múltiplas regiões cerebrais. Até ao momento, não há nenhum tratamento que modifique a progressão da doença e, conseqüentemente, esta permanece uma doença fatal e incurável, para a qual as únicas opções disponíveis consistem na utilização de fisioterapia e compostos farmacológicos para aliviar sintomas específicos.

O silenciamento de genes através do mecanismo de interferência de RNA (iRNA), representa uma das abordagens mais diretas para o tratamento da DMJ, permitindo bloquear a produção da proteína causadora da doença, e assim impedir a progressão da doença. Estudos anteriores exploraram o potencial da iRNA para o tratamento da DMJ e mostraram a sua eficácia em diferentes modelos animais. No entanto, estas experiências bem-sucedidas envolveram a administração intracraniana de vetores virais sendo desejável um procedimento menos invasivo e mais seguro. Portanto, o objetivo deste projeto foi desenvolver uma estratégia não-viral para entregar sequências silenciadoras ao cérebro através de uma via de administração não-invasiva, e a avaliação do seu potencial terapêutico em dois modelos animais geneticamente modificados da DMJ.

Na primeira parte deste projeto, descrita no capítulo 2, gerámos com sucesso nanopartículas de base lipídica – SNALPs – direcionadas para o cérebro através da incorporação de um pequeno peptídeo derivado da glicoproteína do vírus da raiva (RVG-9r). Estes SNALPs direcionados para o cérebro apresentaram características importantes para administração sistémica: elevada eficiência de encapsulação para siRNAs, capacidade de proteger os siRNAs encapsulados, tamanho de partículas homogéneo e adequado. Estudos de citometria de fluxo e microscopia confocal revelaram a entrega específica dos siRNAs a células neuronais, *in vitro*. Além disso, os SNALPs direcionados para o cérebro diminuíram significativamente os níveis da ataxina-3 mutante, a proteína

que causa a DMJ, numa linha celular neuronal. Experiências *in vivo* demonstraram que o peptídeo RVG-9r aumentou a acumulação das nanopartículas no cérebro de murganhos, após administração intravenosa, um dos objetivos mais importantes deste projeto.

No capítulo 3, avaliamos o potencial terapêutico da administração intravenosa de SNALPs direcionados com o peptídeo RVG-9r num modelo lentiviral murino da DMJ. Os nossos estudos facultam evidências que a administração não-invasiva de SNALPs direcionados para o cérebro diminuiu o número de inclusões ubiquitina-positivas e mediou neuroprotecção num modelo murino lentiviral e estriatal da DMJ, um resultado extremamente promissor.

Por fim, no capítulo 4, como o cerebelo é uma das regiões cerebrais mais afetadas nos doentes de Machado-Joseph, avaliamos a eficácia e os resultados do silenciamento da ataxina-3 mutante usando SNALPs direcionados com o peptídeo RVG-9r num modelo murino transgênico cerebelar da DMJ, quando implementado após o início da doença. Os SNALPs direcionados com o peptídeo RVG-9r internalizaram no parênquima cerebelar, onde os siRNAs entregues reduziram os níveis de ataxina-3 mutante, melhoraram o desempenho motor dos animais, atenuaram a neuropatologia e não induziram uma resposta imune evidente, constituindo assim uma terapia promissora para a DMJ.

Em resumo, esta dissertação apresenta evidências que uma formulação clinicamente relevante baseada em nanopartículas é uma estratégia terapêutica promissora para tratar a DMJ. Os nossos estudos reforçam outros que revelaram os benefícios da iRNA para a terapia da DMJ, revelando uma nova estratégia que tem um elevado potencial para ser utilizada na prática clínica para o tratamento de diversas doenças neurodegenerativas ligadas à produção de proteínas patogénicas.

CHAPTER 1

General Introduction

1.1. Machado-Joseph disease

1.1.1. Machado-Joseph disease and associated clinical symptoms

Machado-Joseph disease (MJD), also known as spinocerebellar ataxia type 3 (SCA3), belongs to a group of nine polyglutamine diseases that are caused by an unstable expansion of a cytosine-adenine-guanine (CAG) trinucleotide: spinobulbar muscular atrophy (SBMA), Huntington's disease (HD), dentatorubropallidoluysian atrophy (DRPLA) and spinocerebellar ataxias (SCA1, SCA2, SCA3, SCA6, SCA7, SCA17) (Riess, 2008). This disorder was originally described in people of Portuguese descendant, particularly from the Azores islands (Nakano *et al.*, 1972; Rosenberg *et al.*, 1976), but it was subsequently identified in several other countries, being nowadays the most common form of autosomal dominantly inherited ataxia worldwide (Bird, 1998). The highest worldwide prevalence can be found in the portuguese Flores island, where 1 in each 239 inhabitants have the disease (Bettencourt *et al.*, 2008).

MJD has a late onset and usually appears in the late third decade of life (Dürr A, 1996; Schöls L, 1997). Clinical manifestations are heterogeneous, but progressive ataxia, a dysfunction of motor coordination that can affect gaze, speech, gait and balance is the clinical hallmark of the disease (Taroni, 2004). More specific symptoms include ophthalmoplegia, bulging eyes, nystagmus, dystonia, amyotrophy, postural instability, dysarthria and facial and lingual fasciculations (Lima and Coutinho, 1980; Sudarsky and Coutinho, 1995). In some cases, parkinsonism was also reported to be another clinical feature of this disorder (Gwinn-Hardy *et al.*, 2001). Moreover, non-motor symptoms such as sleep disturbances, chronic pain, cramps and fatigue were also other frequent signs found in MJD patients (Saute and Jardim, 2015).

No effective disease-modifying treatment was developed for MJD so far, consequently it remains a fatal and incurable disease for which the only available option consists in the alleviation of some specific symptoms. Accordingly, parkinsonism and symptoms like restless legs syndrome may respond to levodopa or dopamine agonists (Buhmann *et al.*,

2003; Schöls *et al.*, 1998; Tuite *et al.*, 1995) and the spasticity of lower extremities may be managed by injection of botulinum toxin (Freeman and Wszolek, 2005). A complete overview of the existing therapies to manage the symptoms that MJD patients present, can be found in a review from Jonas Saute and Laura Jardim (Saute and Jardim, 2015). Also non-pharmacological approaches such as physiotherapy, the use of assistive devices (e.g. walkers and wheelchairs) and speech and occupational therapy may help patients in their everyday life activities (D'Abreu *et al.*, 2010). Nevertheless, the lack of therapeutic strategies to tackle the cause of the disease results inevitably in patients death approximately 20 years after disease onset (Kieling *et al.*, 2007).

1.1.2. Molecular genetics of Machado-Joseph disease and the ataxin-3 protein

Genetically, MJD is well characterized being caused by the over-repetition of a CAG tract in the coding region of the *ATXN3/MJD1* gene on chromosome 14q32.1 (Kawaguchi *et al.*, 1994; Takiyama *et al.*, 1993). This results in an expanded polyglutamine tract at the C-terminus of ataxin-3, which confers a toxic gain-of-function to the protein. While in healthy individuals normal alleles range from 12 to approximately 43 CAG repeats, MJD patients present between ~60 and 87 CAG repeats in the mutant allele (Cancel G, 1995; Dürr A, 1996; Maciel *et al.*, 1995; Matilla *et al.*, 1995; Matsumura *et al.*, 1996; Ranum *et al.*, 1995; Sasaki *et al.*, 1995). Intermediate expansions as low as 45 CAG repeats were also reported to give rise to SCA clinical features (Padiath *et al.*, 2005). Moreover, the length of the polyglutamine tract is inversely correlated with the age at onset of the disease (Cancel G, 1995; Maciel *et al.*, 1995; Maruyama, 1995).

Ataxin-3 protein is ubiquitously expressed in neuronal and non-neuronal tissues (do Carmo Costa *et al.*, 2004; Ichikawa *et al.*, 2001; Nishiyama *et al.*, 1996; Paulson *et al.*, 1997a; Schmidt T, 1998; Trottier *et al.*, 1998; Wang *et al.*, 1997) and interestingly, while in normal neurons ataxin-3 appears mainly in the cytoplasm, in diseased neurons the protein tends to concentrate in neuronal cell nuclei (Goti *et al.*, 2004; Nishiyama *et al.*, 1996; Paulson *et al.*, 1997a; Paulson *et al.*, 1997; Schmidt T, 1998). Although the biological functions of ataxin-3 are still not fully understood, several studies demonstrate the

involvement of ataxin-3 in the ubiquitin-proteasome pathway, the principal mechanism for protein catabolism in mammalian cells, as a deubiquitinating enzyme and a poly-ubiquitin binding protein (Berke *et al.*, 2005; Burnett *et al.*, 2003; Chai Y, 2004; Doss-Pepe *et al.*, 2003; Durcan *et al.*, 2011; Kuhlbrodt *et al.*, 2011; Mao *et al.*, 2005; Nicastro *et al.*, 2009; Nicastro *et al.*, 2005; Nicastro *et al.*, 2010; Scaglione *et al.*, 2011; Schmitt *et al.*, 2007; Todi *et al.*, 2009; Winborn *et al.*, 2008). Ataxin-3 has been further linked to aggresome formation and cytoskeletal organization (Burnett and Pittman, 2005; Costa *et al.*, 2010; Mazzucchelli *et al.*, 2009; Rodrigues *et al.*, 2010), in the cellular response to heat or oxidative stress (Araujo *et al.*, 2011; Reina *et al.*, 2010; Rodrigues *et al.*, 2011) and as a participant in transcription regulation (Evert *et al.*, 2006b; Li *et al.*, 2002; Rodrigues *et al.*, 2007). Interestingly, these ataxin-3 functions link ataxin-3 to pathways that were already implicated in the pathogenesis of several polyglutamine diseases.

1.1.3. Neuropathology of Machado-Joseph disease

Neuronal dysfunction and degeneration occurs in the spinal cord and in multiple brain regions including: cerebellum (spinocerebellar pathways and dentate nuclei), brainstem (pons and medulla), substantia nigra, thalamus, striatum and less extensively in the cerebral cortex (Alves *et al.*, 2008b; Jacobi *et al.*, 2012; Klockgether *et al.*, 1998; Rüb *et al.*, 2008; Rüb *et al.*, 2013; Schulz *et al.*, 2010; Sudarsky and Coutinho, 1995; Taniwaki *et al.*, 1997; Wullner *et al.*, 2005; Yamada *et al.*, 2001), as represented in Figure 1.1.

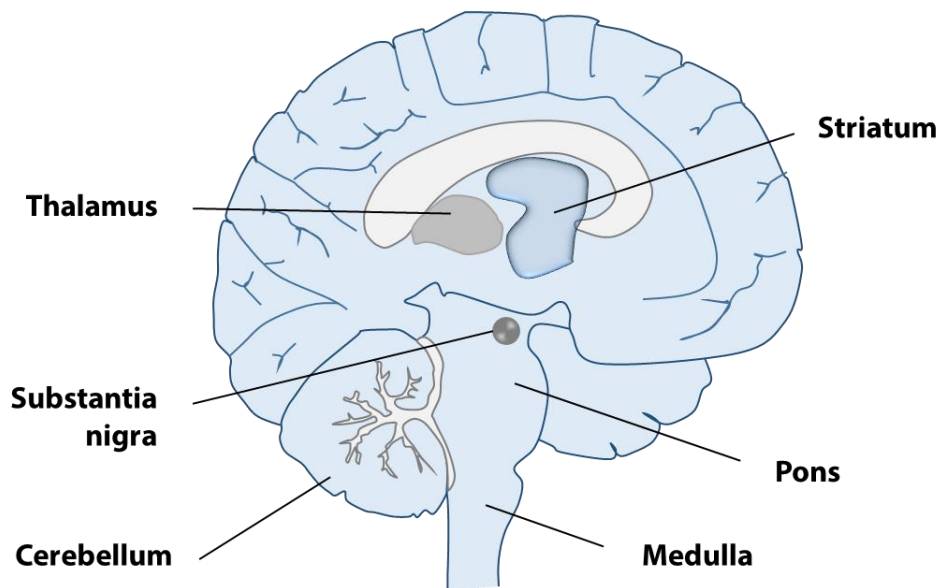


Figure 1.1. MJD neurodegeneration and neurodysfunction profile. The principal sites of neuronal loss and neuronal dysfunction in MJD are indicated: cerebellum, brainstem (pons and medulla), substantia nigra, thalamus and striatum.

1.1.4. Neuronal intranuclear inclusions

While ataxin-3 is ubiquitously expressed throughout the whole brain and predominantly in the cytoplasm, the formation of neuronal intranuclear inclusions (NII) resulting from mutant ataxin-3 accumulation appear in specific brain regions (Paulson *et al.*, 1997; Schmidt T, 1998). These inclusions represent the pathological hallmark of MJD, but whether they are toxic or protective is still a matter of debate (Muñoz *et al.*, 2002; Ross and Poirier, 2005; Takahashi *et al.*, 2010; Uchihara *et al.*, 2002).

The first evidences suggested that NII were toxic because of their ability to physically impair the axonal transport (Gunawardena *et al.*, 2003) and sequester functional proteins such as proteasome components, chaperones, transcription factors and ubiquitin, causing perturbation of the normal cellular activities (Chai *et al.*, 1999b; Chai *et al.*, 1999a; Chai *et al.*, 2002; Donaldson *et al.*, 2003; Schmidt *et al.*, 2002; Shimohata *et al.*, 2000). However, more recently, other groups reported that there is a partial correlation between the presence of NII and neuronal cell loss, suggesting that other factors distinct from NII formation may be involved in neuronal death (Evert *et al.*, 2006a; Muñoz *et al.*, 2002). Furthermore, Evert and colleagues suggested that the formation of aggregates might even

be considered a cellular protective response to large quantities of misfolded protein (Evert *et al.*, 2006a).

1.1.5. Pathogenesis of Machado-Joseph disease

The pathogenesis of MJD is still poorly understood, but the presence of mutant ataxin-3 with an expanded polyglutamine tract is the triggering factor of several events that lead to neurodegeneration. There is evidence that proteolytic cleavage might be the initial step of a cascade of events that origins different toxic species (Goti *et al.*, 2004; Haacke *et al.*, 2007; Ikeda *et al.*, 1996; Jung *et al.*, 2009; Simões *et al.*, 2012). The first toxic species are protein fragments with an altered conformation which may then undergo aggregation, giving rise to soluble oligomers and ultimately, insoluble intracellular inclusions. Expanded ataxin-3 may also misfold and self-associate originating oligomers that can accumulate in intracellular inclusions. Interestingly, soluble oligomers have been shown to induce greater toxicity than polyglutamine monomers or intracellular inclusions (Takahashi *et al.*, 2008).

As described in several reviews (Costa Mdo and Paulson, 2012; Evers *et al.*, 2014; Matos *et al.*, 2011; Nóbrega and Pereira de Almeida, 2012; Paulson, 2012), the principal toxic effects of these aberrantly folded species may include, among others: failure of the quality control system, dysregulation of transcription, mitochondrial dysfunction, aberrant protein-protein interactions, calcium-homeostasis dysregulation and axonal-transport disruption (Figure 1.2).

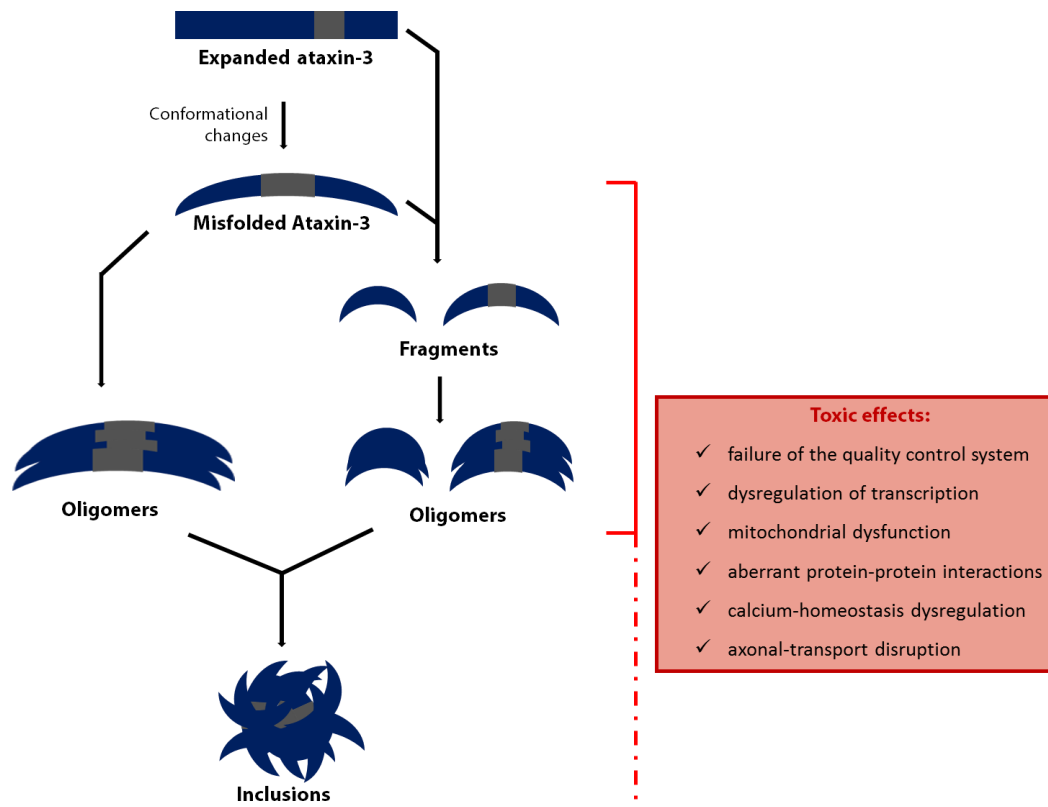


Figure 1.2. Molecular mechanisms underlying MJD pathogenesis. Schematic representation of several toxic species that may be involved in MJD pathogenesis: misfolded ataxin-3, misfolded fragments, oligomers (soluble micro-aggregates) and intracellular inclusions (insoluble aggregates). These toxic species give rise to deleterious effects on multiple cell pathways: failure of the quality control system, dysregulation of transcription, mitochondrial dysfunction, aberrant protein-protein interactions, calcium-homeostasis dysregulation and axonal-transport disruption.

Even though, as previously explained, MJD results primarily from a toxic gain-of-function mechanism owing to the presence of the expanded polyglutamine tract in the ataxin-3 protein, growing evidence suggests that the CAG expansion on RNA might also contribute somehow to the pathogenesis of the disease (Hsu *et al.*, 2011; Li *et al.*, 2008; Wang *et al.*, 2011b).

1.1.6. Promising therapeutic strategies for Machado-Joseph disease

As discussed before, there is no therapy to modify disease progression and the available options to alleviate MJD rely in the use of pharmacological compounds to deal with some specific symptoms, as reviewed by Jonas Saute and Laura Jardim (Saute and Jardim, 2015). However, the extensive research on molecular mechanisms underlying disease

pathogenesis brought to light several studies that revealed potential therapeutic options for MJD management in the future. These studies can be categorized into five different groups according to its goal: 1) reducing mutant ataxin-3 protein levels, 2) preventing mutant ataxin-3 misfolding, cleavage, oligomerization and aggregation, 3) targeting specific cellular mechanisms (e.g. transcriptional dysregulation, calcium homeostasis and oxidative stress), 4) neuroprotection and 5) cell-replacement (Evers *et al.*, 2014; Matos *et al.*, 2011; Nóbrega and Pereira de Almeida, 2012). The first group encompasses strategies that decrease diseased-protein levels either by blocking its production – gene editing, RNA interference and exon skipping strategies – or by increasing its degradation – upregulation of autophagy and ubiquitin proteasome system (Evers *et al.*, 2014). Figure 1.3 outlines these potential therapeutic strategies for MJD.

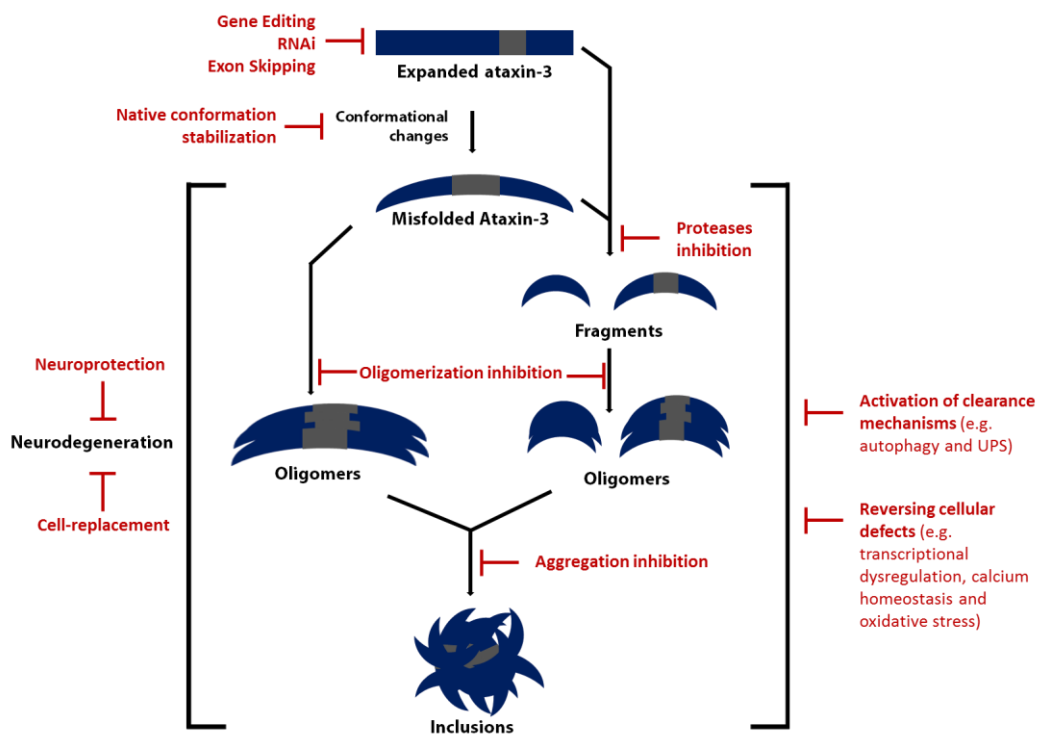


Figure 1.3. Outline of the potential therapeutic strategies for MJD. Gene editing, RNAi and exon skipping represent the most straightforward approach towards MJD treatment, enabling the suppression of the expanded protein before deleterious effects happen. Other effective strategies aim to prevent the mechanisms responsible for the production of toxic species: mutant ataxin-3 misfolding (native conformation stabilizers), cleavage (proteases inhibitors), oligomerization (oligomerization inhibitors) and aggregation (aggregation inhibitors). Some approaches involve the activation of clearance mechanisms like autophagy and ubiquitin-proteasome system, others try to reverse cellular defects that are mediated by toxic species. Neuroprotection and cell-replacement strategies were also used successfully to alleviate MJD.

Although several approaches demonstrated promising results on MJD, the most effective therapy for a monogenic disease such as MJD is a strategy that eliminates the production of the causative protein, before significant deleterious effects happen to the affected neuronal cells. Therefore, this thesis focuses on the use of the RNA interference mechanism to block the production of the disease-causing protein, in an attempt to stop disease progression. Studies exploring the RNA interference potential for the treatment of MJD, will be discussed in section 1.2.

1.2. RNA interference

1.2.1. RNA interference and its mechanism

In 1998, in experiments using the nematode *Caenorhabditis elegans*, Fire and Mello uncovered the RNA interference (RNAi) mechanism, through which double-stranded RNA molecules (dsRNAs) trigger silencing of complementary messenger RNA sequences (Fire *et al.*, 1998). Just eight years later, Fire and Mello were awarded with the Nobel Prize in Physiology or Medicine, emphasizing the importance of their discovery. Another important finding came out in 2001, when *Elbashir and collaborators* showed that shorter synthetic dsRNAs – small interfering RNAs (siRNAs) – could mediate RNAi in cultured mammalian cells (Elbashir *et al.*, 2001a; Elbashir *et al.*, 2001b). Subsequently, several groups demonstrated potent gene suppression *in vivo* by RNAi in animals, including non-human primates (Lewis *et al.*, 2002; McCaffrey *et al.*, 2002; Song *et al.*, 2003; Xia *et al.*, 2002; Zimmermann *et al.*, 2006). Altogether, these findings were the driving force for the development of gene-specific silencing therapeutics for human diseases. Notably, in 2010, the first evidence of successful RNAi-mediated gene-silencing in humans from the delivered siRNAs was reported (Davis *et al.*, 2010).

The mechanism of RNAi can be initiated with distinct RNA molecules, including endogenous small non-coding microRNAs (miRNAs) or exogenously introduced siRNAs, short hairpin RNAs (shRNAs) or artificial miRNAs (Figure 1.4).

As highlighted in several reviews (Boudreau *et al.*, 2011; Davidson and McCray, 2011; Lee *et al.*, 2002; Pecot *et al.*, 2011; Rana, 2007), mature miRNAs (19–25 nucleotides) are processed from primary-miRNA transcripts (pri-miRNAs), which contain hairpin structures. Upon expression, pri-miRNAs are cleaved by Drosha producing precursor-miRNAs (pre-miRNAs) (Gregory *et al.*, 2004; Kim, 2005; Lee *et al.*, 2003). Pre-miRNAs are subsequently trafficked by exportin-5 to the cytoplasm where they are further processed by Dicer, giving rise to the miRNA duplex (Bohnsack *et al.*, 2004; Provost *et al.*, 2002; Yi *et al.*, 2003). Mature miRNAs are then loaded onto RNA-induced silencing complex (RISC), recognize its target and bind to the 3'untranslated region (3'UTR) of the target mRNA (Khvorova *et al.*, 2003; Schwarz *et al.*, 2003). If there is a perfect complementarity between mature miRNA and its target, the cleavage of the transcript happens (Bagga *et al.*, 2005). Instead, imperfect binding results in the repression of the translation (Doench *et al.*, 2003; Zeng *et al.*, 2003).

Synthetic siRNAs are small double stranded RNA molecules that contain a guide (or antisense) strand that is complementary to the target mRNA, and a passenger (or sense) strand. Each strand has approximately 19-21 nucleotides and contain 2 nucleotide overhangs on each 3' end (Elbashir *et al.*, 2001a; Elbashir *et al.*, 2001b). siRNAs are synthesized to mimic mature miRNAs duplexes entering the RNAi pathway after Dicer-cleavage step. Once in the cytoplasm, the siRNA sense strand is degraded, whereas the antisense strand is incorporated into the RISC (Zamore *et al.*, 2000). The antisense strand is designed to present perfect complementarity to the target mRNA, triggering potent cleavage-based silencing of the target gene.

Besides synthetic siRNAs, the RNAi mechanism can also be exogenously initiated with the use of shRNAs or artificial miRNAs, but this requires the use of expression vectors, such as viral vectors, to be introduced in the cell nuclei. These molecules are transcribed as a sense and complementary antisense sequence, connected by a non-complementary loop, and enter the RNAi pathway mimicking pri-miRNAs (artificial miRNAs) or pre-miRNAs (shRNAs) (Paul *et al.*, 2002; Zeng *et al.*, 2002).

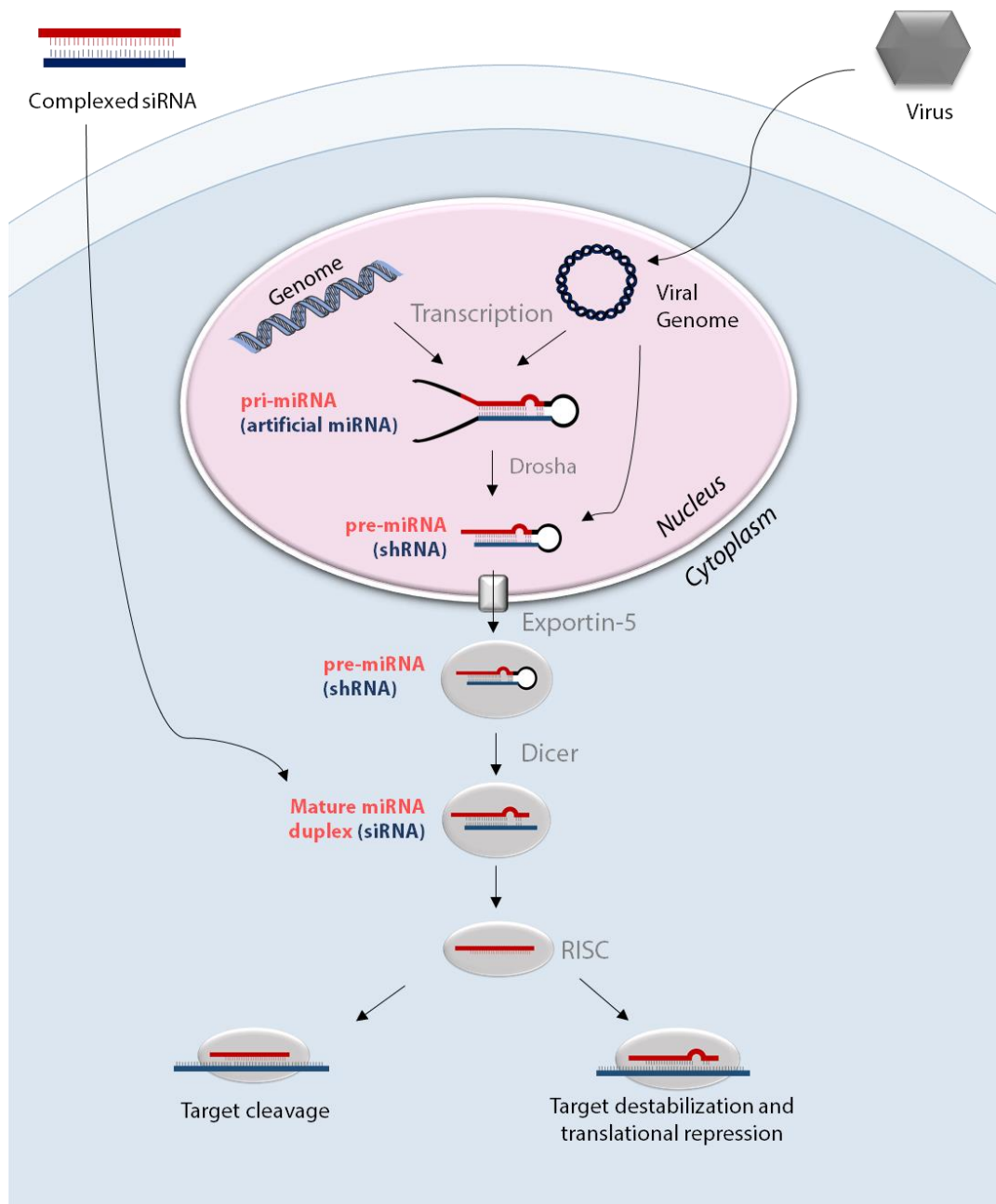


Figure 1.4. RNAi mechanism and exogenous components that trigger RNAi-mediated gene silencing. The RNAi mechanism can be triggered by endogenous miRNAs or exogenously introduced siRNAs, shRNAs or artificial miRNAs. siRNAs need to be introduced in the cell cytoplasm, and enter the RNAi pathway after Dicer-cleavage step. Artificial miRNAs and shRNAs require the use of expression vectors, such as viral vectors, to be introduced in the cell nuclei, and enter the RNAi pathway mimicking pri-miRNAs and pre-miRNAs, respectively. Mature miRNAs (19–25 nucleotides) are processed from primary-miRNA transcripts (pri-miRNAs), which contain hairpin structures. Upon expression, pri-miRNAs are cleaved by Drosha producing precursor-miRNAs (pre-miRNAs). Pre-miRNAs are subsequently trafficked by exportin-5 to the cytoplasm where they are further processed by Dicer, giving rise to the miRNA duplex. Mature miRNAs are then loaded onto RNA-induced silencing complex (RISC), recognize its target and bind to the 3'untranslated region (3'UTR) of the target mRNA. If there is a perfect complementarity between mature miRNA and its target, the cleavage of the transcript happens. Instead, imperfect binding results in the repression of the translation.

1.2.2. Clinical trials using RNAi to treat human diseases

The enormous therapeutic potential of RNAi lead to the development of several biotechnology companies including Alnylam Pharmaceuticals, Tekmira Pharmaceuticals, Calando Pharmaceuticals, Quark Pharmaceuticals and Sylentis, that are currently supporting the pre-clinical and clinical development of several RNAi-based products.

Currently, there are more than 20 clinical trials ongoing using RNAi-based products, and the clinical applications under study vary from viral infections to hereditary disorders and cancers (ClinicalTrials.gov). Nevertheless, the world is still waiting for the release of the first RNAi product into the marketplace. Table 1.1 presents an overview of RNAi-drugs that have entered clinical trials, based on previous publications (Kanasty *et al.*, 2013; Ozcan *et al.*, 2015) and updated for the current status (ClinicalTrials.gov).

Table 1.1. RNAi-based drugs in clinical trials

Drug	Vehicle	Route	Target	Phase and Status	Clinical trial ID	Sponsor
Bevasiranib	Naked siRNA	IVT	VEGF	I Completed II Completed II Completed III Terminated III Withdrawn	NCT00722384 NCT00259753 NCT00306904 NCT00499590 NCT00557791	OPKO Health, Inc.
AGN211745	Naked siRNA	IVT	VEGFR1	I/II Completed II Terminated	NCT00363714 NCT00395057	Allergan siRNA Therap. Inc.
PF-04523655	Naked siRNA	IVT	RTP801	I Completed II Terminated II Completed II Completed	NCT00725686 NCT00701181 NCT00713518 NCT001445899	Quark Pharmac.
ALN-RSV01	Naked siRNA	IN	RSV nucleocapsid	II Completed II Completed II-b Completed	NCT00496821 NCT00658086 NCT01065935	Alnylam Pharmac.
I5NP	Naked siRNA	IV	P53	I Completed I Terminated I/II Completed	NCT00802347 NCT00683553 NCT00802347	Quark Pharmac.

TD101	Naked siRNA	Foot inj.	K6A (N171K mutation)	I Completed	NCT00716014	Pachyonychia Congenita Project
CALAA-01	CD NP	IV	RRM2	I Terminated	NCT00689065	Calando Pharmac.
ALN-VSP02	LNP	IV	KSP and VEGF	I Completed I Completed	NCT00882180 NCT01158079	Alnylam Pharmac.
PRO-040201	LNP	IV	ApoB	I Terminated	NCT00927459	Tekmira Pharmac.
Atu027	Cationic Lipoplex	IV	PKN3	I Completed Ib/Ila Active, not recruiting	NCT00938574 NCT01808638	Silence Therapeutics
SYL040012	Naked siRNA	Ophtha.	ADRB2	I Completed I/II Completed II Completed II Recruiting	NCT00990743 NCT01227291 NCT01739244 NCT02250612	Sylentis, S.A.
QPI-1007	Naked siRNA	IVT	CASP2	I Completed II Active, not recruiting II/III Not yet opened	NCT01064505 NCT01965106 NCT02341560	Quark Pharmac.
ALN-TTR01	LNP	IV	TTR	I Completed	NCT01148953	Alnylam Pharmac.
ALN-TTR02	LNP	IV	TTR	I Completed II Completed II Active, not Recruiting III Recruiting I Completed III Recruiting by invitation	NCT01559077 NCT01617967 NCT01961921 NCT01960348 NCT02053454 NCT02510261	Alnylam Pharmac.
ALN-TTRSC	siRNA-GalNAc conjugate	SC	TTR	I Active, not Recruiting II Completed II Active, not Recruiting III Recruiting	NCT01814839 NCT01981837 NCT02292186 NCT02319005	Alnylam Pharmac.
SIG12D LODER	LODER polymer	EUS biopsy needle	KRAS G12D	I Completed II Not yet recruiting	NCT01188785 NCT01676259	Silenseed Ltd.

SYL1001	Naked siRNA	Ophtha.	TRPV1	I Completed I/II Completed II Recruiting	NCT01438281 NC01776658 NCT02455999	Sylentis, S.A.
TKM-080301	LNP	IV	PK1	I Completed I/II Completed I/II Recruiting	NCT01437007 NCT01262235 NCT02191878	National Cancer Inst. Tekmira Pharmac.
ALN-PCS02	LNP	IV	PCSK9	I Completed	NCT01437059	Anylam Pharmac.
ALN-PCSSC	LNP	SC	PCSK9	I Active, not recruiting	NCT02314442	Anylam Pharmac.
TKM-100201	LNP	IV	ZEBOV Polym. VP24, VP35	I Terminated	NCT01518881	Tekmira Pharmac.
ND-L02-s0201	LNP	IV	HSP47	I Completed I Recruiting	NCT01858935 NCT02227459	Nitto Denko Corp.
TKM-100802	LNP	IV	ZEBOV Polym. VP24, VP35	I Terminated	NCT02041715	Tekmira Pharmac.
ALN-AT3SC	siRNA-GalNAc conjugate	SC	AT TG	I Recruiting	NCT02035605	Anylam Pharmac.
APN401	Mononuclear cells	IV	E3 ubiquitin ligase Cbl-b	I Recruiting	NCT02166255	Wake Forest Univ.
DCR-MYC	LNP	IV	MYC	I/II Recruiting I Recruiting	NCT02314052 NCT02110563	Dicerna Pharmac.
SiRNA-EphA2-DOPC	LNP	IV	EphA2	I Recruiting	NCT01591356	MD Anderson Cancer Center

ABBREVIATIONS: LNP= lipid nanoparticle; CD NP= cyclodextrin nanoparticle; IVT= intravitreal; IV= intravenous; IN= intranasal; SC= subcutaneous; EUS= endoscopic ultrasound.

The most advanced RNAi drug candidates are ALN-TTR02 and ALN-TTRsc, two therapeutic candidates from Anylam Pharmaceuticals in phase III trials (Haussecker and Kay, 2015). These siRNA-based drugs are indicated for the treatment of transthyretin-mediated amyloidosis (TTRA) and inhibit specifically transthyretin (TTR) mRNA, thereby reducing TTR protein (Kubowicz *et al.*, 2013). The commercialization of these products is expected to occur as early as 2017 (Haussecker and Kay, 2015).

1.2.3. RNAi and neurodegenerative diseases

There are no available therapies for the most devastating neurodegenerative diseases. Therefore, for these group of diseases, but particularly for those in which neurodegeneration is linked to the synthesis of mutant proteins coded by dominant mutant alleles, therapies based on RNAi hold great promise. Some examples of successful experiments involving RNAi to rescue the neurological phenotype in animal models of neurodegenerative diseases include: Huntington's disease (HD), SCA1, MJD/SCA3, SCA7, Alzheimer's disease (AD) and Parkinson's disease (PD). These examples are summarized in Table 1.2.

Table 1.2. Successful experiments using RNAi-based therapeutics in animal models of neurodegenerative diseases

Disease	Target gene	RNAi Approach	Delivery vehicle	Injection Site	References
HD	<i>HTT</i>	shRNAs, artificial miRNAs, siRNAs or antisense oligonucleotides	AAV1, AAV2, AAV5, AAV2/1 Adenoviral vector Lentivirus ExGen500 or Lipofectamine 2000 Cholesterol-conjugates	Striatum or ICV	(Boudreau <i>et al.</i> , 2009; Carroll <i>et al.</i> , 2011; DiFiglia <i>et al.</i> , 2007; Drouet <i>et al.</i> , 2009; Grondin <i>et al.</i> , 2012; Harper <i>et al.</i> , 2005; Huang <i>et al.</i> , 2007a; Kordasiewicz <i>et al.</i> , 2012; Machida <i>et al.</i> , 2006; McBride <i>et al.</i> , 2011; Østergaard <i>et al.</i> , 2013; Rodriguez-Lebron <i>et al.</i> , 2005; Stiles <i>et al.</i> , 2012; Wang <i>et al.</i> , 2005; Yu <i>et al.</i> , 2012)
SCA1	<i>ATXN1</i>	shRNAs or artificial miRNAs	AAV2, AAV2/1, AAV2/5	Cerebellar midline lobules IV/V or Deep cerebellar nuclei (DCN)	(Keiser <i>et al.</i> , 2014; Keiser <i>et al.</i> , 2013; Xia <i>et al.</i> , 2004)
SCA3	<i>ATXN3</i>	shRNAs or artificial miRNAs	Lentivirus AAV2/1	Striatum or DCN	(Alves <i>et al.</i> , 2008a; Alves <i>et al.</i> , 2010; Costa Mdo <i>et al.</i> , 2013; Nóbrega <i>et al.</i> , 2014; Nóbrega <i>et al.</i> , 2013b; Rodriguez-Lebron <i>et al.</i> , 2013)
SCA7	<i>ATXN7</i>	Artificial miRNAs	AAV2/1	DCN	(Ramachandran <i>et al.</i> , 2014)
AD	<i>BACE1</i> <i>APP</i> <i>CDK5</i>	siRNAs, shRNAs or artificial miRNAs	Lentivirus AAV2/5	Hippocampus	(Piedrahita <i>et al.</i> , 2010; Rodriguez-Lebron <i>et al.</i> , 2009; Singer <i>et al.</i> , 2005)
PD	α - <i>synuclein</i>	shRNAs	Lentivirus AAV 5, AAV2	Striatum or Substantia Nigra	(Gorbatyuk <i>et al.</i> , 2010; Khodr <i>et al.</i> , 2011; Sapru <i>et al.</i> , 2006)

Despite the encouraging results obtained in all these studies, before considering its clinical application, several issues need to be addressed. One of the most important concerns is related with the lack of efficient systems to enable *in vivo* gene transfer to the CNS by a non-invasive administration. As a consequence, all the documented experiments were performed through an invasive route – either after intracranial or intracerebroventricular (ICV) administration – which results in a more circumscribed expression, that may be insufficient to treat all the disease-relevant brain regions. There is a need to develop alternative systems to achieve robust silencing of the mutant protein over larger areas of the human brain. Another concern is related with the potential side effects that long term expression of siRNA treatment can mediate, and the inability to interrupt it. For these two concerns, the development of efficient systems for *in vivo* gene transfer to the CNS upon intravenous administration is expected to provide the most useful therapeutic strategy for the alleviation of several neurological diseases.

1.2.4. RNAi and Machado-Joseph disease

As highlighted in table 1.2, several recent studies showed the efficacy of RNAi in animal models of Machado-Joseph disease. However, all these studies involved craniotomy to inject viral vectors codifying the silencing sequences into the brain parenchyma. As previously explained, there is a need for a less invasive procedure without the need for craniotomy, general anesthesia and the risks associated with surgical injection in the brain parenchyma. Moreover, safety concerns of regulatory affairs institutions regarding viral vectors suggest that non-viral systems would reach patients within a shorter time frame as compared to viral systems. Therefore, this thesis focuses on the development of a non-viral strategy to enable the delivery of siRNAs to the brain after a non-invasive administration, and its validation in two genetically-modified mouse models of MJD.

1.2.4.1. Non-allele *versus* allele-specific silencing of ataxin-3

To silence the expression of ataxin-3 in MJD cellular and animal models, two different approaches can be explored: non-allele (Alves *et al.*, 2010; Costa Mdo *et al.*, 2013; Rodriguez-Lebron *et al.*, 2013) and allele-specific silencing (Aiba *et al.*, 2013; Alves *et al.*, 2008a; Hu *et al.*, 2011; Hu *et al.*, 2009; Li *et al.*, 2004; Liu *et al.*, 2013a; Liu *et al.*, 2013b; Miller *et al.*, 2003; Nóbrega *et al.*, 2014; Nóbrega *et al.*, 2013b).

As previously described, the ataxin-3 protein is ubiquitously expressed in neuronal and non-neuronal human tissues and has been implicated in several important cell pathways. Therefore, one of the major concerns when implementing RNAi that does not discriminate between mutant and wild type alleles, is the toxicity that can result from reduced expression of the wild-type protein. In fact, in a fly model of MJD, Warrick and collaborators reported that wild type ataxin-3 suppressed polyglutamine neurodegeneration *in vivo*. However, later studies demonstrated that non-expanded ataxin-3 could not alleviate polyglutamine-induced degeneration in mouse and rat models of MJD (Alves *et al.*, 2010; Hübener and Riess, 2010), suggesting that therapeutic approaches that reduce expression of both alleles might be feasible.

Nevertheless, selective inhibition of the mutant allele has a higher probability to translate into a successful treatment for humans, potentially inducing fewer side effects. For that reason, in this project, we used an allele-specific silencing approach to reduce mutant ataxin-3 levels without interfering with the non-expanded ataxin-3. To perform this, and as previously reported by our group, siRNAs were targeted to a single nucleotide polymorphism (SNP) that can be found in 70% of MJD patients (Alves *et al.*, 2008a). This SNP is located at the 3' end of the CAG tract of the ataxin-3 (rs12895357), and while the mutant allele carries the C variant, the wild type allele carries the G variant (Gaspar *et al.*, 2001).

1.3. Non-viral vectors for gene silencing in the Central Nervous System upon systemic administration

1.3.1. Obstacles to the delivery of siRNAs to the brain upon intravenous administration

Despite the potential of siRNAs to treat several diseases that remain untreatable, the development of siRNAs as therapeutics has been challenging. The main barrier to clinical translation of siRNAs is related with its successful delivery to the target cells.

After being introduced into the bloodstream, nucleic acids face several challenges that block their delivery to neuronal cells. On the one hand, siRNAs are susceptible to degradation by extracellular RNases and rapidly eliminated by the kidneys, presenting very short half-lives that range from seconds to minutes (O'Mahony *et al.*, 2013; Peer and Lieberman, 2011). siRNAs also have unfavorable characteristics such as: large molecular weight (~13 kDa), net negative charge and hydrophilic nature which strongly impair its cellular internalization (O'Mahony *et al.*, 2013). However, the biggest challenge to the delivery of nucleic acids to the Central Nervous System (CNS) is the presence of the blood-brain barrier (BBB), which precludes the entry of most therapeutic substances from the blood into the brain.

To overcome these major problems, the majority of the successful pre-clinical studies using RNAi-based therapeutics on neurodegenerative diseases, used viral vectors to introduce silencing sequences into the brain (reviewed in section 1.2.3). Besides the fact that these strategies require, in most situations, invasive administration of the viral vectors into the brain, these approaches have also other drawbacks, especially safety concerns (e.g. insertional mutagenesis), high cost of production and the possibility to elicit an immune response against the viral agent (Pérez-Martínez *et al.*, 2012; Posadas *et al.*, 2010; Thomas *et al.*, 2003). Therefore, to overcome these issues, there is an extreme need to develop alternative non-viral vectors. Non-viral vectors are recognized to be stable, easy to produce and to involve minimal safety risks (Posadas *et al.*, 2010). Moreover, they enable the use of less invasive procedures, like intravenous administration, to administer the siRNA-based treatment. Consecutively, intravenous administration would provide the ideal non-invasive way for delivery throughout the brain, because of its rich vascularity,

which may be necessary given the diffuse neuropathology of several neurodegenerative diseases (Pardridge, 2002; Schlachetzki *et al.*, 2004). Additionally, the transient nature of expression mediated by non-viral vectors, allows an interruption of administration if at any moment there is a development of side-effects.

1.3.1.1. The BBB and how to overcome the BBB

The BBB is a physical barrier composed of brain capillary endothelial cells (BCECs), characterized by the presence of tight junctions that dramatically limit the traffic of compounds from the blood into the brain (Weksler *et al.*, 2005). On the brain side, this layer of non-fenestrated BCECs is in intimate contact with other cell types such as: pericytes, astrocytes and neurons. In addition to the physical barrier, the BBB has also several receptors, ion channels and influx/efflux transport proteins that act as a transport barrier (Abbott *et al.*, 2006; Pérez-Martínez *et al.*, 2011; Wong *et al.*, 2012).

The main routes of molecular traffic at the BBB, as represented in Figure 1.5, include: paracellular aqueous pathway (limited to small water-soluble compounds), transcellular lipophilic pathway (for lipid-soluble compounds), transport proteins (that act like carriers for glucose, amino acids, and other substances; and efflux transporters) adsorptive-mediated transcytosis (for albumin and other native plasma proteins after cationization) and receptor-mediated transcytosis (for proteins such as insulin and transferrin) (Abbott *et al.*, 2006; Chen and Liu, 2012).

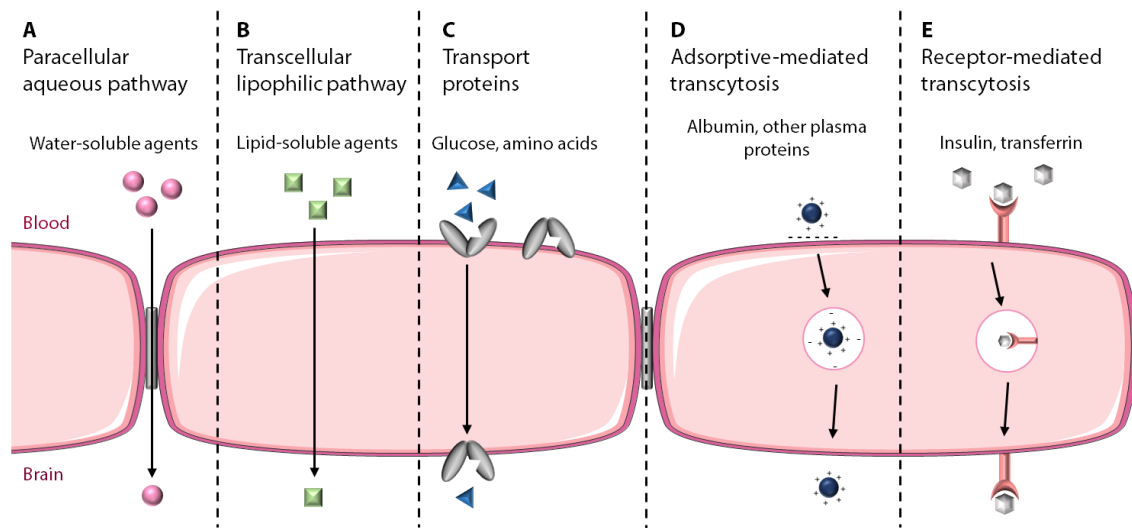


Figure 1.5. Primary routes of molecular traffic at the BBB. (A) Paracellular aqueous pathway, for small hydrophilic compounds. (B) Transcellular lipophilic pathway, for lipophilic agents. (C) Transport proteins, for influx or efflux of different molecules. (D) Adsorptive-mediated transcytosis, for plasma proteins after cationization. (E) Receptor-mediated transcytosis, for larger proteins essential to the brain functions.

Most conventional drugs that are known to cross the BBB are lipophilic molecules that have a low molecular weight (< 500 Da) and, therefore, enter the CNS exploiting the transcellular lipophilic pathway (Nishina *et al.*, 2013; Pérez-Martínez *et al.*, 2011). As siRNAs have a high molecular weight (~13 KDa) and are hydrophilic molecules, in order to achieve gene silencing in the CNS, it is imperative to use a delivery system.

One of the most promising ways to facilitate the delivery of gene therapeutics across the BBB consists in the association of monoclonal antibodies, ligands or optimized ligand fragments to the non-viral delivery system, to promote receptor-mediated transcytosis of the nano-system. As reviewed by Ruben Boado (Boado, 2007), the first effective studies, that enabled the delivery of gene-therapeutics to the brain after intravenous administration, conjugated molecular antibodies to bind endogenous receptors that are present in BCECs (insulin and transferrin receptors) to liposomes, resulting in receptor-mediated transcytosis of the nanoparticles containing gene therapeutics. More recent studies reported that ligands that bind to the nicotinic acetylcholine receptors (nAChRs), that are widely expressed in the brain and in the BCECs, such as small peptides derived from rabies virus (Kumar *et al.*, 2007) or from a neurotoxin (Zhan *et al.*, 2010), could

undergo receptor-mediated transcytosis. These strategies will be further discussed in the next section.

Another alternative pathway to avoid crossing the BBB after peripheral administration, uses the natural trans-synaptic retrograde transport, that occurs with some pathogens and toxins, to deliver nanoparticles through peripheral nerves until the CNS (Pérez-Martínez *et al.*, 2011).

1.3.2. Non-viral strategies with proven brain distribution of gene-therapy molecules upon intravenous administration

Non-viral vectors allow CNS delivery of nucleic acids after non-invasive administration mainly for two main reasons: first, they enable encapsulation or complexation of the therapeutic cargo, avoiding degradation that would occur in the bloodstream and second, they enable the transport across the BBB after association of BBB targeting-ligands. Moreover, the use of nanoparticles (such as liposomes, polymers or exosomes) is expected to avoid extensive systemic distribution, enhancing the transport across the BBB. Please refer to Table 1.3 to see reported non-viral strategies with proven brain distribution of gene-therapy molecules, after intravenous administration. Figure 1.6 has an illustrative representation of selected examples from Table 1.3.

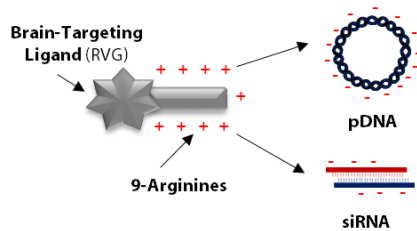
The non-viral strategies discussed below, due to their dimensions in the nanometer range, are considered nano-systems, with respect to either biological molecules (i.e., peptides, natural polymers) or synthetic materials customized at the nanometric scale (i.e., lipid nanoparticles, polymeric nanoparticles).

Table 1.3. Non-viral strategies with proven brain distribution of gene-therapy molecules across the BBB

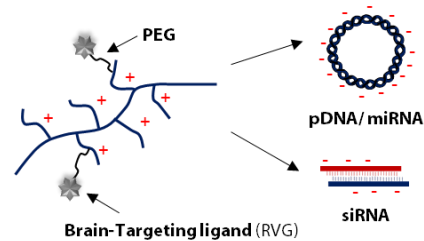
Targeting-ligand	Formulation	Brain disorder	Gene Therapy	Important findings	Ref.
RVG	RVG-9r	Viral encephalitis	siRNAs	Gene silencing within the brain; robust protection against fatal viral encephalitis	(Kumar <i>et al.</i> , 2007)
	PAMAM-PEG	Not tested in a disease condition	pDNA	Widespread expression of an exogenous gene in the brain	(Liu <i>et al.</i> , 2009)
	Cationic Liposomes	Prion disease	siRNAs	Silencing of cellular prion protein in the brain	(Pulford <i>et al.</i> , 2010)
	SSPEI-PEG	Not tested in a disease condition	pDNA	Widespread expression of an exogenous gene in the brain	(Son <i>et al.</i> , 2011)
	SSPEI-PEG (mannitol)	Not tested in a disease condition	miRNAs	Accumulation of miRNA in the brain. Further enhancement using mannitol	(Hwang <i>do et al.</i> , 2011)
	Exosomes	Alzheimer's disease	siRNAs	Gene silencing of BACE1 in the brain; immunologically inert	(Alvarez-Erviti <i>et al.</i> , 2011)
	RVG-9rR	Not tested in a disease condition	pDNA	Widespread expression of an exogenous gene in the brain	(Gong <i>et al.</i> , 2012)
	RVG-9r	Not tested in a disease condition	siRNAs	Gene silencing of calpain-2; impaired learning and memory	(Zadran <i>et al.</i> , 2013)
	Dendrigrft poly-L-lysines-PEG	Parkinson's disease	shRNAs	Gene silencing of activated caspase-3, improving locomotor activity and rescuing neuronal loss	(Liu <i>et al.</i> , 2013c)
	Trimethylated chitosan-PEG	Not tested in a disease condition	siRNAs	siRNA accumulation in the brain	(Gao <i>et al.</i> , 2014)
	Exosomes	Parkinson's disease	siRNAs	Gene silencing of α -synuclein, reducing aggregates	(Cooper <i>et al.</i> , 2014)
	Poly(mannitol-co-PEI)-PEG	Alzheimer's disease	siRNAs	Delivery and gene silencing of BACE1	(Park <i>et al.</i> , 2015)
TfR and/or IR mAbs	PILs	Not tested in a disease condition	pDNA	Widespread gene expression in the rodent and primate brain	(Shi and Pardridge, 2000; Zhang <i>et al.</i> , 2003d)
	PILs	Brain cancer	shRNAs	The delivery of shRNAs against EGFR prolonged survival	(Boado, 2005; Zhang <i>et al.</i> , 2004; Zhang <i>et al.</i> , 2002)

	PILs	Brain cancer	shRNAs	Decrease of luciferase expression by 90% in the brain tumor	(Zhang <i>et al.</i> , 2003b)
	PILs	Parkinson's disease	pDNA	Normalization of the brain enzyme activity after non-invasive delivery of TH; functional motor improvement	(Zhang <i>et al.</i> , 2003c)
	Avidin-biotin technology	Brain cancer	siRNAs	Decrease of luciferase expression (69-81%) in the brain tumor	(Xia <i>et al.</i> , 2007)
	PILs	Type VII mucopolysaccharidosis	pDNA	Increased β -glucuronidase enzyme activity in the brain	(Zhang <i>et al.</i> , 2008)
Transferrin	PAMAM-PEG	Not tested in a disease condition	pDNA	Widespread expression of an exogenous gene in the brain	(Huang <i>et al.</i> , 2007b)
Lactoferrin	PAMAM-PEG	Not tested in a disease condition	pDNA	Widespread expression of an exogenous gene in the brain	(Huang <i>et al.</i> , 2008)
Angiopep	PAMAM-PEG	Not tested in a disease condition	pDNA	Widespread expression of an exogenous gene in the brain	(Ke <i>et al.</i> , 2009)

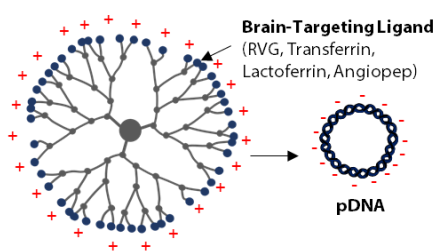
A. Cell-targeting peptide



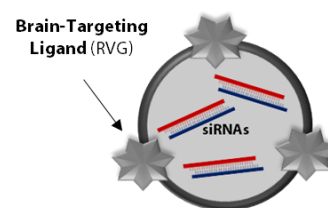
B. Branched polyethyleneimine



C. Dendrimers



D. Exosomes



E. Immunoliposomes

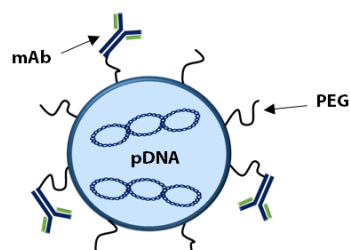


Figure 1.6. Illustrative examples of selected non-viral delivery systems that proved to be efficient for systemic delivery of gene therapies to the brain. (A) A short peptide derived from rabies virus glycoprotein, with 29 amino acids (RVG29) and 9-arginine residues, delivers gene therapies across the BBB. **(B)** Branched polyethyleneimine linked to the RVG29 peptide enables brain delivery of siRNAs, pDNA and miRNAs. **(C)** Polyamidoamine (PAMAM) dendrimers coupled to specific ligands (RVG29, transferrin, lactoferrin or angiopep) enables the delivery of pDNA into the brain. **(D)** RVG29-targeted exosomes deliver siRNAs to the brain. **(E)** Neutral immunoliposomes have been targeted to the brain associating monoclonal antibodies directed against either the transferrin receptor (TfR) and/or the insulin receptor (IR) and increase the absorption of gene therapies to the CNS.

1.3.2.1. Cell-targeting peptides

One of the most striking findings that contributed for the advance of the non-viral vectors for the delivery of nucleic acids to the brain across the BBB, was the discovery, in 2007, of a short peptide derived from rabies virus glycoprotein, with 29 amino acids (RVG29), that had the ability to bind to the nicotinic acetylcholine receptors present on BCECs and on neurons, promoting endothelial permeation and neuronal uptake (Kumar *et al.*, 2007). In this study, Kumar and collaborators reported that RVG-29 with nine-arginine residues (RVG-9r), used for complexation of siRNAs, was suitable for systemic administration, crossed the BBB and promoted reduction in target gene expression, thereby promoting therapeutic effects in mice with Japanese encephalitis viral infection (Kumar *et al.*, 2007). In another study, the RVG-9r peptide showed to promote the delivery of a luciferase plasmid DNA into the brain after intravenous administration, resulting in efficient luciferase gene expression in the brain with reduced expression in other organs such as liver, heart, kidney and muscle (Gong *et al.*, 2012). Figure 1.6A illustrates the electrostatic interaction between RVG-9r-peptide and siRNA or pDNA.

Interestingly also, several other reports showed that certain cell-penetrating peptides (CPPs), like Penetratin and Tat, enhance the accumulation of drugs and proteins in the brain after non-invasive administration (Heitz *et al.*, 2009). However, until now, there are no reports exploring their applicability for the systemic delivery of gene therapeutics. Hopefully several other ligands that demonstrated to promote brain accumulation after intravenous administration, will also prove their efficiency for the transvascular delivery of gene therapeutics (van Rooy *et al.*, 2011; Zhan *et al.*, 2010).

1.3.2.2. Polymer-derived nanoparticles

The most widely used polymeric nanoparticles, to deliver gene therapeutics to the brain after systemic administration, are polyethyleneimine (PEI) derivatives and dendrimers.

There are two forms of PEI – linear and branched – wherein the branched structure is more efficient to condense nucleic acids (Dunlap *et al.*, 1997). Branched PEI presents some other important characteristics for gene delivery: it is able to deliver gene therapies intracellularly, is associated with low immune response and has the ability to escape from endosomes (Boussif *et al.*, 1995). But a major concern using PEI is that it is non-biodegradable, presenting dose-dependent cytotoxicity. To overcome this, it was shown that the introduction of a disulfide linkage (-S-S-) in the branched PEI (SSPEI) introduced biodegradable capability (Son *et al.*, 2011). Importantly, SSPEI covalently linked to the RVG peptide enabled brain delivery of pDNA (Son *et al.*, 2011) and miRNAs (Hwang do *et al.*, 2011), after intravenous administration (Figure 1.6B). In another study, Park and collaborators demonstrated that another derivative from branched PEI, poly(mannitol-co-PEI), when associated to the RVG peptide, was efficient to deliver siRNAs to the brain, silencing β -secretase 1 (BACE1) expression, which plays an early role in amyloid plaque generation in Alzheimer's disease (Ohno *et al.*, 2007; Park *et al.*, 2015).

Dendrimers are highly organized polymers with three distinct domains: a central core, branches emanating from the core (organized in concentric layers) and terminal functional groups located in the exterior (Tomalia *et al.*, 1985). Although they have a good toxicity profile, dendrimers with high number of terminal amino groups are cytotoxic. This can be circumvented through the association of targeting-ligands to the periphery, masking the amino groups (Duncan and Izzo, 2005). Polyamidoamine (PAMAM) dendrimers are the most widely used because of their ability to encapsulate efficiently gene therapies. Actually, several studies showed that coupling specific ligands such as RVG (Liu *et al.*, 2009), transferrin (Huang *et al.*, 2007b), lactoferrin (Huang *et al.*, 2008) or angiopep (Ke *et al.*, 2009) to the surface of PAMAM dendrimers, enabled the delivery of pDNA to the brain, resulting in widespread expression of an exogenous gene, upon intravenous administration (Figure 1.6B).

Dendrigrft poly-L-lysines (DGLs) are synthetic polymers consisting of lysines and have been used for gene therapy because of their capability to efficiently encapsulate pDNA.

One study reported that intravenous administration of DGLs associated with the RVG peptide, resulted in the delivery of a plasmid DNA encoding caspase-3 shRNA to the brain. Even more importantly, this strategy demonstrated to improve locomotor activity and to rescue dopaminergic neuronal loss in a Parkinson's disease animal model (Liu *et al.*, 2013c).

As referred, a fundamental concern when using synthetic polymers *in vivo* is that the vast majority are non-biodegradable, presenting dose-dependent cytotoxicity upon systemic administration. Remarkably, all the referenced studies involving polymer-derived nanoparticles, used polyethylene glycol (PEG) and targeting-ligands, in an attempt to decrease their toxicity and increase their efficacy.

Another cationic polymer that has been explored as non-viral vector is chitosan because as it is a natural polymer, presents adequate features such as biodegradability and biocompatibility (Wang *et al.*, 2011a). However, chitosan is poorly soluble at physiological pH, being unable to interact properly with nucleic acids (Mao *et al.*, 2010). Trimethylation of chitosan demonstrated to improve its solubility and, consequently, the ability to complex nucleic acids (Dehousse *et al.*, 2010). Interestingly, there is one study showing that intravenous administration of trimethylated chitosan, linked to the RVG peptide through a covalent bound, bypasses the BBB delivering siRNAs to the brain (Gao *et al.*, 2014).

1.3.2.3. Exosomes

Exosomes are extracellular vesicles of endocytic origin, with a diameter between 40 and 120 nm, that can transport mRNA, miRNAs and proteins from one cell to another, mediating communication between cells (Valadi *et al.*, 2007). Because of these characteristics, they have an enormous potential as delivery vehicles for RNAi-based therapeutics. Indeed, two reports showed their efficacy for brain delivery of siRNAs, after systemic administration (Alvarez-Erviti *et al.*, 2011; Cooper *et al.*, 2014). These studies combined biotechnology to bind the RVG brain-targeting peptide to the surface of exosomes, encapsulated siRNAs targeting BACE1 (Alvarez-Erviti *et al.*, 2011) or α -synuclein (Cooper *et al.*, 2014) and demonstrated that this strategy resulted in efficient

gene knockdown in different brain regions (Figure 1.6D). Importantly, intravenous administration of siRNA-RVG exosomes, confirmed the immunologically inert profile of the exosomes treatment, as it did not change the levels of all cytokines studied (Alvarez-Erviti *et al.*, 2011).

1.3.2.4. Lipid-based nanoparticles

Lipid-based nanoparticles (LNPs) are a mature technology: at least eight LNP formulations for conventional drugs have been approved by the FDA, primarily for the treatment of cancer and its complications; and at least ten LNP formulations for other small molecule drugs are in clinical trials (Allen and Cullis, 2013).

The LNPs best characterized are liposomes, lipid vesicles with an aqueous core that can complex or encapsulate hydrophilic molecules such as nucleic acids, protecting them from degradation. Liposomes have also other interesting characteristics like the ease of surface modification, the good biocompatibility profile, and low toxicity (in comparison with inorganic nanoparticles and viral vectors), which make them an appealing solution to overcome some delivery issues (Pérez-Martínez *et al.*, 2012).

Although cationic liposomes have been extensively studied, there is only one report using these to deliver siRNAs to the brain after intravenous administration. In this study, *Mark Zabel and collaborators* demonstrated that cationic liposomes (constituted by a cationic lipid, DOTIM, and cholesterol), when associated to siRNAs and RVG-9r, mediated the silencing of a cellular prion protein in the brain (Pulford *et al.*, 2010). Nevertheless, these compounds, obtained from electrostatic interaction between negatively charged nucleic acids and positively charged lipids, have a high positive charge density on their surface resulting in: non-specific interactions with serum proteins, immunogenic response and rapid removal from the blood circulation (Kedmi *et al.*, 2010; Lin *et al.*, 2013).

An attractive alternative is to use PEG-grafted immunoliposomes (PILs) that were developed by the Pardridge group. These neutral immunoliposomes have been targeted to the brain associating monoclonal antibodies directed against either the transferrin receptor (TfR) and/or the insulin receptor (IR) present in endothelial cells of the BBB, increasing their absorption to the CNS (Figure 1.6E). In several papers published during

the last years, intravenous administration of PILs showed to enable the delivery of gene therapeutics to the brain (shRNAs or pDNA) (Boado, 2005; Shi and Pardridge, 2000; Zhang *et al.*, 2003b; Zhang *et al.*, 2003c; Zhang *et al.*, 2003d; Zhang *et al.*, 2008; Zhang *et al.*, 2004; Zhang *et al.*, 2002): prolonging survival in animal models of brain cancer (Boado, 2005; Zhang *et al.*, 2004; Zhang *et al.*, 2002), promoting functional motor improvement in an experimental animal model of Parkinson's disease (Zhang *et al.*, 2003c) and replacing a lysosomal enzyme, β -glucuronidase (GUSB), in GUSB null mice (Zhang *et al.*, 2008). Importantly, *Pardridge and his collaborators* also reported that chronic (weekly) intravenous administration of PILs encapsulating plasmid DNA in rats did not cause any detectable toxic side effect (Zhang *et al.*, 2003a). This promising technology is being developed nowadays by Armagen's biotechnological company.

1.3.3. Formulating an ideal non-viral vector for the delivery of nucleic acids to the brain

The use of nanoparticles is expected to overcome the challenges related with non-invasive delivery of nucleic acids to the CNS, promoting: biocompatibility and biodistribution, BBB crossing, targeted delivery and effective endosomal escape.

A rational approach to design therapeutic nanoparticles, the ABCD nanoparticle concept, was introduced by *Kostarelos and Miller* in 2005. This paradigm defines that an appropriate non-viral vector should be composed by four main components: A – complexed or encapsulated nucleic acids, B – envelope layer around nucleic acids (e.g. liposomes), C – stealth/ biocompatibility layer (e.g. PEG) and D – biological recognition layer, mediated by the use of targeting ligands (Kostarelos and Miller, 2005). The complexation or encapsulation of nucleic acids using nanoparticles, is expected to protect them from degradation while the use of PEG, for instance, aims to minimize toxicity and prolong circulation time. Finally, the use of CNS-targeting ligands (e.g. RVG, transferrin, lactoferrin, angioprep or molecular antibodies targeting receptors expressed at the BBB) is essential to enable brain delivery upon intravenous administration.

Besides this, other manufacturing and safety concerns should be addressed when designing the ideal formulation: particle size, immunogenicity of PEG and protein and

peptide components, aggregation of proteins and peptides and potential for scale-up (O'Mahony *et al.*, 2013).

1.3.4. Stable Nucleic Acid Lipid Particles

Stable nucleic acid lipid particles (SNALPs) are one of the most promising non-viral approaches for *in vivo* delivery of siRNAs (Costa *et al.*, 2013; Di Martino *et al.*, 2014; Geisbert *et al.*, 2006; Geisbert *et al.*, 2010; Judge *et al.*, 2009; Morrissey *et al.*, 2005; Zimmermann *et al.*, 2006).

SNALPs are composed by at least three basic lipids: ionizable cationic lipid (e.g. DODAP, DLinDMA, DLinKC2-DMA or DLinMC3-DMA), neutral helper lipid (e.g. cholesterol) and a PEG-derivatized lipid (Lin *et al.*, 2013). The development of ionizable cationic lipids, with pKa around 7 or lower, was one of the biggest advances in the field (Semple *et al.*, 2001). These enable the efficient encapsulation of siRNAs at acidic pH, where the lipid acquire a positive charge, and reduce toxicity as the lipid acquires a neutral charge at physiological pH (Semple *et al.*, 2001). The use of ionizable cationic lipids has also an important role at the endosome level, where they are thought to interact with the anionic endosomal lipids promoting the release of siRNAs into the cytosol (Hafez *et al.*, 2001). Another important component in SNALPs formulation is PEG that forms an aqueous shield around the liposomes, decreasing the extent of interaction with blood components and subsequent elimination by the macrophages. This results in an increase of the residence time of the nanoparticles in the blood circulation (Allen *et al.*, 1991).

Other important features that make SNALPs adequate for systemic administration are: efficient protection of nucleic acids from nucleases, appropriate particle size diameter (between 70-150 nm) and an overall charge close to neutrality (Lin *et al.*, 2013; Wan *et al.*, 2014). Furthermore, besides nucleic acids, SNALPs are a versatile platform that allows simultaneous delivery of multiple components such as imaging agents (Kraft and Ho, 2014) or drugs (Mendonca *et al.*, 2010b; Zhang *et al.*, 2013).

1.3.4.1. SNALPs in clinical trials

The vast majority of the first clinical trials exploring the potential of RNAi-based therapies, involved local administration of naked nucleic acids and, not surprisingly, failed or their future development is doubtful. Since then, and as a result of the development of promising delivery systems like SNALPs, many clinical trials with RNAi-based therapies shifted from local to systemic administration (Haussecker, 2012). Actually, there are, at least, seven SNALP formulations in clinical development for different conditions, as represented below in Table 1.4, and these candidates have been administered by intravenous administration.

Table 1.4. Ongoing clinical trials with SNALPs

Drug	Start year	Disease	Target	Phase and Status	Clinical Trial ID	Company
ALN-VSP02	2009	Solid Tumors with liver involvement	KSP and VEGF	I Completed I Completed	NCT00882180 NCT01158079	Alnylam Pharmac.s
PRO-040201	2009	Hypercholesterolemia	ApoB	I Terminated	NCT00927459	Tekmira Pharmac.
ALN-TTR01	2010	Transthyretin-mediated amyloidosis	TTR	I Completed	NCT01148953	Alnylam Pharmac.
TKM-080301	2010	Solid cancers and lymphoma	Polo-kinase 1	I Completed I/II Completed I/II Recruiting	NCT01437007 NCT01262235 NCT02191878	Tekmira Pharmac.
ALN-PCS02	2011	Hypercholesterolemia	PCSK9	I Completed	NCT01437059	Alnylam Pharmac.
TKM-100201	2011	Ebola virus infection	VP24, VP35, Zaire Ebola L polym.	I Terminated	NCT01518881	Tekmira Pharmac.
ALN-TTR02	2012	Transthyretin-mediated amyloidosis	TTR	I Completed II Completed II Active, not Recruiting III Recruiting I Completed III Recruiting by invitation	NCT01559077 NCT01617967 NCT01961921 NCT01960348 NCT02053454 NCT02510261	Alnylam Pharmac.

As reviewed by *Ozcan and collaborators*, until now, 5 out of 7 candidates showed safe clinical profiles and promising efficacy results, therefore the clinical trials for these therapies is still ongoing (*Ozcan et al.*, 2015).

Hopefully, the appropriate characteristics presented by SNALPs will give the boost that was needed for the definitive clinical implementation of siRNA-based therapies.

1.3.4.2. Brain-targeting of SNALPs

Although SNALPs present appropriate features for systemic administration of siRNAs, *per se* they are not able to deliver therapeutic cargo to distant sites of disease, such as the brain. In fact, several studies using SNALPs demonstrated that these nanoparticles naturally accumulate mainly in the liver and spleen (*Akinc et al.*, 2010; *Geisbert et al.*, 2006; *Judge et al.*, 2009; *Kim et al.*, 2007; *Morrissey et al.*, 2005; *Zimmermann et al.*, 2006). Despite this limitation, SNALPs present an opportunity for the targeted delivery of siRNAs to the brain, upon covalent coupling of ligands that promote crossing of the BBB.

As reviewed in section 1.3.2, one of the well-studied ligands with proven efficacy in the delivery of siRNAs to the brain upon intravenous administration is a short peptide derived from rabies virus glycoprotein (RVG) (*Alvarez-Erviti et al.*, 2011; *Cooper et al.*, 2014; *Gao et al.*, 2014; *Kumar et al.*, 2007; *Pulford et al.*, 2010; *Zadran et al.*, 2013). Therefore, in this thesis, we generated brain-targeted SNALPs through the incorporation of the RVG peptide and investigated its potential for the treatment of MJD, a fatal neurodegenerative disorder for which there is no available disease-modifier. The RVG peptide will be discussed in more detail in the next section.

1.3.4.2.1. Rabies virus glycoprotein derived peptide

1.3.4.2.1.1. Rabies Virus

Although it is known that the rabies virus glycoprotein is responsible for the entry, membrane fusion and release of the rabies virus inside cells, the exact mechanism behind this is still unclear (Schnell *et al.*, 2010). The first identified receptor for rabies virus was the nicotinic acetylcholine receptor (Lentz *et al.*, 1982). Then, other receptors – the neuronal cell adhesion molecule (NCAM) (Thoulouze *et al.*, 1998) and the low-affinity nerve growth factor receptor (p75^{NTR}) (Tuffereau *et al.*, 1998) – also showed to bind or facilitate the entry of rabies virus into cells. Figure 1.7 has a schematic representation of the rabies virus virion.

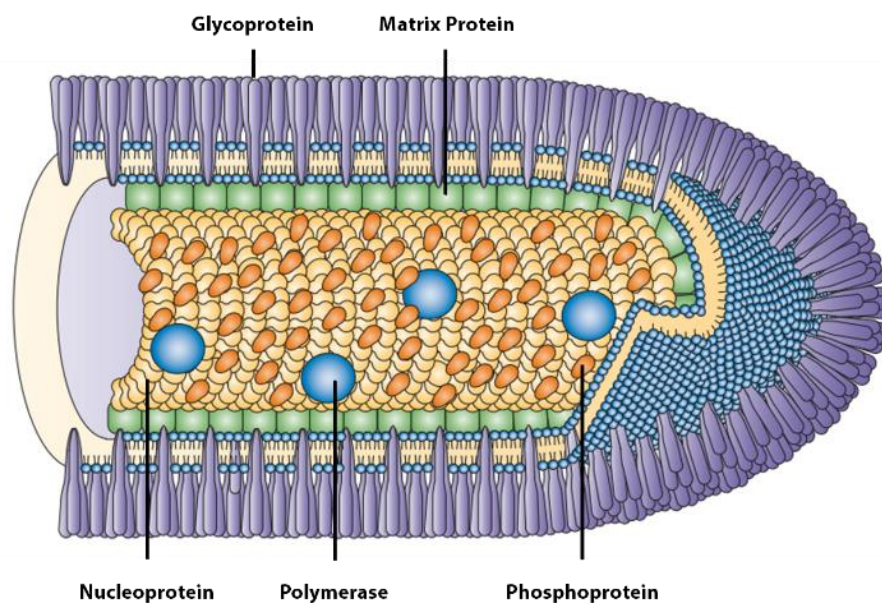


Figure 1.7. The rabies virus virion. The capsid of the rabies virus is composed of two different proteins, matrix protein and glycoprotein that are schematically represented. The matrix protein functions as a bridge between the capsid and the virion. The glycoprotein has a role in virus entry, membrane fusion and virus release. Image adapted from the reference (Schnell *et al.*, 2010), with permission granted from the author.

1.3.4.2.1.2. Studies with RVG peptide

A small peptide derived from rabies virus glycoprotein (RVG29), showed in several reports an enormous potential to deliver gene therapies, proteins and drugs to the brain, following intravenous administration. Please refer to Table 1.5 for references and details related to these studies.

Table 1.5. Studies that show the potential of the RVG peptide to deliver gene-therapies, proteins and drugs to the brain, upon intravenous administration

Cargo	Formulation	Year of publication	Reference
siRNAs	Cell-targeting peptide	2007	(Kumar <i>et al.</i> , 2007)
pDNA	Dendrimer	2009	(Liu <i>et al.</i> , 2009)
siRNAs	Cationic liposomes	2010	(Pulford <i>et al.</i> , 2010)
Protein	Cell-targeting peptide	2010	(Xiang <i>et al.</i> , 2010)
Drug	Albumin nanoparticles	2010	(Chen <i>et al.</i> , 2010)
pDNA	PEI	2011	(Son <i>et al.</i> , 2011)
miRNA	PEI	2011	(Hwang do <i>et al.</i> , 2011)
siRNAs	Exosomes	2011	(Alvarez-Erviti <i>et al.</i> , 2011)
pDNA	Cell-targeting peptide	2012	(Gong <i>et al.</i> , 2012)
siRNAs	Cell-targeting peptide	2012	(Zadran <i>et al.</i> , 2013)
No cargo	PEGylated liposomes	2012	(Tao <i>et al.</i> , 2012)
Protein	Cell-targeting peptide	2012	(Fu <i>et al.</i> , 2012)
shRNA	Poly-L-lysines	2013	(Liu <i>et al.</i> , 2013c)
Protein	Chitosan	2013	(Kim <i>et al.</i> , 2013)
siRNAs	Chitosan	2014	(Gao <i>et al.</i> , 2014)
siRNAs	Exosomes	2014	(Cooper <i>et al.</i> , 2014)
siRNAs	PEI	2015	(Park <i>et al.</i> , 2015)

Even though there is no consensus about the exact mechanism through which RVG29 promotes crossing of the BBB, it is believed that the uptake is related with the $\alpha 7$ subunit of the nicotinic acetylcholine receptors and/or GABA_B receptors (Kumar *et al.*, 2007; Liu *et al.*, 2009), as represented in Figure 1.8. Indeed, evidences show that the $\alpha 7$ -subunit of the acetylcholine receptor, is widely expressed in the brain including in BCECs (Gotti and Clementi, 2004), supporting the idea that RVG29 conserves the ability of the rabies virus glycoprotein to bind to the nicotinic acetylcholine receptors. Nevertheless, another study reported that different agonists or antagonists of nicotinic acetylcholine receptors could not block the uptake of RVG29-targeted nanoparticles (Liu *et al.*, 2009). Despite the possibility of these agonists or antagonists to bind different sites from RVG29, they also

observed that GABA, an inhibitory neurotransmitter that binds to GABA_B receptors, affected the cellular internalization of the RVG29-targeted nanoparticles. Importantly also, GABA_B receptors are widely expressed in the brain and in BCECs (Benke *et al.*, 1999; Fritschy *et al.*, 2004). Altogether, these studies suggest that RVG29 might promote crossing of the BBB through a receptor-mediated transcytosis mechanism.

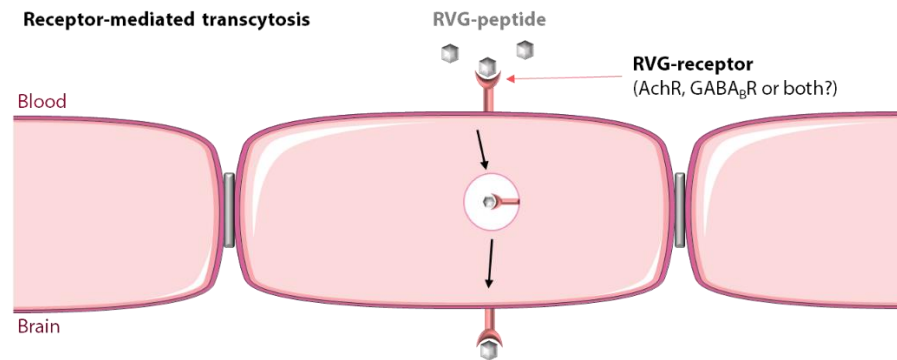


Figure 1.8. Mechanism through which the RVG peptide might promote crossing of the BBB. The uptake of the RVG peptide across the BBB is thought to be linked to the $\alpha 7$ subunit of the nicotinic acetylcholine receptors and/or GABA_B receptors, through receptor-mediated transcytosis.

1.4. Objectives

The main goal of this dissertation was the development and application of a non-viral and non-invasive strategy for the treatment of Machado-Joseph disease, using silencing sequences and brain-targeted stable nucleic acid lipid particles (SNALPs).

To achieve our goal, the specific objectives of this thesis were the following:

- ✓ To develop and characterize brain-targeted SNALPs, through the incorporation of a short peptide derived from rabies virus glycoprotein (RVG) (chapter 2),
- ✓ To evaluate the efficiency of the developed formulation as a therapeutic tool *in vitro* and *in vivo* (chapter 2),
- ✓ To investigate the therapeutic potential of brain-targeted SNALPs to prevent the striatal neuropathology induced by mutant ataxin-3 expression, in a lentiviral-based mouse model of MJD (chapter 3),
- ✓ To study if brain-targeted SNALPs attenuate behavioural deficits and neuropathology in a cerebellar transgenic mouse model of MJD (chapter 4),
- ✓ To assess the safety of intravenous administration of brain-targeted SNALPs (chapter 4).

CHAPTER 2

A targeted lipid-based strategy to deliver silencing sequences to the brain by intravenous administration

2.1. Abstract

Machado-Joseph disease (MJD) is the most common dominantly-inherited ataxia worldwide, but there is no therapy able to modify disease progression. In this context, small interfering RNAs (siRNAs) represent an extremely promising approach, although its successful clinical application has been limited due to their intrinsic limitations and also because of the presence of the blood-brain barrier (BBB). Therefore, the aim of this study was to develop an efficient delivery system that would circumvent these barriers, enabling the accumulation of the nanoparticles in the mouse brain upon intravenous administration. For this purpose, we successfully generated brain-targeted stable nucleic acid lipid particles (SNALPs) through the incorporation of a short peptide derived from rabies virus glycoprotein (RVG-9r). The developed formulation exhibited important features that make it adequate for systemic administration: high encapsulation efficiency for siRNAs, ability to protect the encapsulated siRNAs, appropriate and homogeneous particle size distribution. Flow cytometry and confocal microscopy studies revealed specific *in vitro* delivery of siRNAs to neuronal cells. Moreover, brain-targeted SNALPs efficiently knocked down mutant ataxin-3 mRNA, resulting in protein level reduction, in a neuronal cell line. Importantly, *in vivo* experiments demonstrated that the RVG-9r-peptide increased the accumulation of the nanoparticles in the mouse brain, upon intravenous administration. In conclusion, we have generated a promising brain-targeted delivery system that may be used for MJD therapy and potentially for the treatment of other neurodegenerative diseases.

2.2. Introduction

The currently available therapies for the most devastating neurodegenerative diseases attenuate the symptoms, but do not block neurodegeneration. For this group of diseases, but particularly for those in which neurodegeneration is linked to the synthesis of mutant proteins coded by dominant mutant alleles, therapies based on RNA interference (RNAi) hold great promise. Machado-Joseph disease (MJD) or spinocerebellar ataxia type 3 (SCA3) is caused by the over-repetition of a CAG tract in the coding region of the ATXN3/MJD1 gene, which confers a toxic gain-of-function to the ataxin-3 protein (Kawaguchi *et al.*, 1994) and, therefore, is one of the disorders that could benefit from the development of a silencing strategy.

As the presence of the blood-brain barrier (BBB) limits the entry of systemically administered therapeutics into the central nervous system (CNS), most experiments of RNAi on neurological disorders until now focused on local administration of the silencing sequences using either viral (Alves *et al.*, 2008a; Harper *et al.*, 2005; Sapru *et al.*, 2006; Singer *et al.*, 2005; Xia *et al.*, 2004) or non-viral strategies (DiFiglia *et al.*, 2007; Kordasiewicz *et al.*, 2012; Lima *et al.*, 2012; Yu *et al.*, 2012). However, this is an extremely invasive procedure and results in circumscribed expression, which may be insufficient to treat all the disease-relevant brain regions. Intravenous administration is safer and less invasive and would be the ideal way to deliver the silencing sequences throughout the brain.

Although promising, small interfering RNA (siRNA) molecules have intrinsic limitations: negative charge and hydrophilic nature, which strongly impair their cellular internalization, and low biological stability being prone to enzymatic degradation in body fluids (O'Mahony *et al.*, 2013). Therefore, there is a huge need to develop effective systems that could enhance the delivery of siRNA-based therapeutics into the brain, after non-invasive administration.

One of the most promising ways to afford siRNA delivery across the BBB is to package the silencing sequences in lipid nanoparticles and conjugate them to brain-targeting ligands. Stable nucleic acid lipid particles (SNALPs) provide a flexible platform to encapsulate and

protect siRNAs from degradation (Costa *et al.*, 2013; Mendonca *et al.*, 2010a) as well as covalent conjugation of brain-targeting ligands, being one of the most promising non-viral approaches for *in vivo* application (Costa *et al.*, 2013; Di Martino *et al.*, 2014; Geisbert *et al.*, 2006; Geisbert *et al.*, 2010; Judge *et al.*, 2009; Morrissey *et al.*, 2005; Zimmermann *et al.*, 2006). These nanoparticles are PEGylated presenting improved pharmacokinetic profiles, increased circulatory half-life and decreased uptake by reticuloendothelial system (RES) (Allen *et al.*, 1991). Furthermore, besides nucleic acids, they provide a good platform to carry multiple components simultaneously such as imaging agents (Kraft and Ho, 2014) or drugs (Mendonca *et al.*, 2010b; Zhang *et al.*, 2013).

One of the well-studied ligands with proven efficacy in the delivery of siRNAs across the BBB is a short peptide derived from the rabies virus glycoprotein (RVG) (Alvarez-Erviti *et al.*, 2011; Cooper *et al.*, 2014; Gao *et al.*, 2014; Kumar *et al.*, 2007; Park *et al.*, 2015; Pulford *et al.*, 2010; Zadran *et al.*, 2013), although the exact mechanism behind crossing the BBB remains unclear.

In this study, we synthesized RVG-9r-targeted SNALPs targeting mutant ataxin-3, the MJD causing protein (Kawaguchi *et al.*, 1994), and investigated their potential to be used for MJD therapy *in vitro* and *in vivo*. Here, we provide *in vitro* evidence that RVG-9r-targeted SNALPs are able to deliver siRNAs to neuronal cells and further release the encapsulated silencing sequences in the cytoplasm, suppressing mutant ataxin-3. Importantly, the RVG peptide promoted the accumulation of the nanoparticles in the brain, upon intravenous administration. Our results suggest that our approach may provide a new therapeutic option for MJD as well as other monogenetic neurodegenerative diseases.

2.3. Materials and Methods

2.3.1. Materials

siRNAs used in these studies included those targeting EGFP (siEGFP), firefly luciferase (siLuc) and mutant ataxin-3 (siMutAtax3) and were synthesized by Dharmacon. 5-carboxyfluorescein (FAM)-labeled siRNA was acquired from Genecust and labeling was performed at the 5' sense strand. Sequences are included in Table 2.1.

Table 2.1. siRNAs sequences

siRNA	Sequence	
	sense	antisense
siMutAtax3	5'AGCAGCAGCGGGACCUAUCdTdT3'	5'GAUAGGUCCCGCUGCUGCUdTdT3'
siEGFP	5'UGAACUUCAGGGUCAGCUdTdT3'	5'AAGCUGACCCUGAAGUUCAdTdT3'
siLuc	5'UCGAAGUACUCAGCGUAAGdTdT3'	5'CUUACGCUGAGUACUUCGAdTdT3'
FAM-labeled siRNA	FAM- 5'AGCAGCAGCGGGACCUAUCdTdT3'	5'GAUAGGUCCCGCUGCUGCUdTdT3'

Peptides RVG-9r (YTIWMPENPRPGTPCDIFTNSRGKRASNGGGGRRRRRRRRR) and RV-MAT-9r (MNLKRKIVKNRRDEDTQKSSPASAPLDGGGGRRRRRRRRR) were synthesized and purified by high performance liquid chromatography (HPLC) to obtain a purity greater than 95%, by ChinaPeptides.

The lipids 1,2-dioleoyl-3-dimethylammonium-propane (DODAP), 1,2-distearoyl-snglycero-3-phosphocholine (DSPC), cholesterol (Chol), N-palmitoyl-sphingosine-1-[succinyl(methoxypolyethylene glycol) 2000] (C16 PEG2000 Ceramide), 1,2-distearoyl-sn-glycero-3-phosphatidylethanolamine-N-[maleimide (polyethylene glycol)-2000] ammonium salt (DSPE-PEG-MAL) and I- α -phosphoethanolamine-N-(lissamine rhodamine B sulfonyl) ammonium salt (Rho-PE) were obtained from Avanti Polar Lipids. Cardiogreen or indocyanine green (ICG), a near infrared dye used in these studies, was obtained from Sigma-Aldrich.

All other reagents were obtained from Sigma-Aldrich unless stated otherwise.

2.3.2. Cell lines and culturing conditions

Neuro2a, HT-22 and HeLa cells were obtained from the American Type Culture Collection (Manassas, VA). Neuro2a and HeLa cells were maintained in Dulbecco's modified Eagle's medium (Sigma-Aldrich) and HT-22 cells were grown on DMEM/F-12 GlutaMAX™ medium (Gibco). In both cases, medium was supplemented with 10% heat-inactivated FBS (Gibco) and 1% Penicillin-Streptomycin (Gibco) and cultured at 37 °C under a humidified atmosphere containing 5% CO₂.

2.3.3. Mice

C57BL/6 ataxin-3 [Q69]-transgenic (Torashima *et al.*, 2008) or wild-type mice were used. The animals were housed in a temperature-controlled room maintained on a 12 h light/12 h dark cycle. Food and water were provided *ad libitum*. The experiments involving mice were previously approved by the Responsible Organization for the Animals Welfare of the Faculty of Medicine and Center for Neuroscience and Cell Biology of the University of Coimbra, Portugal, and were carried out in accordance with the European Community directive (86/609/EEC) for the care and use of laboratory animals. The researchers received adequate training (Felasa-certified course) and certification to perform the experiments from the Portuguese authorities (Direcção Geral de Veterinária, Lisbon, Portugal).

2.3.4. Synthesis and characterization of stable nucleic acid lipid particles

2.3.4.1. Preparation of ligand-coupled micelles

Targeted liposomes were prepared by the post-insertion technique previously described (Moreira *et al.*, 2002). Briefly for RV-MAT-9r-coupled liposomes, the peptide was modified with the addition of thiol groups through a one hour-reaction with freshly prepared 2-iminothiolane hydrochloride (2-IT). The reaction was performed at a 1:10 peptide: 2-IT molar ratio in HEPES buffer (20 mM HEPES, 145 mM NaCl, pH 8). For RVG-9r, the pre-existing cysteine residue in the peptide composition enabled direct conjugation of the peptide to the micelles. DSPE-PEG-MAL micelles were prepared in MES buffer (20 mM

MES, 20 mM HEPES, pH 6.5) immediately before peptide conjugation, and then thiolated peptides were coupled to the micelles by a thioester linkage (1:1 peptide: DSPE-PEG-MAL molar ratio). The coupling reaction was performed overnight, in the dark, at room temperature and with gentle stirring. For non-targeted liposomes, HEPES buffer was directly added to the DSPE-PEG-MAL micelles.

2.3.4.2. Encapsulation of siRNAs or NIR dye into liposomes and subsequent postinsertion of ligand-coupled micelles

The preparation of liposomes encapsulating siRNAs was performed as previously described (Costa *et al.*, 2013; Mendonca *et al.*, 2010a). Briefly, a lipid mixture in absolute ethanol containing DODAP:DSPC:CHOL:C16-PEG2000-Ceramide (25:22:45:8 molar ratio percentages relative to total lipid) and siRNAs in 20 mM citrate buffer, pH 4 (final charge ratio of cationic lipid:siRNAs of 2:1) were heated at 60°C. The lipid mixture was then slowly added under strong vortex to the siRNA solution. For some experiments, liposomes were labeled with rhodamine including 1 mol% of Rho-PE in the lipids mixture. To prepare liposomes encapsulating indocyanine green (ICG) we added the dye, previously dissolved on absolute ethanol, to the lipid film (ICG:total lipid molar ratio 1:50).

The resulting liposomes were extruded 21 times through 100 nm diameter polycarbonate membranes using a LiposoFast basic extruder (Avestin, Ottawa, ON). Removal of ethanol and non-encapsulated siRNA or dye was carried out upon running extruded liposomes through a Sepharose CL-4B column equilibrated with HEPES buffer.

To determine total lipid concentration, cholesterol was quantified using the Liebermann-Burchard test (Xiong *et al.*, 2007). Briefly, 200 µL of Liebermann-Burchard reagent were added to 5 µL of cholesterol standards or liposome samples followed by incubation at 37°C for 20 minutes. Absorbance was measured at 625 nm in a SpectraMax Plus 384 spectrophotometer (Molecular Devices) and the concentration assessed against a cholesterol standard curve.

Next, 2 mol% of targeted- (peptide conjugated) or non-targeted (plain) micelles relative to the total lipid concentration were added to the liposomes and the conjugation was performed incubating approximately 15 hours in a water bath at 39°C.

Finally, to remove non-conjugated micelles and chemical reagents used during liposomal preparation, targeted and non-targeted liposomes were purified by size exclusion chromatography on a Sepharose CL-4B column equilibrated with HEPES buffer.

2.3.4.3. Liposomes characterization

The final total lipid concentration was inferred from the cholesterol quantification, as described above.

The siRNA that was encapsulated into the liposomes was determined using SYBR Safe (Life Technologies, Carlsbad, CA) in the presence of the detergent octaethylene glycol monododecyl ether ($C_{12}E_8$), and using a siRNA standard curve. The fluorescence ($\lambda_{ex}502$ nm, $\lambda_{em}530$ nm) was measured using a SpectraMax Gemini EM fluorimeter (Molecular Devices). To assess if the siRNA was fully encapsulated and protected by the lipid nanoparticle, the ability of the SYBR Safe to intercalate with siRNA in the absence of $C_{12}E_8$ detergent was evaluated.

To quantify encapsulation efficiency for FAM-labeled siRNA the $C_{12}E_8$ detergent and a standard curve with FAM-labeled siRNA were used. The fluorescence ($\lambda_{ex}494$ nm, $\lambda_{em}520$ nm) was also measured using the SpectraMax Gemini EM fluorimeter.

ICG quantification was performed measuring the fluorescence ($\lambda_{ex}780$ nm, $\lambda_{em}820$ nm) with a fluorimeter, and using an ICG standard curve.

To determine the amount of DSPE-PEG-MAL-peptide conjugate associated with liposomes, peptides were quantified using the BCA protein assay kit (Thermo Scientific) using a peptide standard curve. After incubation during 40 minutes at 37°C, absorbance was measured at 562 nm in a spectrophotometer.

The mean diameter of the resulting liposomes was determined by photon correlation spectroscopy using an N5 submicrometer particle size analyzer (Beckman Coulter).

2.3.5. Assessment of cellular uptake by flow cytometry

Neuro2a, HT-22 and HeLa cells were seeded in 12-well plates at densities of 1×10^5 cells per well. Twenty-four hours later cells were incubated with rhodamine-labeled liposomes (non-targeted-, RV-MAT-9r-targeted, RVG-9r THIO-targeted or RVG-9r-targeted-) with different concentrations of total lipid (0.06, 0.16 and 0.32 mM) in media with 10% FBS at

37°C for 4 hours. Cells were then washed with PBS, collected with trypsin and fixed with BD Cytofix/Cytoperm solution (BD Biosciences) for 20 minutes at 4°C. Cells were then washed with PBS and analyzed by flow cytometry with a FACScalibur (BD Biosciences). Rhodamine signal was evaluated in the FL-2 channel and a total of 10,000 events per sample were collected. Data were analyzed using Cell Quest Pro software (BD Biosciences).

2.3.6. Assessment of cellular internalization by confocal microscopy

Neuro2a cells were seeded on glass coverslips in 12-well plates at densities of 1×10^5 cells per well. Twenty-four hours later, cells were incubated with targeted- or non-targeted- liposomes encapsulating 0.5 μM FAM-labeled siRNA during 4 hours at 37 or 4°C. Where indicated, receptors were saturated by incubation of the cells for 30 minutes with 50 μM of free RVG-9r-peptide prior to the addition of the liposomes.

Cells were then washed with PBS, fixed for 20 minutes at room temperature with 4% paraformaldehyde, washed again with PBS, nucleus was stained with the DNA-binding dye DAPI for 5 minutes, washed with PBS and finally mounted onto a slide with mowiol mounting medium. Fluorescent images were obtained in a laser scanning confocal microscope Zeiss LSM 510 Meta (Carl Zeiss Microscopy) using a diode (405 nm for DAPI) and an argon (488 nm for FAM) excitation lasers, and a 63x oil immersion objective. All fluorescence parameters were maintained constant to enable sample comparison.

2.3.7. Production of lentiviral vectors encoding for the human mutant ataxin-3

Lentiviral vectors encoding for the human mutant ataxin-3 (ATX-3 72Q) (Alves *et al.*, 2008b) were produced in HEK293T cells with a four-plasmid system, as previously described (de Almeida *et al.*, 2001). The lentiviral particles were resuspended in 0.5% bovine serum albumin in phosphate-buffered saline (PBS) and the viral particle content determined using an ELISA to detect HIV-1 p24 antigen levels (RETROtek, Gentaur), according to the manufacturer's instructions.

2.3.8. Evaluation of mutant ataxin-3 mRNA and protein levels by quantitative real-time PCR (qRT-PCR) and Western Blot (WB), respectively

To obtain a neuronal cell line stably-expressing mutant ataxin-3, Neuro2a cells were transduced with lentiviral vectors encoding for human mutant ataxin-3. Briefly, 2×10^5 Neuro2a cells were incubated with 200 ng of p24 antigen in the presence of polybrene and, to achieve stable expression of the vectors, cells were allowed to grow for two weeks before performing the experiments.

For silencing experiments, 5×10^4 of infected cells were seeded in 24-well plate. Twenty-four hours later, cells were incubated during 4 hours at 37°C with different concentrations (0.1, 0.2 and 0.5 μ M) of control siRNA (siLuc) or siRNA against mutant ataxin-3 (siMutAtax3) encapsulated in RVG-9r- or RV-MAT-9r-targeted liposomes. Media was then replaced and a second transfection was performed 44 hours later with the same formulation and concentrations of siRNA used for the first transfection.

To detect mutant ataxin-3 mRNA levels, total RNA was extracted from cultured cells 24 hours after the second transfection using Nucleospin RNA kit (Macherey-Nagel). After RNA quantification, 1 μ g of total RNA was converted into cDNA using iScript cDNA synthesis kit (Bio-Rad, Hercules, CA), in a Veriti 96-well thermocycler (Applied Biosystems). RNA extraction and cDNA synthesis for mRNA quantification were performed following the manufacturer's instructions. qRT-PCR was performed using SsoAdvanced™ Universal SYBR® Green Supermix (Bio-Rad), in a Step One Plus Real-Time PCR System from Applied Biosystems. Primers used to detect human ataxin-3 (QT00094927) and mouse HPRT (QT00166768) were obtained from Qiagen. Briefly, the cDNA obtained was diluted 10-fold with RNase-free water and quantitative PCR was performed using 1 μ L per sample as follows: one single cycle at 95°C for 30 s, followed by 45 cycles of two steps (5 s at 95°C, 15 s at 55°C). The melt curve stage started immediately after, and consisted of 5 s heating at 65°C with a 0.5°C temperature increase in each step until 95°C. The StepOne Software generated automatically threshold cycle (Ct) values and mutant ataxin-3 levels were normalized using HPRT housekeeping gene and calculated compared to non-treated cells. To analyze mutant ataxin-3 protein levels, cells were collected 48 hours after the second transfection and protein detection was performed by Western Blot. Cells were collected using RIPA lysis buffer (50 mM Tris-HCl pH 8, 150 mM NaCl, 1% NP-40, 0.5% sodium deoxycholate, 0.1% sodium dodecyl sulphate) mixed with a protease inhibitor cocktail

(Roche). The lysate was further sonicated and centrifuged at 12,000 rpm for 20 minutes at 4°C. Supernatant was collected and protein concentration estimated through the Bradford method (Bio-Rad). Twenty micrograms of total denatured protein were then loaded in a 4% stacking, 12% resolving polyacrylamide gel for electrophoretic separation. Proteins were then transferred to polyvinylidene difluoride (PVDF) membranes (Merck Millipore) and blocked in 5% nonfat milk. Immunoblotting was performed using the mouse monoclonal anti-ataxin-3 antibody (1H9; 1:5,000; Chemicon) and mouse monoclonal anti- β -tubulin 1 (clone SAP.4G5; 1:10,000; Sigma-Aldrich). Proteins were detected by chemifluorescence using a goat anti-mouse alkaline phosphatase-conjugated secondary antibody (1:5,000; Thermo Scientific) and revealing with the enzyme substrate ECF (Amersham Biosciences). Protein labeling was then imaged using a VersaDoc Imaging System (Model 3000 from Bio-Rad). Semi-quantitative analysis was carried out using Quantity-one 1-D image analysis software version 4.5. Beta-tubulin was used as reference protein to normalize the amount of loaded protein.

2.3.9. Analysis of the biodistribution properties of targeted-liposomes using an *in vivo* imaging technology platform

To perform these experiments mice were tail-vein injected with RV-MAT-9r or RVG-9r-targeted liposomes encapsulating ICG. The amount of ICG was adjusted according to the mouse weight, being administered 10 nmol of ICG liposomes per 15 g of animal. 3 hours after injection, images were acquired using an IVIS Lumina XR equipment (Perkin Elmer).

2.3.9.1. *in vivo* NIR fluorescence images of the brain after intravenous administration of targeted-liposomes

7-week-old C57BL/6 mice were intravenously injected and *in vivo* imaging was performed in anesthetized mice that were shaved around the brain region using a Wella Contura Trimmer (Harvard Apparatus). The imaging parameters were as follows: λ_{ex} 745 nm, λ_{em} 810-875 nm, fluorescence exposure time of 2 seconds, medium binning, f/stop=2 and a field of view of 12.5 cm.

2.3.9.2. *ex vivo* NIR fluorescence images of brain and major organs after intravenous administration of targeted-liposomes

6-to-7-week-old C57BL/6 ataxin-3 [Q69]-transgenic or wild-type mice were used to assess the body distribution of the nanoparticles in the brain and major organs. Mice were sacrificed by intracardiac perfusion with 20 mL of ice-cold PBS and NIR fluorescence images were obtained. The imaging parameters for the brain and major organs of the animals were as follows: λ_{ex} 745 nm, λ_{em} 810-875 nm, fluorescence exposure time varied from 2 to 5 seconds (for brain) and from 0.5 to 2 seconds (for major organs), medium binning, f/stop=2 and a field of view of 7.5 to 12.5 cm.

For all the NIR fluorescent measurements, radiant efficiency units were selected because these units are normalized to the incident light. For each experiment, three animals were imaged at the same time: a non-injected animal, an animal injected with RV-MAT-9r-targeted liposomes encapsulating ICG and a third animal injected with RVG-9r-targeted liposomes encapsulating ICG. The results show the fold change in ICG radiant efficiency units in mice injected with RVG-9r-targeted liposomes encapsulating ICG, when compared to the control formulation (RV-MAT-9r).

2.3.10. Statistical analysis

Data are presented as mean \pm standard error of mean (SEM) of at least three independent experiments. Student's *t*-test, one- or two-way ANOVA combined with Bonferroni's post-test were used to determine statistically significant differences of the means. Statistical differences are presented at probability levels of * $p < 0.05$, ** $p < 0.01$ and *** $p < 0.001$ and considered non-significant (n.s.) when $P < 0.05$. Calculations were performed using GraphPad Prism version 5.00 for Windows (San Diego).

2.3. Results

2.3.1. Generation of brain-targeted SNALPs

To generate lipid nanoparticles with the capacity, upon intravenous administration, to deliver siRNAs through the BBB into neuronal cells, we covalently attached a rabies-derived RVG-9r-peptide to the surface of a liposomal formulation composed of DODAP/DSPC/CHOL/C16 PEG2000 ceramide. This ligand was used to confer brain-targeting capability (-RVG counterpart) and to improve cellular uptake and cytosolic release (-9r, nine-arginines counterpart) of the nanoparticles (Biswas *et al.*, 2013; El-Sayed *et al.*, 2008; Wender *et al.*, 2000; Zeller *et al.*, 2015). As a control, we used a peptide with similar length derived from rabies viral matrix protein (RV-MAT) that does not have the ability to cross the BBB, and maintained the nine-arginines (RV-MAT-9r) to enable results comparison (Kumar *et al.*, 2007). Note that the arginines *per se* already increase the uptake of the liposomes.

The schematic representation for the preparation of RVG-9r-targeted SNALPs is shown in Fig. 2.1.

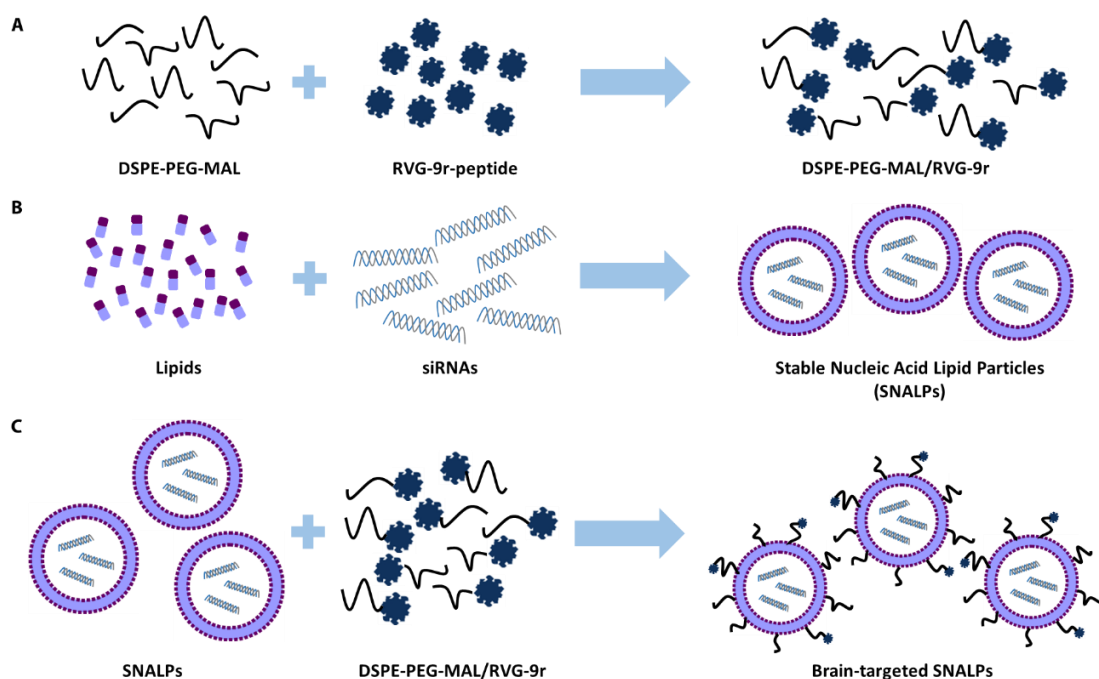


Figure 2.1. Synthesis of brain-targeted stable nucleic acid lipid particles. (A) RVG-9r peptide was directly conjugated to DSPE-PEG-MAL overnight, with gentle stirring. **(B)** To encapsulate siRNAs in

liposomes, a lipid mixture in absolute ethanol was added to the siRNAs solution in citrate buffer, pH 4. **(C)** Conjugation of the liposomes encapsulating siRNAs to RVG-9r-micelles was performed overnight.

2.3.2. Characterization of brain-targeted SNALPs

As previously reported (Costa *et al.*, 2013; Mendonca *et al.*, 2010a), we verified that the encapsulation efficiency for siRNAs was very high ($94.2\% \pm 4.69$) independently from the post-inserted peptide. Moreover, our formulation was able to fully protect siRNAs from degradation, since in the absence of the detergent $C_{12}E_8$ the intercalation of the probe SYBR Safe with the encapsulated siRNAs did not occur (data not shown).

Even though the RVG-9r-peptide already has a cysteine residue in its composition, that enables direct conjugation of the peptide to the micelles, we tested postinsertion efficiency and cellular uptake for RVG-9r-targeted liposomes for both cases: after peptide modification with the addition of thiol groups (RVG-9r THIO) or without any further modification (RVG-9r).

We verified that, when compared to RVG-9r modified with the addition of thiol groups, direct conjugation of RVG-9r to DSPE-PEG-MAL micelles gave rise to a significantly higher postinsertion efficiency ($26.5 \pm 4.14\%$ versus $79.3 \pm 1.16\%$, respectively; Fig. 2.2A). Furthermore, we also evaluated the extent of cellular uptake of non-targeted, RVG-9r THIO-targeted or RVG-9r-targeted liposomes by a neuronal (Neuro2a) and a non-neuronal cell line (HeLa cells). To perform this experiment, we used rhodamine-labeled liposomes and incubated cells with growing concentrations of total lipid (0.06, 0.16 and 0.32 mM) and evaluated the extent of cellular uptake by flow cytometry. The uptake of RVG-9r-targeted liposomes by Neuro2a cells was significantly higher, when compared to RVG-9r THIO-targeted liposomes (Fig. 2.2B).

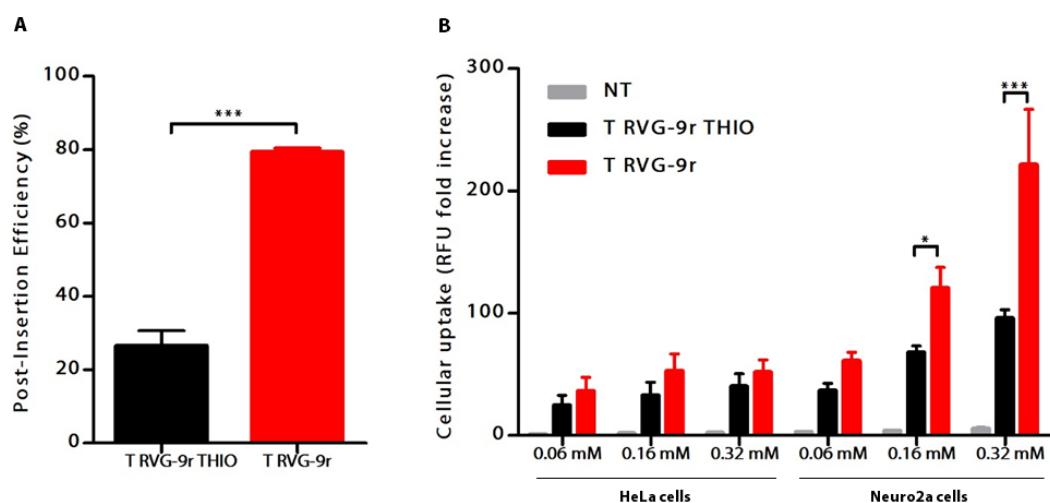


Figure 2.2. Comparison between thiolated and non-thiolated RVG-9r-targeted liposomes. (A) Postinsertion efficiency for liposomes conjugated with thiolated (THIO) or non-thiolated RVG-9r-peptide. Values are presented as mean \pm SEM of n=6. Unpaired t-test with Welch's correction was used for comparison (**p<0.01). **(B)** HeLa and Neuro2a cells were transfected with growing concentrations of total lipid of non-targeted, RVG-9r THIO-targeted or RVG-9r-targeted liposomes at 37°C during 4 hours. After incubation, rhodamine signal was assessed by flow cytometry and the fold increase in relative fluorescence units (RFU) to non-treated cells is indicated. Values are presented as mean \pm SEM of n=4/5. Two-way ANOVA analysis of variance combined with Bonferroni post-test was used for comparison of RVG-9r THIO- and RVG-9r-targeted liposomes (*p<0.05 and ***p<0.001).

For RV-MAT-9r-coupled liposomes, the post-insertion efficiency was also high (60.78 \pm 15.43%). In this regard, when liposomes were incubated with 2 mol% of peptide-micelles, we obtained 12.2 \pm 1.88 nmol RV-MAT-9r/ μ mol total lipid and 15.8 \pm 0.18 nmol RVG-9r/ μ mol total lipid.

As shown in table 2.2, as measured through photon correlation spectroscopy, the obtained size for RV-MAT-9r and RVG-9r-targeted liposomes encapsulating siRNAs was under 200 nm which makes them suitable for intravenous administration (190 \pm 22.89 and 195.8 \pm 4.47 nm, respectively). The polydispersity index was also low (0.299 \pm 0.064 and 0.162 \pm 0.015, respectively), which indicates that liposomes exhibit a narrow particle size distribution.

Table 2.2. Size and polydispersity index of non-targeted or targeted-SNALPs

SNALPS	Size (nm)	Polydispersity index
Non-targeted	122.8±2.15	0.197±0.016
RV-MAT-9r-targeted	190±22.89	0.299±0.064
RVG-9r-targeted	195.8±4.47	0.162±0.015

*Values represent the mean ± SEM of at least four independent formulations.

2.3.3. RVG-9r promotes robust association of liposomes to neuronal cells

To study neuronal cell targeting specificity of RVG-9r-targeted liposomes *in vitro* we incubated cells with growing concentrations of total lipid of non-targeted, RV-MAT-9r-targeted or RVG-9r-neuronal-targeted liposomes. The evaluation of the extent of cellular uptake of these liposomes labeled with rhodamine by two neuronal cell lines – HT-22 and Neuro2a cells – and a non-neuronal cell line – HeLa cells – was performed. As assessed by flow cytometry, extensive uptake was observed four hours after incubation of Neuro2a and HT-22 cells with RVG-9r-targeted liposomes, when compared to non-targeted or RV-MAT-9r-targeted liposomes (Fig. 2.3). Upon incubation with 0.32 mM of total lipid (RVG-9r-targeted liposomes), a 116-fold or a 65-fold increase in the rhodamine signal for Neuro2a and HT-22, respectively, was observed. Nevertheless, in a non-neuronal cell line (HeLa cells), there was no significant difference in the cellular uptake between RVG-9r- and RV-MAT-9r-targeted liposomes. Beyond that, we also found that cellular uptake for the different liposomes was dose-dependent for all the tested cell lines.

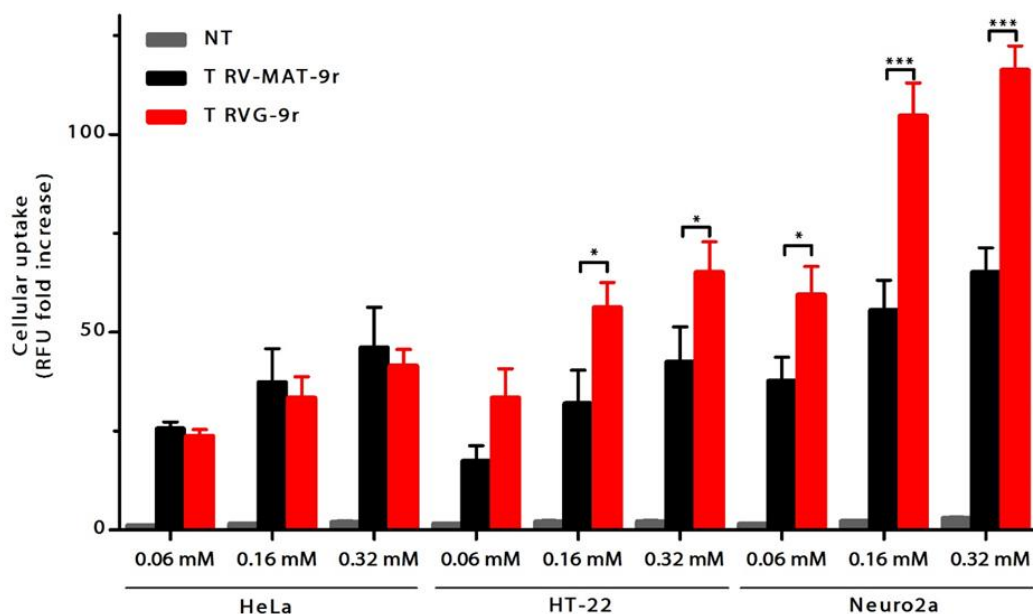


Figure 2.3. Cellular uptake of RVG-9r-targeted liposomes by neuronal and non-neuronal cell lines. Neuronal (Neuro2a, HT-22) and non-neuronal (HeLa) cells were transfected with growing concentrations of total lipid of non-targeted, RV-MAT-9r-targeted or RVG-9r-targeted rhodamine-labeled liposomes at 37°C during 4 hours. After incubation, rhodamine signal was assessed by flow cytometry and the fold increase in relative fluorescence units (RFU) to non-treated cells is indicated. Values are presented as mean±SEM of at least 3 independent experiments. Two-way ANOVA analysis of variance with Bonferroni's post-test was used for comparison of RV-MAT-9r- and RVG-9r-targeted liposomes (**p<0.001 and *p<0.05).

To evaluate the delivery of siRNAs to the cytoplasm of a neuronal cell line, we encapsulated FAM-labeled siRNAs in targeted- (RV-MAT-9r or RVG-9r) or non-targeted liposomes and assessed cellular internalization by confocal microscopy. Four hours after incubation, we observed that RVG-9r-targeted liposomes efficiently delivered siRNA into the cytoplasm of Neuro2a cells, as can be visualized by the intense green fluorescence from FAM-labeled siRNA (Fig. 2.4A, c), while much lower levels of fluorescence were observed when cells were incubated with non-targeted or RV-MAT-9r-coupled liposomes (Fig. 2.4A, a, b, respectively).

To demonstrate that RVG-9r was responsible for the cellular uptake of RVG-9r-targeted liposomes through receptors present at the cell surface, we performed transfection at 4°C (where energy-dependent mechanisms like endocytosis are inhibited) and at 37°C after saturation of the receptors (RS – with excess of RVG-9r peptide). Decreased levels of internalization were observed for both cases (Fig. 2.4A, d, e, respectively; and 2.4B).

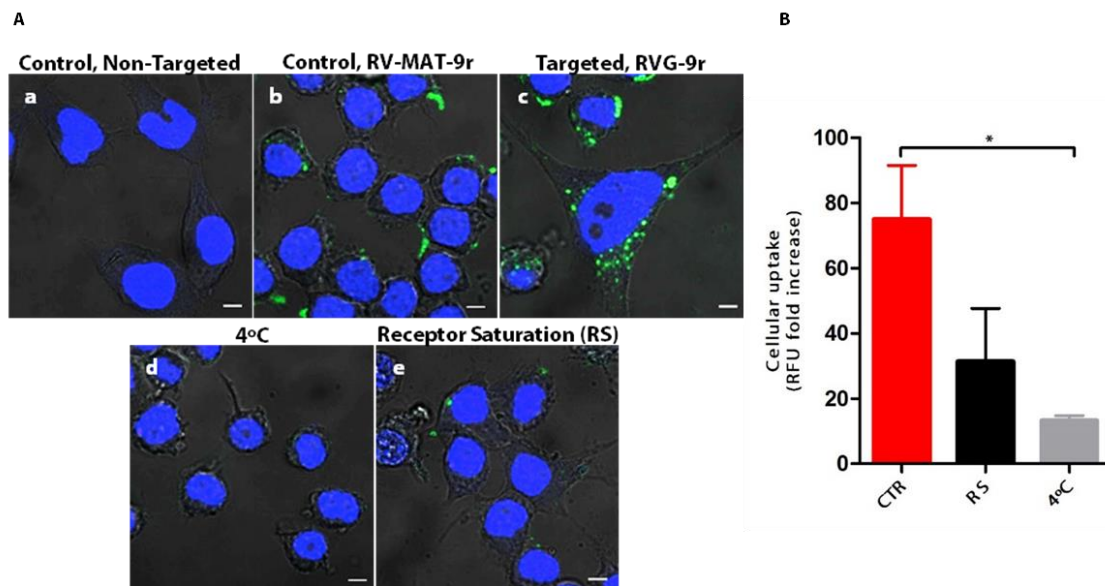


Figure 2.4. RVG-9r-targeted liposomes efficiently deliver siRNAs to neuronal cells, possibly through receptor-mediated endocytosis. (A) Neuro2a cells were incubated at 37°C with 0.5 μ M of FAM-labeled siRNA encapsulated in (a) non-targeted liposomes, (b) RV-MAT-9r-targeted liposomes or (c) RVG-9r-targeted liposomes. Neuro2a cells were also incubated with the same amount of FAM-labeled siRNA encapsulated in RVG-9r-targeted liposomes at 4°C (d) or after receptor saturation (RS) in the presence of an excess of free RVG-9r at 37°C (e). Four hours post-transfection, the nucleus of fixed cells was stained with DAPI and cells were visualized in a confocal microscope with a 63x plan-apochromat oil immersion objective. Images are representative of two independent experiments. Scale bars represent 10 μ m. (B) Neuro2a cells were transfected with 0.16 mM of total lipid of RVG-9r-targeted liposomes at 37°C (CTR), in the presence of an excess of free RVG-9r at 37°C (RS) or at 4°C. Values are presented as mean \pm SEM of at least 3 independent experiments. One-way ANOVA analysis of variance with Bonferroni's post-test was used for multi-comparison (* p <0.05).

Together, these results indicate that targeting liposomes with the RVG-9r-peptide robustly increases association and delivery of siRNAs to neuronal cells, possibly through a receptor-mediated endocytosis mechanism.

2.3.4. RVG-9r-targeted liposomes encapsulating siRNAs targeting mutant ataxin-3 efficiently reduce mutant ataxin-3 levels

Since we had shown that RVG-9r-targeted liposomes efficiently deliver siRNA to neuronal cells, we next evaluated the functionality of the developed formulation by testing whether we could reduce mutant ataxin-3 levels in Neuro2a cells stably-expressing mutant ataxin-3. To perform these experiments, cells were transfected with growing concentrations of control siRNAs (siCTR) or siRNAs targeting mutant ataxin-3 (siMutAtax3) encapsulated in

RV-MAT-9r- (control peptide) or RVG-9r-targeted liposomes. Transfection with 0.5 μM of siMutAtax3 encapsulated in RVG-9r-targeted liposomes resulted in a significant decrease of mutant ataxin-3 mRNA (approximately $39\pm 5.2\%$, Fig. 2.5A), which was particularly robust regarding protein levels ($68\pm 11.4\%$, Fig. 2.5B), when compared to control formulations (RVG-9r-targeted liposomes encapsulating siCTR or RV-MAT-9r-targeted liposomes encapsulating siMutAtax3). Silencing was sequence-specific because, relatively to non-treated cells, the treatment of cells with liposomes encapsulating siCTR did not significantly alter mutant ataxin-3 mRNA and protein levels. Moreover, as previously demonstrated for cellular uptake, we observed that the downregulation of mutant ataxin-3 with RVG-9r-targeted liposomes was also concentration-dependent.

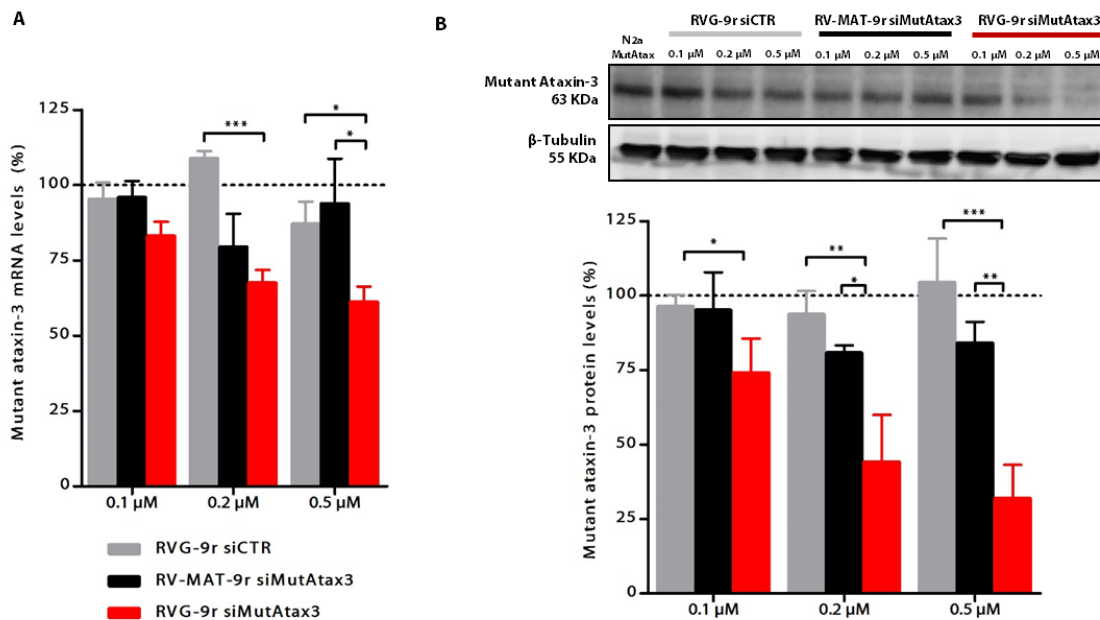


Figure 2.5. *in vitro* suppression of mutant ataxin-3 by RVG-9r-targeted liposomes encapsulating siMutAtax3. Neuro2a cells stably-expressing mutant ataxin-3 were double-transfected with different concentrations of siMutAtax3 or siCTR encapsulated in RVG-9r-targeted liposomes or with RV-MAT-9r-targeted liposomes encapsulating siMutAtax3. **(A)** To analyze mutant ataxin-3 mRNA levels, cells were collected 24 hours after the second transfection and detection was performed by qRT-PCR. Samples were normalized using HPRT housekeeping gene. The results show the levels of mutant ataxin-3 mRNA in treated cells, when compared to non-treated cells. **(B)** Representative membrane showing mutant ataxin-3 and β -tubulin protein levels in treated and non-treated cells. To analyze mutant ataxin-3 protein levels, cells were collected 48 hours after the second transfection and protein detection was performed by Western Blot. Mutant ataxin-3 bands were corrected with β -tubulin (endogenous protein) signal intensity. The results present mutant ataxin-3 expression levels of treated samples, relatively to non-treated samples. Values are presented as mean \pm SEM of at least 3 independent experiments. Two-way ANOVA

analysis of variance combined with Bonferroni's post-test was used for multiple comparisons (** $p < 0.001$, ** $p < 0.01$ and * $p < 0.05$).

Thus, our results show that RVG-9r-targeted liposomes are able to deliver siMutAtax3 to neuronal cells, resulting in efficient mutant ataxin-3 knockdown.

2.3.5. Intravenous administration of RVG-9r-targeted liposomes promotes accumulation in the brain

Having demonstrated the efficacy of RVG-9r-targeted liposomes *in vitro*, we then investigated whether the RVG-9r-peptide could increase the accumulation of the nanoparticles in the mouse brain, upon intravenous administration. For this purpose, we encapsulated a near infrared dye (NIR) in liposomes – indocyanine green (ICG) – and used an *in vivo* imaging technology platform (IVIS Lumina equipment) to visualize biodistribution in the brain and peripheral organs (Fig. 2.6A). As shown in Fig. 2.6B, intravenous administration of RVG-9r-targeted liposomes increased ICG accumulation in the brain of living animals three hours post-injection, when compared to RV-MAT-9r-coupled liposomes.

To evaluate the biodistribution of the nanoparticles between the brain and major organs of the animals, mice were injected with ICG liposomes and sacrificed by intracardiac perfusion with PBS three hours post-injection. We observed that intravenous administration of RVG-9r-targeted liposomes, when compared to a formulation targeted with RV-MAT-9r, allowed a significant increase in the accumulation of ICG in the mouse brain (Fig. 2.6C, D) but not in major organs such as heart, lungs, liver, spleen and kidneys (Fig. 2.6E, F). Moreover, RVG-9r-targeted liposomes exhibited a decreased accumulation in the heart and lungs of the injected animals (Fig. 2.6F).

These results reveal that intravenous administration of RVG-9r-targeted liposomes promotes the accumulation of the nanoparticles in the brain of the injected animals.

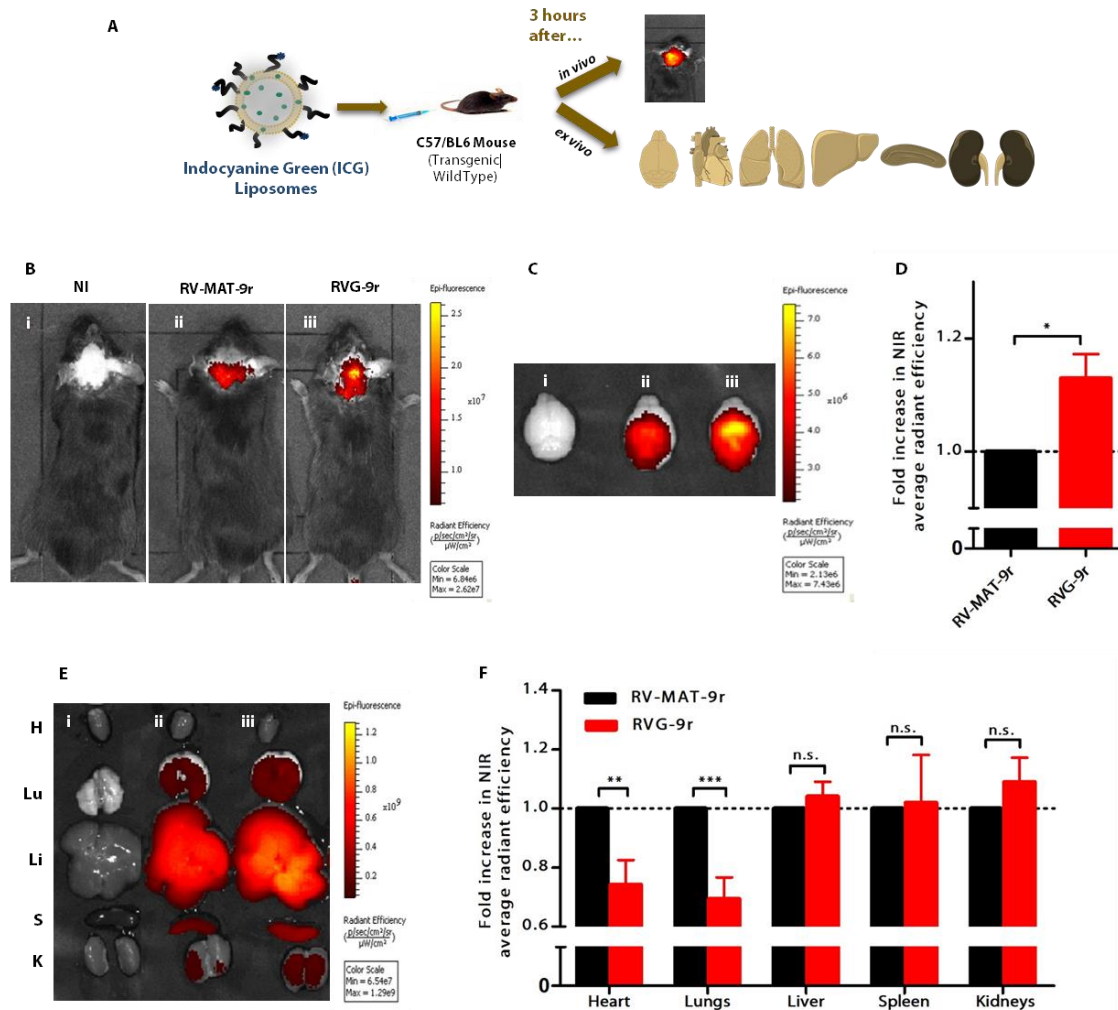


Figure 2.6. *in vivo* and *ex vivo* NIR fluorescence images upon intravenous administration of RVG-9r-targeted nanoparticles. (A) Schematic representation of the *in vivo* study. Mice were intravenously injected through tail vein injection with RV-MAT-9r or RVG-9r-targeted liposomes encapsulating ICG. Three hours after injection, images of a non-injected animal (NI) (i), and mice injected with RV-MAT-9r-targeted ICG liposomes (ii) or RVG-9r-targeted ICG liposomes (iii) were acquired using an IVIS Lumina equipment. (B) *in vivo* imaging was performed in anesthetized mice that were shaved around the brain region. (C-F) To get the body distribution of the nanoparticles in the brain and major organs, mice were sacrificed by intracardiac perfusion with PBS and NIR fluorescence images were obtained. (C) Representative image of the *ex vivo* ICG accumulation in the brain. (D) Fold increase in the NIR fluorescence in the brain of animals injected with RVG-9r-targeted liposomes, comparatively to mice injected with RV-MAT-9r-targeted liposomes. (E) Representative image of the *ex vivo* ICG accumulation in major organs (H, Heart; Lu, Lungs; Li, Liver; S, Spleen and K, Kidneys). (F) Quantification of the NIR fluorescence in major organs of mice injected with RVG-9r-targeted liposomes, when compared to RV-MAT-9r-targeted liposomes. Values in C) and E) are presented as mean \pm SEM of n=6. Student's t-test was used to compare animals injected with RVG-9r- to RV-MAT-9r-targeted liposomes (** $p < 0.01$, *** $p < 0.001$, * $p < 0.05$ and n.s. $p > 0.05$).

2.4. Discussion

Despite the potential of RNAi for the treatment of dominantly-inherited neurodegenerative disorders such as MJD, the successful clinical application has been limited due to the presence of the BBB and the intrinsic limitations of gene-silencing molecules. To solve these problems, the development of an effective delivery system is extremely needed.

Previous studies, showed that RVG could deliver siRNAs to the brain through a specific ligand-receptor mediated transcytosis mechanism, using either siRNA directly complexed to RVG-9r (Kumar *et al.*, 2007; Zadran *et al.*, 2013), associating cationic liposomes (Pulford *et al.*, 2010), cationic polymers (Gao *et al.*, 2014; Park *et al.*, 2015) or exosomes (Alvarez-Erviti *et al.*, 2011; Cooper *et al.*, 2014). However, apart from exosomes, the other formulations rely on electrostatic interactions between negatively charged siRNA molecules and positively charged components. Several disadvantages arise from the use of non-viral vectors based on electrostatic interactions: uncontrollable interaction between formulation components, causing weak reproducibility of the manufacturing process; positive charge of the complexes, which leads to poor pharmacokinetic properties, short circulatory half-life and significant reticuloendothelial system (RES) uptake and immune recognition, which gives rise to inflammatory toxicity (Sakurai *et al.*, 2008; Shim and Kwon, 2010; Wu and McMillan, 2009).

SNALPs emerged as a promising platform to overcome these major drawbacks, being able to deliver the silencing sequences to their target (Costa *et al.*, 2013; Di Martino *et al.*, 2014; Geisbert *et al.*, 2006; Geisbert *et al.*, 2010; Judge *et al.*, 2009; Morrissey *et al.*, 2005; Zimmermann *et al.*, 2006). Therefore, in this part of the work we synthesized brain-targeted SNALPs using the RVG-9r-peptide, and evaluated its potential *in vitro* and *in vivo*. For our experiments, we maintained 9-arginines (9r) in the peptide composition because previous studies suggest that they improve cellular uptake and cytosolic release of the nanoparticles (Biswas *et al.*, 2013; El-Sayed *et al.*, 2008; Zeller *et al.*, 2015).

We first tested if we would need to modify the RVG-9r peptide with the addition of thiol groups, before conjugation to micelles. Our results demonstrated that direct conjugation

of RVG-9r to the micelles gave rise to higher postinsertion efficiencies and cellular uptake, which makes the production protocol simpler and easier to implement.

DODAP, an ionizable cationic lipid, enables efficient encapsulation of siRNAs at acidic pH, and reduces toxicity as the lipid acquires a neutral charge at physiological pH (Semple *et al.*, 2001). It is also believed that ionizable cationic lipids interact with the endosomal membrane, promoting the release of the siRNAs into the cytosol (Hafez *et al.*, 2001). Therefore, in an attempt to benefit from its important characteristics, we used DODAP in the composition of our liposomes.

Overall, the RVG-9r-targeted SNALPs exhibited important features that make them adequate for systemic administration: high encapsulation efficiency for siRNAs, ability to protect the encapsulated siRNAs, appropriate and homogeneous particle size distribution. Moreover, from a production point-of-view, this technology exhibited high reproducibility of the manufacturing process. Ligand post-insertion efficiencies were higher than the ones that were earlier shown (Costa *et al.*, 2013; Mendonca *et al.*, 2010a) and this may be attributable to the arginines included in the peptide composition, because we observed good yields for both RVG-9r and RV-MAT-9r peptides.

Flow cytometry and confocal microscopy studies revealed that the attachment of RVG-9r to the liposomal surface enhanced the uptake of the liposomes by neuronal cells (HT-22, Neuro2a) but not non-neuronal cells (HeLa), when compared to the RV-MAT-9r-coupled liposomes (Fig. 2.3 and 2.4). These results are also in accordance to what was previously reported by different groups (Gao *et al.*, 2014; Hwang do *et al.*, 2011; Kumar *et al.*, 2007; Park *et al.*, 2015; Pulford *et al.*, 2010; Son *et al.*, 2011). Moreover, we observed a decrease in cellular association and internalization when RVG-9r-targeted liposomes were incubated with Neuro2a cells at 4°C or at 37°C after receptor saturation, which indicates that an energy-dependent process, most likely receptor-mediated endocytosis, is involved in the uptake of these liposomes (Fig. 2.4). These were important observations because clinically, the fact that the RVG-9r-nanoparticles associate more with neuronal cells and through receptor-mediated endocytosis, may reduce the undesired side effects that result from targeting of other tissues.

Additionally, we targeted mutant ataxin-3, the MJD-causing protein (Kawaguchi *et al.*, 1994), using RVG-9r-targeted SNALPs and observed that this formulation efficiently

knocked down mutant ataxin-3 mRNA, resulting in protein level reduction in a neuronal cell line (Fig. 2.5). These results confirmed that the RVG-9r-targeted liposomes are able to further release encapsulated siRNAs in the cytoplasm of neuronal cells and mediate downregulation of the target gene. Importantly, the target sequence of these siRNAs includes a single nucleotide polymorphism that we previously showed to enable allele-specific silencing of mutant ataxin-3, while preserving wild-type ataxin-3 (Alves *et al.*, 2008a; Nóbrega *et al.*, 2014; Nóbrega *et al.*, 2013b).

To evaluate brain-targeting efficiency after intravenous administration, we used an *in vivo* imaging platform to detect signal from encapsulated NIR dye. We observed that RVG-9r conjugation to our nanoparticles enhanced the ability to cross the BBB, as shown by the higher accumulation of ICG in the brain of the animals injected with RVG-9r- when compared to RV-MAT-9r-targeted liposomes (Fig. 2.6B-D). Additionally, RVG-9r-targeted liposomes appear to be less retained by heart and lungs of the animals (Fig. 2.6F) probably due to the brain-targeting capability.

In conclusion, we developed an appropriate brain-targeted delivery system that may be used for MJD therapy and potentially for the treatment of other neurodegenerative diseases. The developed strategy will be further explored for the treatment of MJD, in the next two chapters of this thesis.

CHAPTER 3

Non-invasive silencing of mutant ataxin-3 decreases striatal neuropathology in a lentiviral mouse model of Machado-Joseph disease

3.1. Abstract

Machado-Joseph disease (MJD) is the most common dominantly-inherited ataxia worldwide and it is caused by the over-repetition of a CAG tract in the coding region of the *ATXN3/MJD1* gene. The expanded polyglutamine tract on mutant ataxin-3 confers a toxic gain-of-function to the ataxin-3 protein, leading to neuronal dysfunction and degeneration in multiple brain regions, including the striatum. Although MJD is an extremely debilitating disorder, it remains a fatal and incurable disease.

Gene silencing by RNA interference (RNAi) is one of the most promising approaches towards MJD therapy and has shown promising results in MJD animal models. However, until now, all the performed experiments involved intracranial administration of viral vectors, and there is a need for a safer and less invasive procedure. Therefore, we evaluated the therapeutic potential of intravenous administration of brain-targeted SNALPs in a lentiviral-based mouse model of MJD. Notably, our study provides evidence that brain-targeted SNALPs decrease the number of ubiquitin-positive inclusions and mediate neuroprotection in a striatal lentiviral-based mouse model of MJD. These data strengthen the benefits of RNAi towards MJD therapy and show that our non-viral and non-invasive strategy may constitute a promising therapeutic strategy for MJD patients.

3.2. Introduction

Machado-Joseph disease (MJD), also known as spinocerebellar ataxia type 3 (SCA3), is the most common autosomal dominantly inherited ataxia worldwide and one of the nine known polyglutamine (polyQ) diseases (Bird, 1998; Riess, 2008). This disorder is caused by the over-repetition of a CAG tract in the coding region of the *ATXN3/MJD1* gene on chromosome 14q32.1, which results in an expanded polyglutamine tract at the C-terminus of ataxin-3 (Kawaguchi *et al.*, 1994; Takiyama *et al.*, 1993). While in normal alleles the number of CAG repeats is usually below 43, MJD patients present between ~60 and 87 CAG repeats in the mutant allele (Cancel G, 1995; Dürr A, 1996; Maciel *et al.*, 1995; Matilla *et al.*, 1995; Matsumura *et al.*, 1996; Ranum *et al.*, 1995; Sasaki *et al.*, 1995).

The presence of mutant ataxin-3 with an expanded polyglutamine tract is the triggering factor of several events that lead to neuronal dysfunction and degeneration in multiple brain regions, including: cerebellum, brainstem, substantia nigra, thalamus and striatum (Alves *et al.*, 2008b; Dürr A, 1996; Scherzed *et al.*, 2012; Sudarsky and Coutinho, 1995; Taniwaki *et al.*, 1997; Wullner *et al.*, 2005). The pathological hallmark of MJD is the presence of neuronal intranuclear inclusions, which contain aggregates of expanded ataxin-3 and other ubiquitin-proteasome components (Paulson *et al.*, 1997). Although this is an extremely debilitating disorder, no effective disease-modifying treatment was developed for MJD so far, consequently it remains a fatal and incurable disease.

Therapies based on RNA interference (RNAi) hold great promise for the treatment of diseases in which neurodegeneration is linked to the production of mutant proteins coded by dominant mutant alleles. Indeed, there are several examples of successful experiments involving RNAi to rescue neurological phenotype in animal models of neurodegenerative diseases, including: Huntington's disease (DiFiglia *et al.*, 2007; Kordasiewicz *et al.*, 2012; Yu *et al.*, 2012), SCA1 (Keiser *et al.*, 2014; Keiser *et al.*, 2013; Xia *et al.*, 2004), SCA7 (Ramachandran *et al.*, 2014), Alzheimer's disease (Piedrahita *et al.*, 2010; Rodriguez-Lebron *et al.*, 2009; Singer *et al.*, 2005) and Parkinson's disease (Gorbatyuk *et al.*, 2010; Khodr *et al.*, 2011; Sapru *et al.*, 2006). Furthermore, using different animal models of MJD we and others have shown that RNAi may be an effective therapy for MJD (Alves *et al.*, 2008a; Alves *et al.*, 2010; Costa Mdo *et al.*, 2013; Nóbrega *et al.*, 2014; Nóbrega *et al.*,

2013b; Rodriguez-Lebron *et al.*, 2013). Besides promising, the referred experiments were performed upon intracranial administration of viral vectors and there is a need for a safer and less invasive procedure that could afford the delivery of RNAi-therapeutics throughout all the disease-relevant brain regions.

In this study we evaluated the therapeutic efficacy of the previously developed formulation (brain-targeted SNALPs) in the striatum of a lentiviral-based mouse model of MJD (Simões *et al.*, 2012). This MJD mouse model is a versatile research tool that replicates late stages of neurodegenerative diseases, enabling to test therapeutic hypothesis in a short period of time and allowing precise quantitative analysis of neuropathology, particularly the number of aggregates and the brain volume depleted of markers such as DARPP-32. As genotyping of MJD patients could allow the initiation of the treatment before the first symptoms appear, these experiments were conducted initiating the treatment at an early time-point. Importantly, the silencing sequences used in these studies targeted a single nucleotide polymorphism that we previously showed to enable allele-specific silencing of mutant ataxin-3, while preserving wild-type ataxin-3 (Alves *et al.*, 2008a; Nóbrega *et al.*, 2014; Nóbrega *et al.*, 2013b). Here, we provide evidence that intravenous administration of RVG-9r-targeted SNALPs is able to significantly decrease striatal neuropathology in a lentiviral-based mouse model of MJD.

3.3. Materials and Methods

3.3.1. Materials

Cy5.5-labeled siRNAs were acquired from Dharmacon and labeling was performed at the 5' sense strand. The remaining materials used in these studies were the same that were mentioned in chapter 2.

3.3.2. Mice

6-weeks-old C57BL/6 mice were obtained from Charles River. Animals were maintained and experiments carried out as referred in chapter 2.

3.3.3. Synthesis and characterization of brain-targeted stable nucleic acid lipid particles

Synthesis and characterization of RVG-9r-targeted SNALPs was performed as described in chapter 2.

3.3.4. Production of lentiviral vectors encoding human mutant ataxin-3

Lentiviral vectors encoding human mutant ataxin-3 (ATX-3 72Q) (Alves *et al.*, 2008b) were produced in HEK293T cells with a four-plasmid system, as previously described (de Almeida *et al.*, 2001). The lentiviral particles were resuspended in 0.5% bovine serum albumin in phosphate-buffered saline (PBS) and the viral particle content determined using a lentivirus qPCR titration kit (abm), according to the manufacturer's instructions.

3.3.5. Injection of lentiviral vectors encoding mutant ataxin-3 into the striatum

After thawing lentivirus on ice, 7-weeks-old mice were anesthetized with a mixture of xylazine-ketamine. 1.25 μ L of lentiviral vectors encoding human mutant ataxin-3 (ATX-3 72Q, 8.6X10⁹ IU/mL) were stereotaxically injected into the right hemisphere of the mouse

striatum using the following coordinates: antero-posterior +0.6 mm, medial-lateral +1.8 mm and dorso-ventral -3.3 mm.

3.3.6. Striatal distribution experiment

Three days after lentivirus injection into the right hemisphere of the mouse striatum, mice were intravenously injected with 3.5 mg/kg of Cy5.5-labeled siRNAs encapsulated in RVG-9r-targeted liposomes. Three hours after injection, animals were sacrificed by intracardiac perfusion with 10 mL of ice-cold PBS followed by 40 mL of 4% paraformaldehyde (PFA). Brain was then post-fixed in 4% PFA for 24 hours, cryoprotected by incubation for 48 hours in 25% sucrose at 4°C and then frozen at -80°C. 25 µm coronal striatal sections were cut using a cryostat (Leica CM3050S) and stored in PBS supplemented with 0.05 mM of sodium azide (in 48-well-plates) at 4°C. Sections were directly mounted on gelatinized slides and Cy5.5 fluorescence from Cy5.5-labeled siRNAs was detected using Zeiss Axio Imager Z2 microscope with x20 objective. To obtain representative images of the left and right striatum, the tiles feature of the Zen software (Zeiss) was used.

3.3.7. Mutant ataxin-3 silencing experiment

Three days after lentivirus injection into the right hemisphere of the mouse striatum, mice were randomly distributed in two different groups of treatment and intravenously injected with RVG-9r-targeted liposomes encapsulating siCTR (siEGFP) or siMutAtax3. Each animal received a total of three injections (3 mg siRNA/ kg each), spaced by ten days, and animals were sacrificed 4 weeks after the stereotaxic injection. qRT-PCR and immunohistochemical analysis was performed as described below.

3.3.8. Mutant ataxin-3 mRNA silencing in the mouse striatum by qRT-PCR

Mice were sacrificed by cervical dislocation and the right injected striata were dissected and stored immediately at -80°C until RNA extraction. To detect striatal mRNA levels, total RNA was extracted using Qiazol solution (Qiagen) followed by purification of the RNA product using the Nucleospin RNA kit (Macherey-Nagel). cDNA synthesis and quantitative

PCR were performed as described in materials and methods of chapter 2, with slight modifications. Briefly, to determine the levels of human mutant ataxin-3, we used 2.5 μ L of cDNA diluted 10 times and an annealing temperature of 55°C. The StepOne Software generated automatically threshold cycle (Ct) values and mutant ataxin-3 levels were normalized using HPRT housekeeping gene. The mRNA relative quantification was performed with the Pfaffl method relatively to control-treated animals. Primers used to detect human ataxin-3 (QT00094927) and mouse HPRT (QT00166768) were obtained from Qiagen.

3.3.9. Immunohistochemical procedure

Mice were sacrificed and brain tissue was processed as described in section 3.3.6 of this chapter.

Visible immunohistochemical procedure was performed as we previously reported (Alves *et al.*, 2008a). Briefly, the protocol began by endogenous peroxidase quenching incubating sections in 0.1% phenylhydrazine in PBS, for 30 minutes at 37°C. Blocking and permeabilization were performed in 0.1% Triton X-100 10% normal goat serum (Gibco) prepared in PBS, for 1 hour at room temperature. Sections were then incubated overnight at 4°C in blocking solution with primary antibodies: rabbit polyclonal anti-ubiquitin antibody (1:500, Dako) and rabbit anti-DARPP-32 antibody (1:2000, Chemicon). After washing, the sections were then incubated with the biotinylated secondary antibody (anti-rabbit, 1:250; Vector Laboratories). Bound antibodies were visualized using the Vectastain ABC kit, with 3,3'-diaminobenzidine tetrahydrochloride (DAB metal concentrate, Pierce) as substrate. The sections were then mounted on slides, dehydrated and coverslipped with Eukitt. Images were acquired using Zeiss Axio Imager Z2 microscope with x5 or x20 objective.

To perform cresyl violet staining, sections were pre-mounted on gelatinized slides and stained with cresyl violet for 5 minutes, differentiated in 70% ethanol, dehydrated by passing through 96% ethanol, 100% ethanol and xylene solutions and mounted with Eukitt. Images were acquired using Zeiss Axio Imager Z2 microscope with x5 objective.

Fluorescence immunohistochemical procedure was performed as we previously reported (Mendonça *et al.*, 2015), with very few alterations. Briefly, the protocol was initiated with

1 h of blocking and permeabilization in 0.3% Triton X-100 10% normal goat serum prepared in PBS at room temperature. Sections were then incubated overnight at 4°C with the following primary antibodies prepared in 2% normal goat serum 0.05% Triton X-100 (in PBS): rabbit polyclonal anti-Iba1 (1:1000, Wako) or rabbit polyclonal anti-GFAP (1:1000, Wako). Sections were washed and incubated with goat anti-rabbit conjugated to Alexa Fluor 568 secondary antibody (1:250, Molecular Probes), prepared in 2% normal goat serum (Gibco), for 2 h at room temperature. Nuclei staining was performed with DAPI, sections were washed and then mounted on gelatinized slides. After being dried, slides were coverslipped with Mowiol reagent. Widefield fluorescence images were acquired using Zeiss Axio Imager Z2 microscope with x5 objective.

3.3.10. Quantification of ubiquitin-positive inclusions and DARPP-32 depleted volume

Quantitative analysis of the total number of ubiquitin-positive inclusions and the extent of DARPP-32 loss in the striatum was performed by scanning 12 stained-sections per animal that were distanced 200 µm from each other (to obtain representative images of the striatum). To quantify the number of ubiquitin-positive inclusions, sections were imaged using the tiles feature of the Zen software (Zeiss) using Zeiss Axio Imager Z2 microscope with x20 objective. To calculate the DARPP-32 loss, sections were imaged using a x5 objective. The quantifications were then performed using an image-analysis software (Image J software, NIH, USA). The DARPP-32-depleted volume was estimated using the following formula: $\text{Volume} = d(a_1 + a_2 + a_3 + \dots)$, where d is the distance between serial sections and a_1, a_2, a_3 are the areas for individual serial sections.

3.3.11. Quantification of condensed pycnotic nuclei volume

Quantitative analysis of the volume of condensed pycnotic nuclei in the striatum was performed by scanning 8 stained-sections per animal that were distanced 200 µm from each other. Sections were imaged using a x5 objective and quantifications were performed using ImageJ. The volume of condensed pycnotic nuclei was estimated using the following formula: $\text{Volume} = d(a_1 + a_2 + a_3 + \dots)$, where d is the distance between serial sections and a_1, a_2, a_3 are the areas.

3.3.12. Quantification of GFAP and Iba-1 immunoreactivity

Quantitative analysis of the GFAP and Iba-1 immunoreactivity was performed by scanning 12 stained-sections per animal that were distanced 200 μm from each other. Left and right striatum were imaged using the tiles feature of the Zen software (Zeiss) using Zeiss Axio Imager Z2 microscope with x5 objective. The immunoreactivity indexes were measured through optic density analysis in the affected striatal regions relative to their corresponding non-affected striatum (left hemisphere, defined as background), using an image-analysis software (Image J software, NIH, USA).

3.3.13. Statistical analysis

Data are presented as mean \pm standard error of mean (SEM) of at least three independent experiments. Student's *t*-test was used to determine statistically significant differences of the means. Statistical differences are presented at probability levels of * $p < 0.05$, ** $p < 0.01$ and *** $p < 0.001$ and considered non-significant (n.s.) when $P < 0.05$. Calculations were performed using GraphPad Prism version 5.00 for Windows.

3.4. Results

3.4.1. RVG-9r-targeted SNALPs deliver siRNAs and decrease mutant ataxin-3 mRNA levels in the striatum of a lentiviral mouse model of Machado-Joseph disease

At 7 weeks-of-age, mice were stereotaxically injected in the right striatum with lentiviral vectors encoding for the human mutant ataxin-3 (Fig. 3.1A). Three days after, mice were tail-vein injected with RVG-9r-targeted liposomes encapsulating Cy5.5-labeled siRNAs and were sacrificed three hours later, as represented in Fig. 3.1B. Fluorescence microscopy images showed that intravenous administration of RVG-9r-targeted SNALPs promoted the accumulation of Cy5.5-labeled siRNAs in the striatal region from the right hemisphere, as can be seen by the intense red fluorescence.

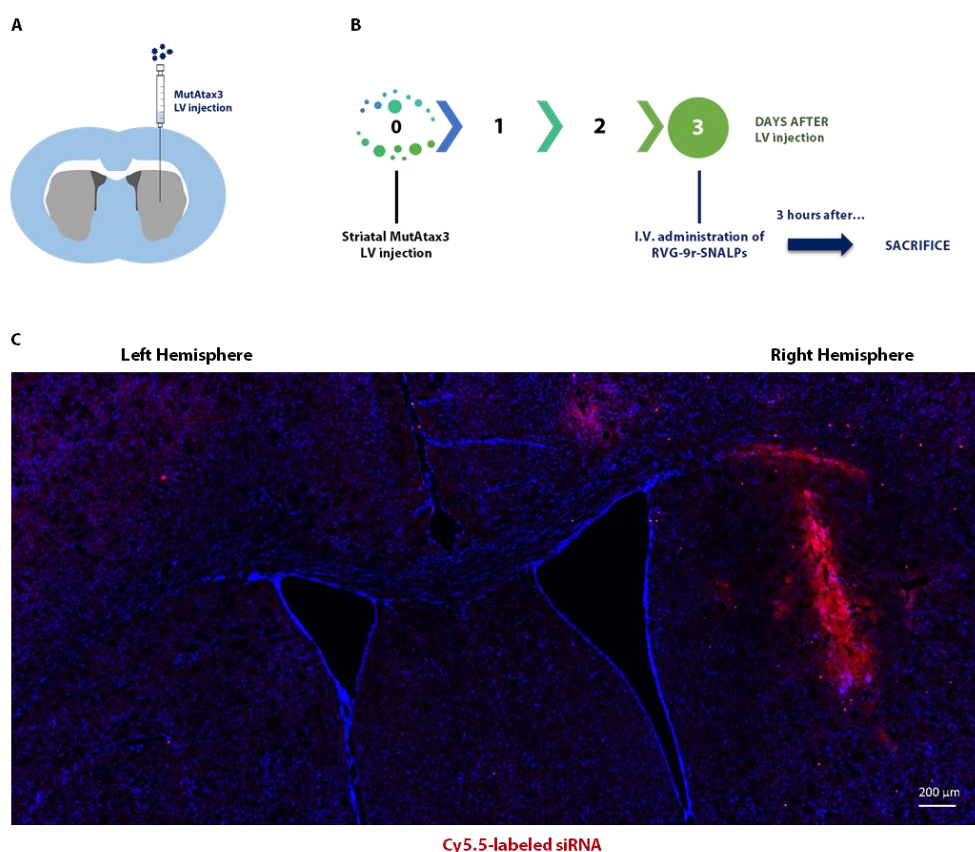


Figure 3.1. RVG-9r-targeted SNALPs deliver siRNAs into the striatum of a lentiviral-based mouse model of Machado-Joseph disease. (A) Schematic representation of the stereotaxic injection of lentiviral vectors encoding for the human mutant ataxin-3 into the mouse striatum (right hemisphere). (B) Timeline indicating the injection of lentiviral vectors (LV) and intravenous administration of RVG-9r-targeted SNALPs. Mice were stereotaxically injected and, three days after, they were intravenously injected with RVG-9r-targeted liposomes encapsulating Cy5.5-

labeled siRNAs. siRNA distribution was evaluated by fluorescence microscopy, 3 hours after tail-vein injection. **(C)** Coronal brain section demonstrating Cy5.5-labeled siRNAs distribution in the striatum of intravenously injected animals. Red dots show Cy5.5-labeled siRNAs.

Following the confirmation of the *in vivo* delivery of siRNAs to the striatum of the lentiviral MJD mouse model, we then evaluated if RVG-9r-targeted SNALPs could decrease mutant ataxin-3 mRNA levels in the striatum of these animals. During the time-course of the experiment, mice were intravenously injected with RVG-9r-targeted liposomes encapsulating a control sequence of siRNA (siCTR) or siRNA against mutant ataxin-3 (siMutAtax3). Each mouse received a total of three tail-vein injections, spaced by 10 days, and animals were sacrificed 4 weeks after stereotaxic injection of lentivirus encoding for the human mutant ataxin-3 (Fig. 3.2A). qRT-PCR data suggest that intravenous administration of RVG-9r-targeted SNALPs encapsulating siMutAtax3, when compared to siCTR, decrease striatal mutant ataxin-3 mRNA levels ($33\pm 14.7\%$, Fig. 3.2B).

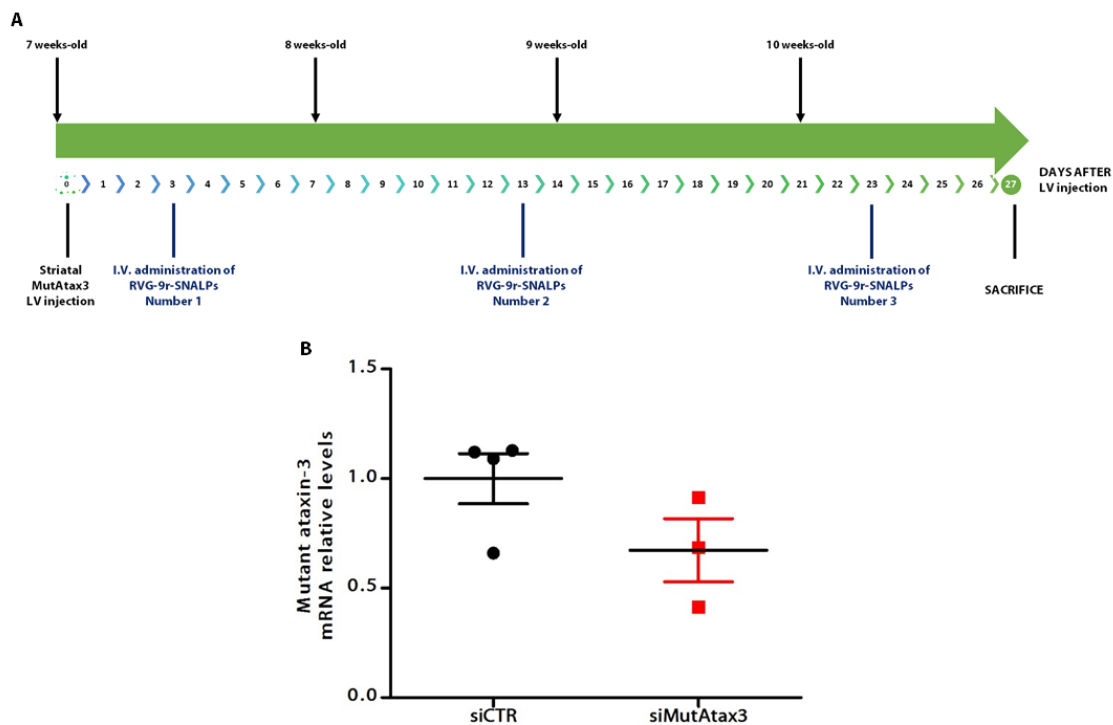


Figure 3.2. RVG-9r-targeted SNALPs decrease mutant ataxin-3 mRNA levels in the striatum of a lentiviral mouse model of MJD. (A) Timeline indicating the injection of lentiviral vectors (LV) and intravenous administration of the liposomes. Mice were stereotaxically injected into the right striatum with lentiviral vectors encoding for the human mutant ataxin-3 (MutAtax3). Three days after, mice were intravenously injected with RVG-9r-targeted SNALPs encapsulating siCTR or siMutAtax3. Each animal received a total of three injections, spaced by ten days, and animals were

sacrificed four weeks after the stereotaxic surgery. **(B)** Mutant ataxin-3 mRNA levels were detected by qRT-PCR. Results were normalized using the HPRT housekeeping gene and show the levels of mutant ataxin-3 mRNA for animals injected with RVG-9r-targeted SNALPs encapsulating siMutAtax-3, when compared with siCTR. Values are presented as mean \pm SEM of n=3/4. Student's t-test was used to compare animals injected with siMutAtax3 to siCTR (n.s. $p < 0.05$).

3.4.2. RVG-9r-targeted SNALPs decrease the number of ubiquitin-positive inclusions and mediate striatal neuroprotection in a lentiviral mouse model of Machado-Joseph disease

The lentiviral-based mouse model of MJD used in this study, which we have previously developed, allows precise quantitative analysis of the neuropathological deficits induced by mutant ataxin-3 expression (Simões *et al.*, 2012). Therefore, we used this animal model to evaluate the therapeutic potential of intravenous administration of RVG-9r-targeted SNALPs on MJD-associated neuropathology. This experiment was conducted as previously described and as represented in Fig. 3.2A.

As the presence of neuronal intranuclear inclusions containing the aggregated mutant ataxin-3 (Paulson *et al.*, 1997) is one of the hallmarks of MJD, we evaluated the potential of RVG-9r-targeted SNALPs to decrease the total number of ubiquitin-positive inclusions. When compared to a control sequence of siRNA (siCTR), we observed that intravenous administration of RVG-9r-targeted liposomes encapsulating siMutAtax3 promoted a 40 \pm 19.2% significant decrease in the total number of ubiquitin-positive inclusions (Fig. 3.3A-E).

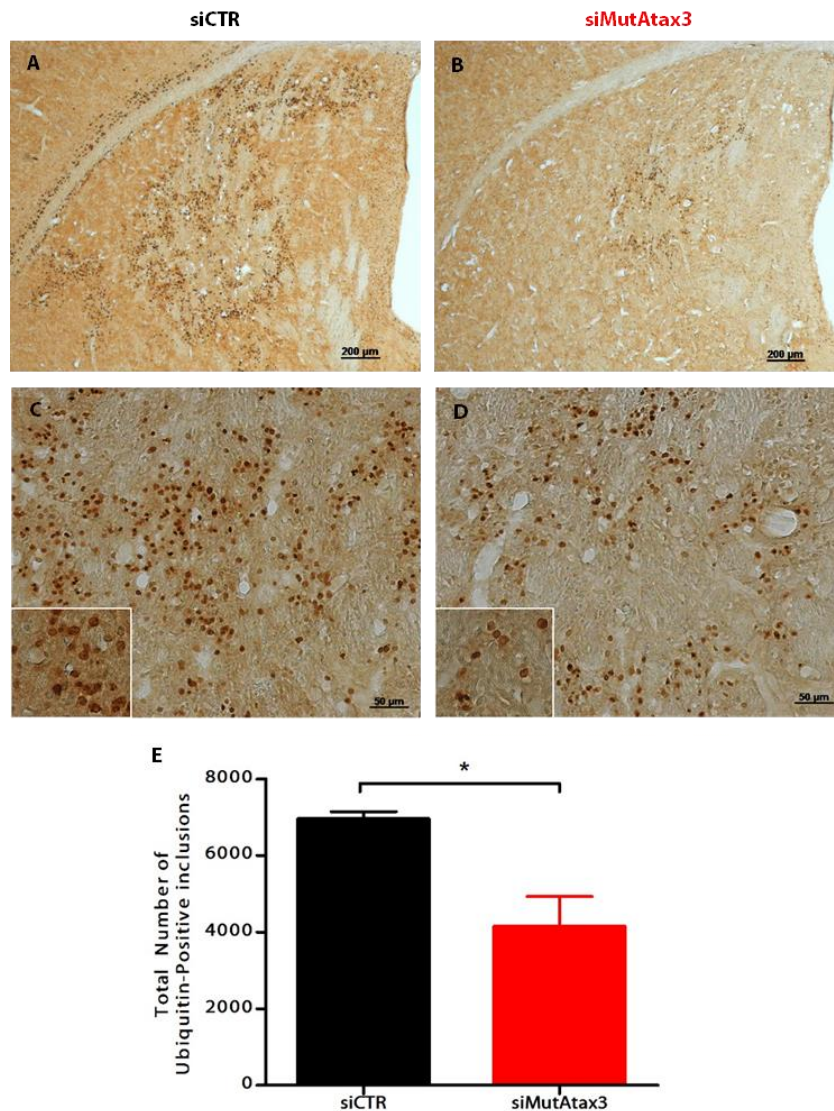


Figure 3.3. RVG-9r-targeted SNALPs decrease the number of ubiquitin-positive inclusions in a lentiviral mouse model of MJD. Immunohistochemical analysis 4 weeks post-injection of lentiviral vectors encoding for the human mutant ataxin-3. **(A, B)** Bright-field microscopy images revealing ubiquitin-positive inclusions after intravenous administration of RVG-9r-targeted liposomes encapsulating siCTR (A) or siMutAtax3 (B). **(C, D)** Higher magnification images of A and B, respectively, revealing ubiquitin-positive inclusions after intravenous administration of RVG-9r-targeted liposomes encapsulating siCTR (C) or siMutAtax3 (D). **(E)** Quantification of the total number of ubiquitin-positive inclusions. Values are presented as mean±SEM of n=5. Student's t-test was used to compare animals injected with siMutAtax3 to siCTR (*p<0.05).

Next, to evaluate if our strategy could mediate striatal neuroprotection, we stained brain sections for DARPP-32, a regulator of dopamine receptor signaling (Greengard *et al.*, 1999), that we previously demonstrated to be a sensitive marker to detect early neuronal dysfunction (Alves *et al.*, 2008b; de Almeida *et al.*, 2002). Intravenous administration of

RVG-9r-targeted liposomes encapsulating siMutAtax3 promoted a $52\pm 25\%$ significant decrease in the loss of DARPP-32 staining when compared to siCTR (Fig. 3.4A-E).

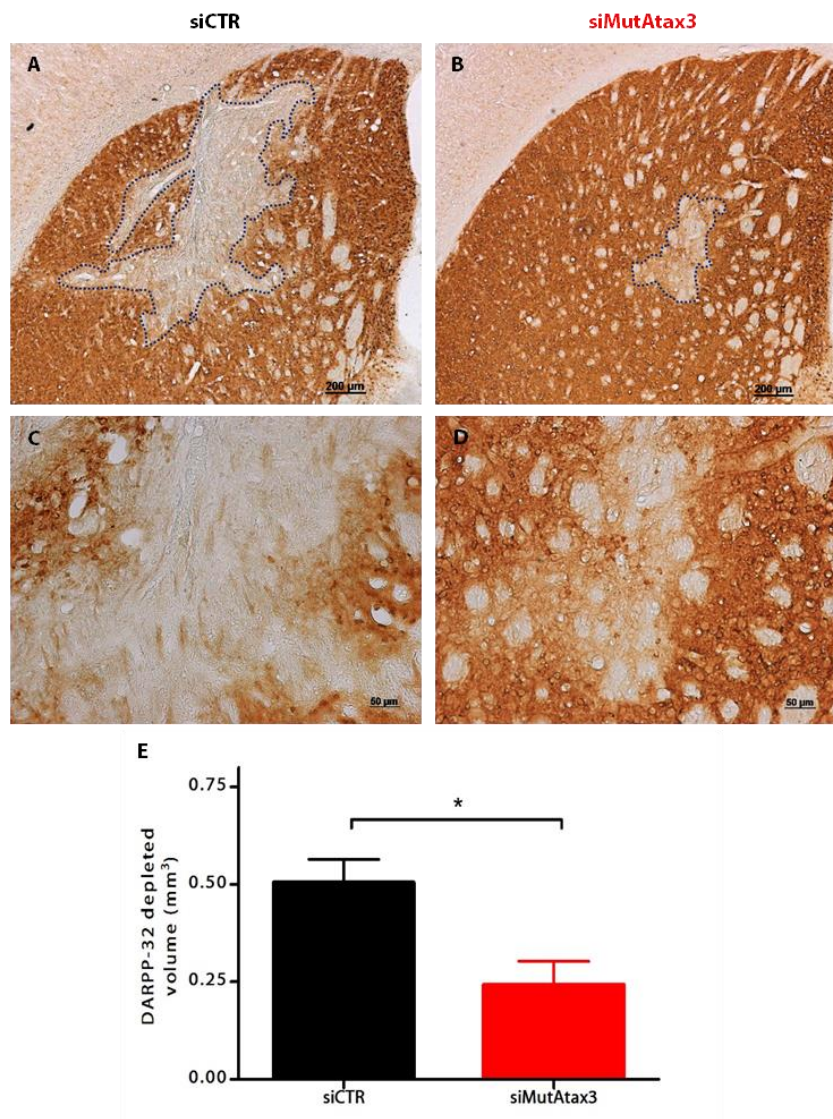


Figure 3.4. RVG-9r-targeted SNALPs decrease neuronal dysfunction in a lentiviral mouse model of MJD. Immunohistochemical analysis 4 weeks post-injection of lentiviral vectors encoding for the human mutant ataxin-3. **(A, B)** Visible microscopy images showing DARPP-32 staining after intravenous administration of RVG-9r-targeted liposomes encapsulating siCTR (A) or siMutAtax3 (B). **(C, D)** Higher magnification images of A and B, respectively, revealing DARPP-32 staining after intravenous administration of RVG-9r-targeted liposomes encapsulating siCTR (C) or siMutAtax3 (D). **(E)** Quantification of DARPP-32 depleted volume (mm³). Values are presented as mean \pm SEM of n=5. Student's t-test was used to compare animals injected with siMutAtax3 to siCTR (*p<0.05).

Additionally, cresyl violet staining demonstrated that non-invasive silencing of mutant ataxin-3 decreased striatal degeneration induced by mutant ataxin-3 expression in the mouse striatum, as shown by the significant decrease in the volume of condensed pycnotic nuclei ($82\pm 11\%$, Fig. 3.5A-C).

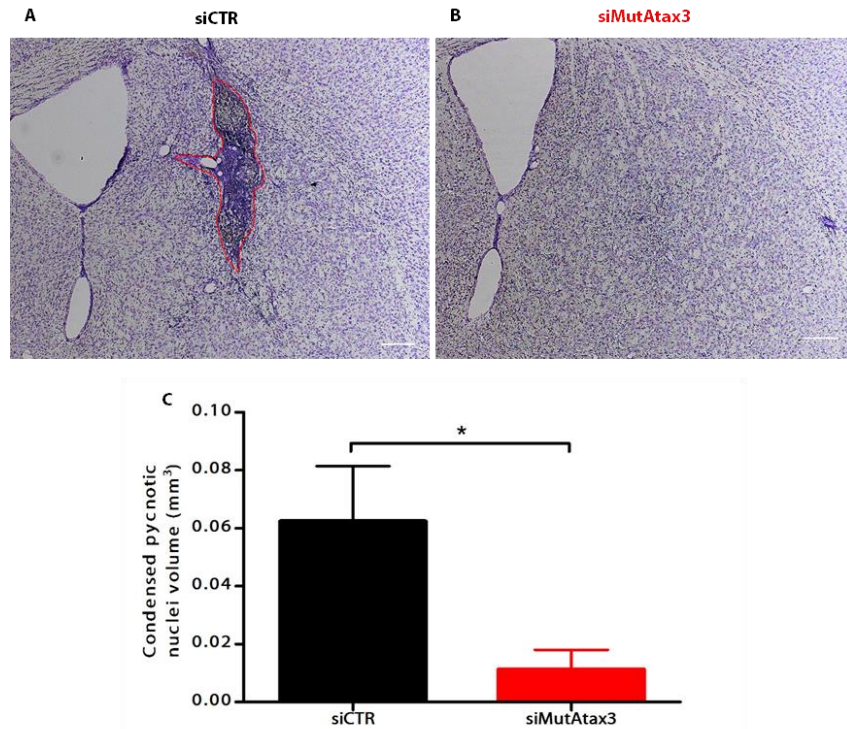


Figure 3.5. RVG-9r-targeted SNALPs decrease striatal degeneration in a lentiviral mouse model of MJD. Immunohistochemical analysis 4 weeks post-injection of lentiviral vectors encoding for the human mutant ataxin-3. **(A, B)** Cresyl violet stained sections revealing pycnotic nuclei area (dark purple region) after intravenous administration of RVG-9r-targeted liposomes encapsulating siCTR (A) or siMutAtax3 (B). Scale bars, 200 μ m. **(C)** Quantification of pycnotic nuclei volume (mm³). Values are presented as mean \pm SEM of n=5. Student's t-test was used to compare animals injected with siMutAtax3 to siCTR (* p <0.05).

Together these results show that RVG-9r-targeted SNALPs promote the clearance of ubiquitin-positive inclusions, preventing cell injury and striatal degeneration in a lentiviral mouse model of MJD.

3.4.3. RVG-9r-targeted SNALPs reduce neuroinflammation in a lentiviral mouse model of Machado-Joseph disease

As we previously reported, mutant ataxin-3 expression induces a local increase of glial fibrillary acidic protein (GFAP) immunoreactivity suggestive of astrocytic activation (Gonçalves *et al.*, 2013). Therefore, we evaluated if intravenous administration of RVG-9r-targeted SNALPs could reverse these effects. Importantly, intravenous administration of RVG-9r-targeted liposomes encapsulating siMutAtax3, when compared to siCTR, was able to significantly reduce GFAP immunoreactivity by $23\pm 6.13\%$ (Fig. 3.6A-C).

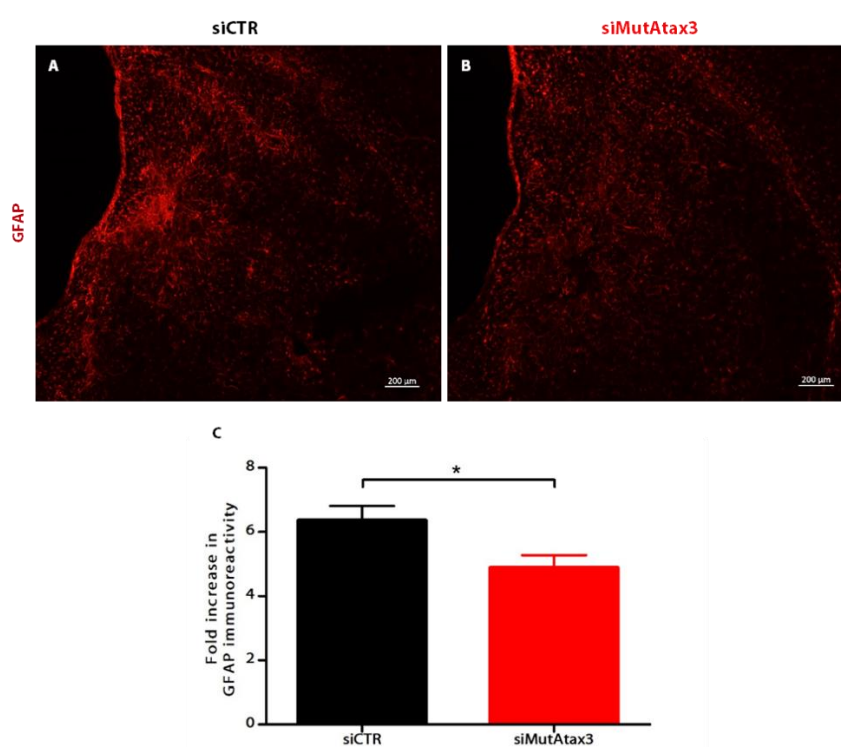


Figure 3.6. RVG-9r-targeted SNALPs decrease neuroinflammation in a lentiviral mouse model of MJD. Immunohistochemical analysis 4 weeks post-injection of lentiviral vectors encoding for the human mutant ataxin-3. **(A, B)** GFAP immunoreactivity after intravenous administration of RVG-9r-targeted liposomes encapsulating siCTR (A) or siMutAtax3 (B). **(C)** Quantification of the fold increase of GFAP immunoreactivity in the injected striatum (right striatum), when compared to the non-injected striatum (left striatum). Values are presented as mean \pm SEM of n=5. Student's t-test was used to compare animals injected with siMutAtax3 to siCTR (*p<0.05).

According to what we previously reported (Duarte-Neves *et al.*, 2015), we found a strong immunoreactivity for a microglia/macrophage-specific calcium-binding protein (Iba-1) in the injected striata, when compared to the non-injected one, revealing microglia activation in the lesion site. However, intravenous administration of RVG-9r-targeted SNALPs did not significantly decrease Iba-1 immunoreactivity (Fig. 3.6D-F), although a slight tendency for diminished Iba-1 staining was observed.

Overall, our data suggest that non-invasive silencing of mutant ataxin-3 improved the neuroinflammation phenotype in this lentiviral mouse model of MJD.

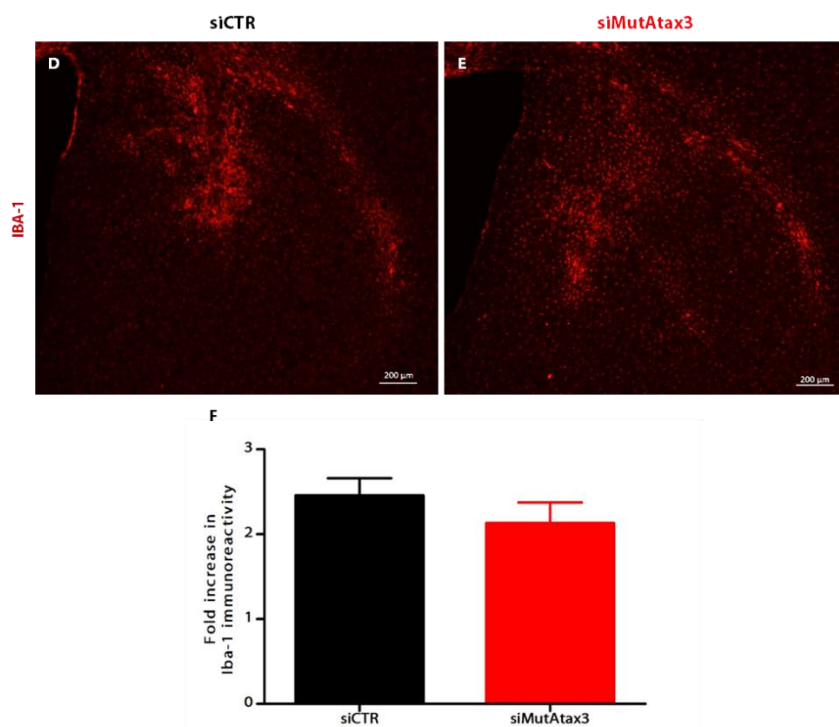


Figure 3.7. RVG-9r-targeted SNALPs do not significantly change Iba-1 immunoreactivity in a lentiviral mouse model of MJD. Immunohistochemical analysis 4 weeks post-injection of lentiviral vectors encoding for the human mutant ataxin-3. (A, B) Iba-1 immunoreactivity after intravenous administration of RVG-9r-targeted liposomes encapsulating siCTR (A) or siMutAtax3 (B). (C) Quantification of the fold increase of Iba-1 immunoreactivity in the injected striatum (right striatum), when compared to the non-injected striatum (left striatum). Values are presented as mean±SEM of n=5. Student's t-test was used to compare animals injected with siMutAtax3 to siCTR (*p<0.05).

3.5. Discussion

RNAi-based therapies represent an enormous therapeutic potential for several diseases that remain untreatable, particularly for monogenic diseases that are triggered by the production of a diseased-protein, such as MJD. However, until now, there is no study evaluating the impact of a non-viral and non-invasive strategy, which has a higher probability for clinical translation, in MJD animal models. Therefore, in this part of the work, we tested if intravenous administration of brain-targeted SNALPs could alleviate the striatal neuropathology in a lentiviral-based mouse model of MJD, that we have previously developed (Simões *et al.*, 2012). Our results demonstrate that RVG-9r-targeted SNALPs, upon intravenous administration a) deliver siRNAs into the striatum, b) silence mutant ataxin-3 expression, c) decrease the number of ubiquitin-positive inclusions and d) mediate neuroprotection, in this striatal lentiviral-based mouse model of MJD.

The ataxin-3 protein is ubiquitously expressed in neuronal and non-neuronal tissues (do Carmo Costa *et al.*, 2004; Ichikawa *et al.*, 2001; Nishiyama *et al.*, 1996; Paulson *et al.*, 1997a; Paulson *et al.*, 1997; Schmidt T, 1998) and its function has been linked to several essential cell pathways. Therefore, selective inhibition of the mutant allele has a higher probability to translate into a successful treatment for humans and for that reason, in our studies, we used an allele-specific silencing approach. The silencing sequences used in our experiments were targeted to a single nucleotide polymorphism that can be found in 70% of MJD patients, according to what we have previously reported (Alves *et al.*, 2008a). The selectivity of this approach was previously demonstrated *in vitro* and *in vivo* and consequently, in our study, we did not further investigate this particular question.

The lentiviral-based rodent models overexpressing the full-length human mutant ataxin-3, that we have been using during the last years, allow the quantitative analysis of neuropathological deficits with high precision, enabling to test therapeutic hypothesis in a short period of time (Alves *et al.*, 2008a; Alves *et al.*, 2010; Alves *et al.*, 2008b; Duarte-Neves *et al.*, 2015; Gonçalves *et al.*, 2013; Nascimento-Ferreira *et al.*, 2013; Nascimento-Ferreira *et al.*, 2011; Nóbrega *et al.*, 2013a; Nóbrega *et al.*, 2014; Simões *et al.*, 2012). Similarly to what we previously reported with intracranial administration of lentivirus

codifying for the silencing sequences (Alves *et al.*, 2008a; Alves *et al.*, 2010; Nóbrega *et al.*, 2014), we found that intravenous administration of RVG-9r-targeted SNALPs promoted a significant reduction in the number of ubiquitin-positive inclusions in the mouse striatum (Fig. 3.3). Importantly, our strategy mediated neuroprotection as shown by the dramatic decrease in i) neuronal dysfunction (reduced DARPP-32 loss, Fig. 3.4), ii) striatal degeneration (lower volume of condensed nuclei, Fig. 3.5) and iii) neuroinflammation (decrease in GFAP immunoreactivity, Fig. 3.6).

The main barrier for the successful clinical application of siRNAs for the treatment of dominantly-inherited neurodegenerative disorders is the lack of an efficient formulation to enable the delivery of siRNAs to the CNS by a non-invasive administration. Consequently, the vast majority of the successful experiments using RNAi-based therapeutics in animal models of neurodegenerative diseases, such as Huntington's disease (Boudreau *et al.*, 2009; Drouet *et al.*, 2009; Grondin *et al.*, 2012; Harper *et al.*, 2005; Huang *et al.*, 2007a; Machida *et al.*, 2006; McBride *et al.*, 2011; Rodriguez-Lebron *et al.*, 2005), SCA1 (Keiser *et al.*, 2014; Keiser *et al.*, 2013; Xia *et al.*, 2004), SCA3 (Alves *et al.*, 2008a; Alves *et al.*, 2010; Costa Mdo *et al.*, 2013; Nóbrega *et al.*, 2014; Nóbrega *et al.*, 2013b; Rodriguez-Lebron *et al.*, 2013), SCA7 (Ramachandran *et al.*, 2014), Alzheimer's (Piedrahita *et al.*, 2010; Rodriguez-Lebron *et al.*, 2009; Singer *et al.*, 2005) or Parkinson's disease (Gorbatyuk *et al.*, 2010; Khodr *et al.*, 2011; Sapru *et al.*, 2006) were performed through an invasive intracranial administration of viral vectors, mainly adeno-associated virus or lentivirus. Non-viral systems are theoretically safer and would reach patients within a shorter time-frame, when compared to the use of viral vectors and the need for craniotomy that they engage. Moreover, they provide silencing effects for a limited period of time, which is a distinctive advantage that makes possible to stop or adapt the treatment if there is the development of side effects. Indeed, there are also some reports showing the beneficial effects of non-viral silencing in Huntington's disease animal models, however, invasive administrations (intracranial or intracerebroventricular injections) were also used in these studies (Carroll *et al.*, 2011; DiFiglia *et al.*, 2007; Kordasiewicz *et al.*, 2012; Østergaard *et al.*, 2013; Stiles *et al.*, 2012; Wang *et al.*, 2005; Yu *et al.*, 2012). Notably, to our best knowledge, our study represents the first report showing

the positive impact of a non-viral strategy in MJD and the first time that a non-invasive systemic administration proved to be beneficial on a polyglutamine disorder.

In summary, we show that a clinically-relevant nanoparticle-based formulation dramatically reduced the striatal neuronal dysfunction and degeneration induced by mutant ataxin-3 expression, in a lentiviral-based mouse model of MJD. Our study shows that brain-targeted SNALPs are a promising therapeutic strategy for MJD.

CHAPTER 4

Non-invasive silencing of mutant ataxin-3 attenuates behavioral deficits and neuropathology in a cerebellar transgenic mouse model of Machado-Joseph disease

4.1. Abstract

Others and we showed that RNA interference holds great promise for the treatment of dominantly inherited neurodegenerative disorders such as Machado-Joseph disease (MJD), for which there is no available treatment. However, successful experiments involved intracranial administration of viral vectors and there is a need for a safer and less invasive procedure. As the cerebellum is one of the mostly affected brain regions in MJD patients, in this work, we evaluated the efficacy and outcomes of mutant ataxin-3 silencing using RVG-9r-targeted SNALPs in a cerebellar-transgenic mouse model of MJD. We observed that intravenous administration of these liposomes was able to deliver siRNAs and suppress mutant ataxin-3 in the cerebellum of this MJD transgenic mouse model. Importantly, non-viral silencing of mutant ataxin-3 by intravenous administration resulted in alleviation of the motor impairments and MJD-associated neuropathology, apparently without inducing toxic effects. To our knowledge, this is the first report showing a beneficial impact of a non-viral strategy in MJD, and the first time that a non-invasive systemic administration proved to be beneficial on a polyglutamine disorder. Our studies open new avenues towards MJD therapy that can also be applied to other neurodegenerative diseases linked to the production of pathogenic proteins.

4.2. Introduction

Machado-Joseph disease (MJD) or spinocerebellar ataxia type 3 (SCA3) is the most common autosomal dominantly-inherited ataxia worldwide (Schols *et al.*, 2004). Clinical manifestations are heterogeneous, but progressive ataxia, a dysfunction of motor coordination that can affect gaze, speech, gait and balance is the clinical hallmark of the disease (Taroni, 2004). Genetically, this disorder is caused by the over-repetition of a CAG tract in the coding region of the ATXN3/MJD1 gene, which confers a toxic gain-of-function to the ataxin-3 protein (Kawaguchi *et al.*, 1994). While in healthy individuals normal alleles range from 12 to approximately 43 CAG repeats, MJD patients present between ~60 and 87 CAG repeats in the mutant allele (Cancel G, 1995; Dürr A, 1996; Maciel *et al.*, 1995; Matilla *et al.*, 1995; Matsumura *et al.*, 1996; Ranum *et al.*, 1995; Sasaki *et al.*, 1995). Neuronal intranuclear inclusions that result from mutant ataxin-3 accumulation are the hallmark of the disease (Paulson *et al.*, 1997) and give rise to neuronal dysfunction and degeneration within different brain regions, particularly the cerebellum, brainstem, substantia nigra and striatum (Alves *et al.*, 2008b; Dürr A, 1996; Rüb *et al.*, 2008; Rüb *et al.*, 2013; Scherzed *et al.*, 2012; Seidel *et al.*, 2012; Sudarsky and Coutinho, 1995; Taniwaki *et al.*, 1997; Wullner *et al.*, 2005). Although this is an extremely debilitating disorder, there is currently no available treatment to modify disease progression.

The extensive research on molecular mechanisms underlying MJD pathogenesis brought to light several studies that revealed potential therapeutic options for MJD management in the future. But one of the most direct and promising approaches towards MJD therapy is the use of the RNA interference (RNAi) mechanism to block the production of the disease-causing protein, before deleterious effects happen. Until now, successful experiments involving intracranial administration of viral vectors showed that silencing mutant ataxin-3 in MJD animal models is beneficial (Alves *et al.*, 2008a; Alves *et al.*, 2010; Costa Mdo *et al.*, 2013; Nóbrega *et al.*, 2014; Nóbrega *et al.*, 2013b; Rodriguez-Lebron *et al.*, 2013). However, craniotomy and injection of viral vectors into the brain parenchyma is an invasive surgical procedure, for which there are still safety concerns, and that results in a circumscribed expression around the injection site that may be insufficient to treat all the disease-relevant brain regions. There is a need for a less invasive procedure that could

reach patients within a shorter time-frame and also able to deliver the silencing sequences throughout the widespread affected brain regions.

Until now, there is no study evaluating the impact of a non-invasive and non-viral strategy in MJD animal models. As the cerebellum is one of the most affected brain regions in MJD patients, that has an essential role in motor coordination, the goal of the present study was to evaluate the therapeutic potential of RVG-9r-targeted SNALPs in a severely impaired cerebellar-transgenic mouse model of MJD (Torashima *et al.*, 2008), when initiated after disease onset. The transgenic mouse model used in this study expresses a truncated form of human mutant ataxin-3 with 69 CAG repeats that results in an early and severe MJD phenotype, being particularly suitable for pre-clinical studies (Torashima *et al.*, 2008). This animal model expresses the mutant protein predominantly in Purkinje cells and presents poor dendritic arborization of Purkinje cells, cerebellar atrophy and severe ataxia. Importantly, our results indicate that non-invasive silencing of mutant ataxin-3 by RVG-9r-targeted SNALPs alleviates motor deficits and MJD-associated neuropathology in this severely impaired transgenic mouse model of MJD.

4.3. Materials and Methods

4.3.1. Materials

Materials used in these studies were the same that were mentioned in chapter 2.

4.3.2. Mice

C57BL/6 ataxin-3 [Q69]-transgenic (Torashima *et al.*, 2008) or wild-type mice were used. Animals were maintained and experiments carried out as referred in chapter 2.

4.3.3. Synthesis and characterization of stable nucleic acid lipid particles

Synthesis and characterization of RV-MAT-9r or RVG-9r-targeted SNALPs was performed as described in chapter 2.

4.3.4. Analysis of siRNA delivery to the cerebellum by flow cytometry

6-to-7-weeks-old ataxin-3 [Q69]-transgenic mice were intravenously injected with 2.5 mg/kg of FAM-labeled siRNA encapsulated in RV-MAT-9r- or RVG-9r-targeted liposomes. Three hours after injection, animals were sacrificed by intracardiac perfusion with 20 mL of ice-cold PBS and cerebellum was isolated and homogenized to analyze by flow cytometry. FAM detection was performed through an indirect method using BD Cytotfix/Cytoperm kit (BD Biosciences). For each condition $\sim 1 \times 10^6$ cells were incubated with an anti-FITC antibody (clone FL-D6; 1:100) for 30 minutes at 4°C, in triplicate. Next, cells were incubated with an Alexa Fluor 488-conjugated anti-mouse secondary antibody (1:100; Molecular Probes) for 30 minutes at 4°C. Alexa Fluor 488 fluorescence for all samples was then evaluated in the FL-1 channel of a FACS Calibur flow cytometer collecting 10,000 events. Data were analyzed using Cell Quest Pro software.

4.3.5. Evaluation of the silencing efficiency of mutant ataxin-3 levels in the cerebellum of a MJD transgenic mouse model

5-weeks-old C57 BL/6 ataxin-3 [Q69] transgenic mice were intravenously injected on three consecutive days with 2.5 mg/kg of siRNA (siEGFP or siMutAtax3) encapsulated in RVG-9r-targeted liposomes or HEPES-buffered saline solution (HBS). To analyze mutant ataxin-3 levels, mice cerebella were harvested 48 hours after the third injection. Half of the cerebellum was used to detect mRNA levels by qRT-PCR and the other half to detect mutant ataxin-3 aggregate levels by Western Blot.

To detect cerebellar mRNA levels, total RNA was extracted using Qiazol solution (Qiagen) followed by purification of the RNA product using the Nucleospin RNA kit (Macherey-Nagel, GmbH & Co. KG, Düren, Germany). cDNA synthesis and quantitative PCR was performed as described in materials and methods of chapter 2, with slight modifications. Briefly, to determine the levels of mutant ataxin-3, we used 2.5 μ L of cDNA diluted 10 times and an annealing temperature of 55°C. For IL-1 β , IL-6 and TNF- α we used 2.5 μ L of cDNA diluted 4 times and annealing temperature of 61°C. For Cebpb we used 2.5 μ L of cDNA diluted 10 times and annealing temperature of 60°C. Pre-designed primers used in these studies (mouse HPRT, IL-1 β , IL-6, TNF- α and Cebpb) were obtained from Qiagen, and primers to detect the truncated form of human mutant ataxin-3 were synthesized by Eurofins, MGW Operon, according to what was previously reported (Torashima *et al.*, 2008). The respective catalog number and sequences can be found in Table 4.1. The levels of the target gene were calculated using HPRT as housekeeping gene. The mRNA relative quantification was performed with the Pfaffl method relatively to control samples.

Table 4.1. Primers sequences or catalog number

Primer	Brand	Sequence/Catalog Number
Human Ataxin-3 [Q69] (Torashima <i>et al.</i>, 2008)	Eurofins, MGW Operon	<i>Forward:</i> 5'GGACCTATCAGGACAGAGTTC3'
		<i>Reverse:</i> 5'CATGGAGCTCGTATGTCAGATA3'
Mouse HPRT	Qiagen	QT00166768
Mouse IL-1β	Qiagen	QT01048355
Mouse IL-6	Qiagen	QT00098875
Mouse TNF-α	Qiagen	QT00104006
Mouse Cebpb	Qiagen	QT00320313

To analyze mutant ataxin-3 aggregates levels, *cerebella* were homogenized using RIPA lysis buffer mixed with a protease inhibitor cocktail and 2mM of dithiothreitol. The lysate was further sonicated and protein concentration estimated through the Bradford method (Bio-Rad Protein Assay, Bio-Rad). Fifty micrograms of total denatured protein were then loaded in a 4% stacking, 10% resolving polyacrylamide gel for electrophoretic separation. The remaining protocol was performed as described in materials and methods of chapter 2. Immunoblotting was performed using the mouse monoclonal antibody anti HA-tag (1:1,000; InvivoGen, San Diego, CA) and mouse monoclonal anti- β -tubulin 1 (clone SAP.4G5; 1:10,000; Sigma-Aldrich).

4.3.6. Motor behavioural assessment

4.3.6.1. Experimental design

To evaluate the impact of mutant ataxin-3 silencing on motor behavior, C57 BL/6 ataxin-3 [Q69] transgenic mice were intravenously injected with HBS, RVG-9r-targeted liposomes encapsulating siMutAtax3 or siCTR (siEGFP). For each group, six animals were injected, in which half were male and the other half female. Behavioural assessment started with 4-week-old animals (T_0) to train them before evaluation of the motor behaviour. Mice were tail-vein injected with 2.5 mg/kg of siRNA (each injection) and each mouse received a total of nine tail-vein injections during the time-course of the experiment. The first three injections were performed on three consecutive days when they were 5-weeks-old, and then the remaining were administered once a week from the second week after starting the treatment (please refer to the timeline, schematically represented in Fig. 4.4). Behavioural assessment was performed every one week until the fourth week after starting the treatment, and then on the sixth and eighth week. All tests were performed in a dark and quiet room, after one hour of acclimatization. Body weight was also evaluated over time.

4.3.6.2. Beam walking analysis

We assessed motor coordination and balance of mice by measuring the time that mice took to cross a beam in seconds, until they reached an enclosed escape platform. We used

two 9 mm beams, a squared one which was easier to cross and a rounded one more difficult to cross. The beams were placed horizontally and raised to a height of approximately 20 cm, and mice had to traverse 40 cm to reach the safe platform. The evaluation was performed progressing from the easiest to the most difficult one. Mice performed four trials for each beam in each time-point, with at least 20 minutes of rest between trials. The mean latency time each animal spent to cross the two beams was recorded. We allowed a maximum of 60 seconds for mice to reach the safe platform.

4.3.6.3. Swimming performance

We evaluated swimming performance in a long narrow swimming pool made of glass, 70 cm long, 12.5 cm wide and with 19.5 cm height-walls. The pool had a platform 8.5 cm high at one end, onto which the animals could climb. The pool was filled with water with temperature around 25°C, until the platform level. Mice performed four trials for each time-point, with at least 20 minutes of rest between trials. The mean latency time each animal spent (in seconds) to swim across the pool and climb the platform (with its four paws) was recorded.

4.3.6.4. Footprint pattern analysis

Gait was evaluated performing footprint analysis, in which the fore and hind paws of the animal were painted with non-toxic dyes of different colors and mice were encouraged to walk in a straight line. The catwalk consisted in a sheet of green paper positioned in a platform 100 cm long, 10 cm wide and with 15 cm height-walls. We measured two parameters of the footprint pattern – overlap and stride length. To measure the uniformity of step alternation, the overlap distance between the center of the fore- and hind-paw placement was quantified. Measurements were performed over a sequence of five consecutive steps, on the left and right sides and the mean from 10 measurements (5 left, 5 right) was recorded. To measure the stride length, the average distance of forward movement between each stride was quantified. Measurements were performed over a sequence of five consecutive steps, for both fore and hindpaws of the animal (left and right, 20 measurements). The final results represent the mean value for the fore and hindpaw stride length.

4.3.6.5. RotaRod Performance

Motor coordination and balance of the animals were analyzed using a rotarod apparatus (Leticia Scientific Instruments, Panlab), measuring the latency to fall (in seconds). The rotarod performance was evaluated at a constant speed (5 rpm) and at an accelerated speed (4 to 40 rpm), both for a maximum of 5 minutes. Mice performed four trials per time-point (first for rotarod at constant speed and then for rotarod at an accelerated speed), with at least 20 minutes of rest between trials.

4.3.7. Neuropathology evaluation

4.3.7.1. Tissue preparation

After an overdose of avertin anesthesia, mice were intracardiacally perfused with 10 mL of PBS followed by 40 mL of 4% paraformaldehyde (PFA) using a perfusion pump (perfusion rate of 2.5 mL per minute). The brains were then removed and post-fixed in 4% PFA for 24 hours, cryoprotected by incubation for 48 hours in 25% sucrose at 4°C and then frozen at -80°C. 30 µm sagittal sections were cut using a cryostat (Leica CM3050S, Wetzlar, Germany) and stored in 48-well-plates as free-floating sections in PBS supplemented with 0.05 mM of sodium azide. For each animal, three 48-well-plates with one sagittal section per well were collected, and the trays stored at 4°C until immunohistochemical processing.

4.3.7.2. Fluorescence immunohistochemical procedure

Immunohistochemical procedure was performed as we previously reported (Mendonça *et al.*, 2015) with very few alterations. Briefly, the protocol was initiated with 1 h of blocking and permeabilization in 0.3% Triton X-100 10% normal goat serum prepared in PBS at room temperature. Sections were then incubated overnight at 4°C with the following primary antibodies prepared in 2% normal goat serum 0.05% Triton X-100 (in PBS): rabbit polyclonal anti-calbindin (1:1000, Millipore), mouse monoclonal anti-HA (1:1000, InvivoGen) or rabbit polyclonal anti-Iba1 (1:1000, Wako). Sections were washed three times with PBS and incubated with the corresponding secondary antibodies coupled to fluorophores, prepared in 2% normal goat serum (Gibco), goat-anti rabbit or mouse

conjugated to Alexa Fluor 594 or 568 (1:250, Molecular Probes, Eugene, Oregon, USA) for 2 h at room temperature. Nuclei staining was performed with DAPI, sections were washed three times with PBS and then mounted on gelatinized slides. After being dried, slides were mounted in Mowiol reagent. Widefield fluorescence images were acquired with x20 and x40 objective on a Zeiss Axiovert 200 imaging microscope.

4.3.7.3. Cresyl Violet staining

Sections were pre-mounted on gelatinized slides and stained with cresyl violet for 5 minutes, differentiated in 70% ethanol, dehydrated by passing through 96% ethanol, 100% ethanol and xylene solutions and mounted with Eukitt.

4.7.3.4. Quantification of Purkinje cell number, mutant ataxin-3 aggregates and thickness of the cerebellar layers

Quantitative analysis of Purkinje-cell number (calbindin-positive cells), mutant ataxin-3 aggregates (haemagglutinin-positive aggregates) and thickness of the cerebellar layers was performed by scanning six sections per animal that were distanced 240 µm from each other (to obtain representative images of the cerebellum). Cerebellar sections were imaged using the MosaiX feature of the Axiovision software (Zeiss) using Zeiss PALM Axiovert 200M microscope with x20 objective. The quantifications were then performed for all lobules of the cerebellum using an image-analysis software (Image J software, NIH, USA). The thickness of the cerebellar layers was assessed in the intersections of the cerebellar lobules.

4.3.8. Quantification of IL-6 serum levels by ELISA

Quantification of IL-6 serum levels for animals subjected to intravenous administration of RVG-9r-targeted SNALPs or HBS, was performed in duplicate, using 50 µl of serum and the Mouse IL-6 ELISA Kit from Merck Millipore according to the manufacturer's protocol. As a positive control, one wild-type animal (with approximately 20 g) was intraperitoneally injected with 200 µg of lipopolysaccharides (LPS) from *Escherichia coli* O26:B6.

4.3.9. Statistical analysis

Data are presented as mean \pm standard error of mean (SEM) of at least three independent experiments. Student's *t*-test or one-way ANOVA combined with Bonferroni's post-test were used to determine statistically significant differences of the means. Statistical differences are presented at probability levels of * $p < 0.05$, ** $p < 0.01$ and *** $p < 0.001$ and considered non-significant (n.s.) when $P < 0.05$. Calculations were performed using GraphPad Prism version 5.00 for Windows (San Diego, CA).

4.4. Results

4.4.1. RVG-9r-targeted SNALPs deliver siRNAs and suppress mutant ataxin-3 in the cerebellum of a Machado-Joseph disease transgenic mouse model

First, to clarify if the RVG-9r-targeted SNALPs would be efficient in delivering their encapsulated siRNAs to the cerebellum of a cerebellar transgenic mouse model of MJD, mice were tail-vein injected with RV-MAT-9r or RVG-9r-targeted liposomes encapsulating 5-carboxyfluorescein (FAM)-labeled siRNAs. Three hours after injection, cerebellar homogenates were analyzed, as represented in Fig. 4.1A. Flow cytometry data showed that RVG-9r increased FAM-labeled siRNAs accumulation in the cerebella of the injected animals (Fig. 4.1B, C), despite the reduced vascularization of these transgenic animals.

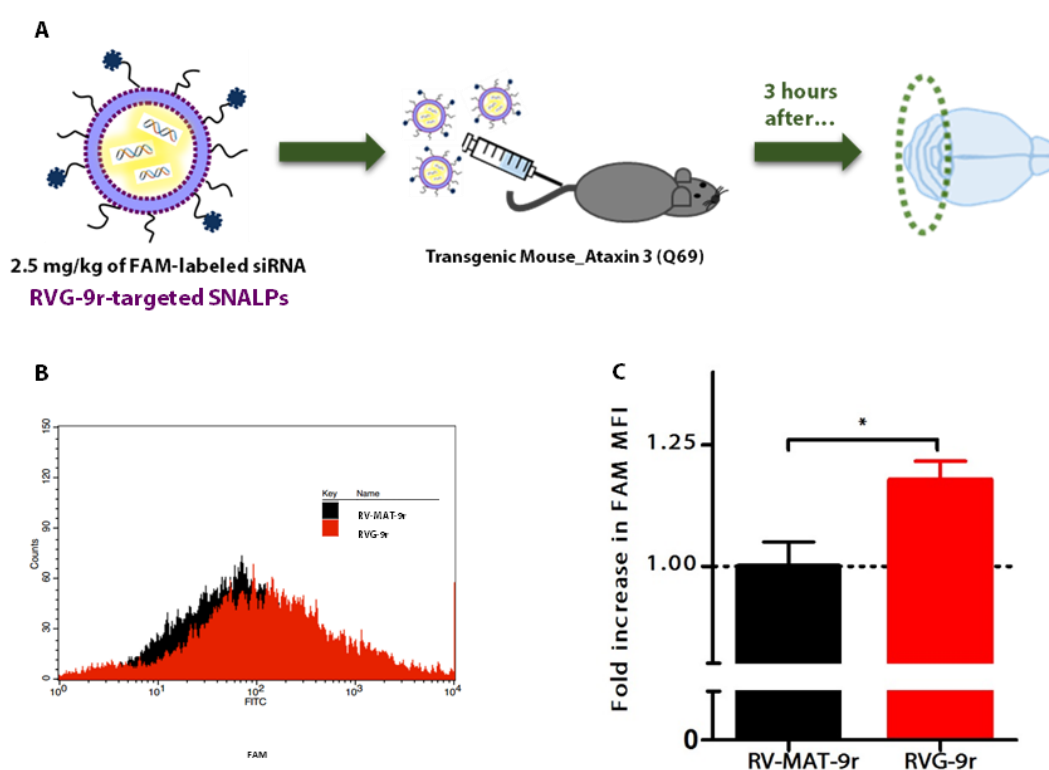


Figure 4.1. siRNA delivery to the cerebellum upon intravenous administration of RVG-9r-targeted liposomes. (A) C57 BL/6 ataxin-3 [Q69] transgenic mice were intravenously injected with 2.5 mg/kg of FAM-labeled siRNA encapsulated in RV-MAT-9r or RVG-9r-targeted liposomes. Three hours after injection, mice were sacrificed and cerebella homogenized for analysis by flow cytometry. **(B)** Representative histogram of the FAM fluorescence in cerebellar cells of mice injected with RV-MAT-9r (black) or RVG-9r targeted liposomes (red). **(C)** Fold increase in FAM MFI in the cerebellum of animals injected with RVG-9r-targeted liposomes, comparatively to mice injected with RV-MAT-9r-targeted liposomes. Values are presented as mean±SEM of n=3.

Student's t-test was used to compare animals injected with RVG-9r- to RV-MAT-9r-targeted liposomes (*p<0.05).

Following confirmation of the *in vivo* delivery of siRNAs to the cerebellum of MJD transgenic mice, we then evaluated whether RVG-9r-targeted SNALPs could suppress mutant ataxin-3 in the cerebellum of these animals. This MJD transgenic mouse model expresses a truncated form of human ataxin-3 with 69 CAG repeats predominantly in Purkinje cells of the cerebellum and exhibits a drastic neurological phenotype adequate for pre-clinical studies (Torashima *et al.*, 2008). C57BL/6 ataxin-3 [Q69]-transgenic mice were intravenously injected on three consecutive days with siMutAtax3 or siCTR encapsulated in RVG-9r-targeted liposomes or with a saline solution (HBS, control). To analyze mutant ataxin-3 levels, mouse cerebella were harvested 48 hours after the third injection (Fig. 4.2A). qRT-PCR and western blot data show that intravenous administration of siMutAtax3, when compared to siCTR, significantly decreased mutant ataxin-3 mRNA and protein aggregate levels in the cerebellum of these animals by approximately 32±5.2% and 32±7.1%, respectively (Fig. 4.2B and C, respectively).

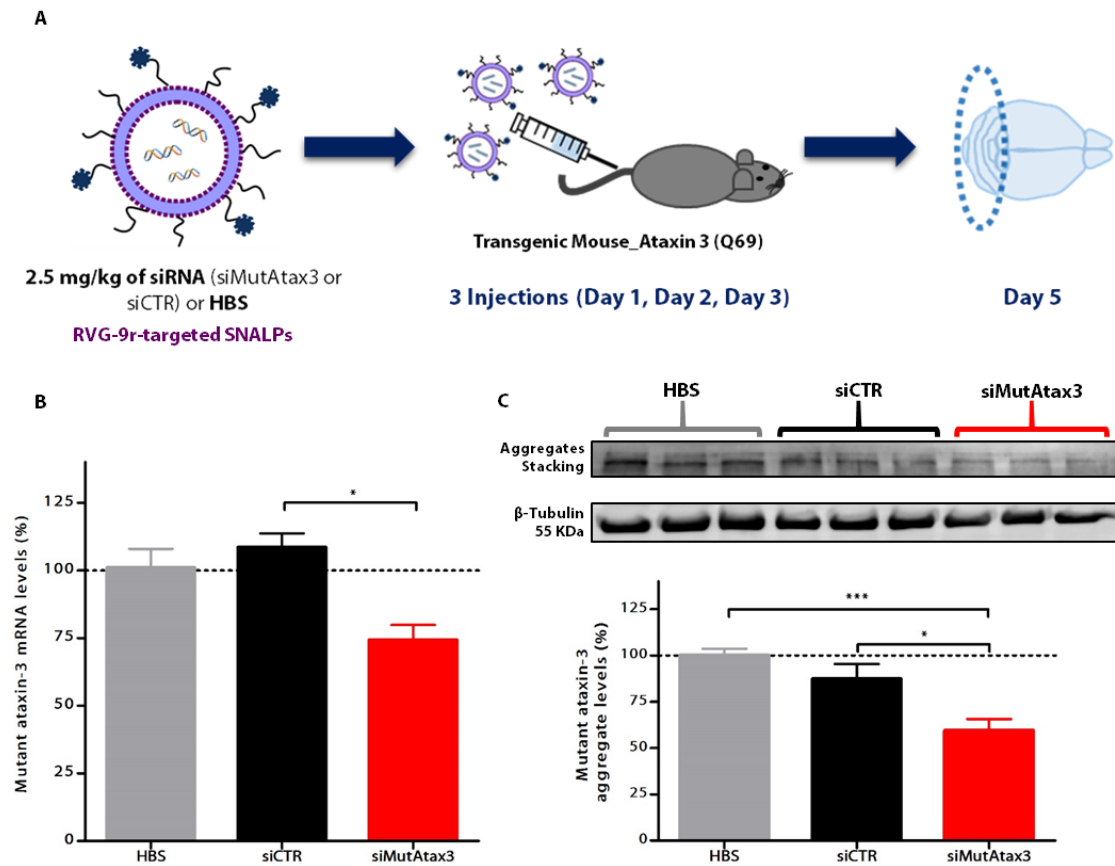


Figure 4.2. Mutant ataxin-3 silencing in the cerebellum after intravenous administration of RVG-9r-targeted liposomes encapsulating siMutAtax3. (A) C57 BL/6 ataxin-3 [Q69] transgenic mice were intravenously injected on three consecutive days with 2.5 mg/kg of siRNA (siCTR or siMutAtax3) encapsulated in RVG-9r-targeted liposomes or HEPES-buffered saline solution (HBS, control). To analyze mutant ataxin-3 levels, mouse cerebella were harvested 48 hours after the third injection. (B) Mutant ataxin-3 mRNA levels were detected by qRT-PCR. Results were normalized using HPRT housekeeping gene and show the levels of mutant ataxin-3 mRNA for animals injected with RVG-9r-targeted SNALPs when compared with mice injected with HBS. (C) Representative membrane showing mutant ataxin-3 aggregate levels in treated and saline-injected mice. Mutant ataxin-3 aggregate levels were detected by Western Blot. Normalization of protein levels was made with β -tubulin protein endogenous levels. The results show the levels of mutant ataxin-3 in treated animals, compared to non-treated ones (HBS-injected). Values are presented as mean \pm SEM of at least 4 independent experiments. One-way ANOVA analysis of variance combined with Bonferroni's post-test was used for multiple comparisons (***p<0.001, *p<0.05).

4.4.2. Intravenous administration of RVG-9r-targeted SNALPs does not stimulate the production of pro-inflammatory cytokines or a microglia-related gene in the cerebellum

To investigate whether intravenous administration would contribute to inflammation, which could preclude repeated administration, we evaluated the mRNA levels of pro-inflammatory cytokines (IL-1 β , IL-6 and TNF- α) and a microglia-related gene (Cebpb) in the cerebella of these animals. No significant difference in the mRNA levels of these mediators were detected between HBS-injected mice or mice injected with RVG-9r-targeted SNALPs (Fig. 4.3A and B).

Altogether, these results demonstrate that intravenous administration of RVG-9r-targeted SNALPs is able to safely suppress mutant ataxin-3 in the cerebellum of a transgenic mouse model of Machado-Joseph disease.

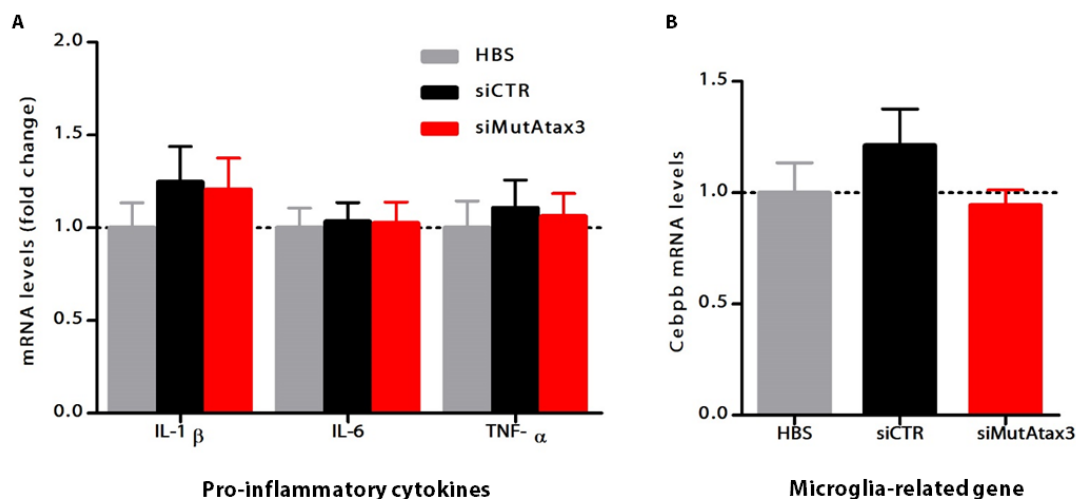


Figure 4.3. Intravenous administration of RVG-9r-targeted SNALPs do not stimulate the production of pro-inflammatory cytokines neither the activation of microglia. (A) mRNA relative levels of pro-inflammatory mediators (IL-1 β , IL-6 and TNF- α) in the cerebellum of MJD transgenic mice injected with RVG-9r-targeted SNALPs (black, red) relatively to animals injected with HBS (grey). Results were normalized using HPRT housekeeping gene. **(B)** mRNA relative levels of a microglia-related gene – Cebpb – in the cerebellum of MJD transgenic mice. Values are presented as mean \pm SEM of at least 4 independent experiments. One-way ANOVA analysis of variance combined with Bonferroni's post-test was used for multiple comparisons (n.s. $p>0.05$).

4.4.3. Non-invasive silencing of mutant ataxin-3 alleviates motor disabilities

Having shown that our formulation was efficient in silencing mutant ataxin-3 in the cerebellum of this transgenic mouse model, we then investigated its potential to promote the recovery of motor performance. The transgenic mouse model used in this study exhibits a severe ataxic phenotype that may be detected very early, even before mice are 3 weeks-old (Torashima *et al.*, 2008).

Three groups of transgenic animals were evaluated over-time: mice intravenously injected with a saline solution (HBS), RVG-9r-targeted liposomes encapsulating siCTR and RVG-9r-targeted liposomes encapsulating siMutAtax3.

Tail-vein injections and behavioural assessment were performed as represented in Fig. 4.4A. Motor behaviour assessment was conducted by performing the following tests: beam walking, swimming, footprint analysis and rotarod. As shown in Fig. 4.4B, the treatment was well tolerated and did not interfere with body weight gain. Accordingly, the ratio of body weight gain between the beginning and end of the experiment was 1.64 for transgenic animals injected with HBS, 1.70 for transgenic animals injected with RVG-9r-targeted liposomes encapsulating siCTR and 1.75 for transgenic animals injected with RVG-9r-targeted liposomes encapsulating siMutAtax3.

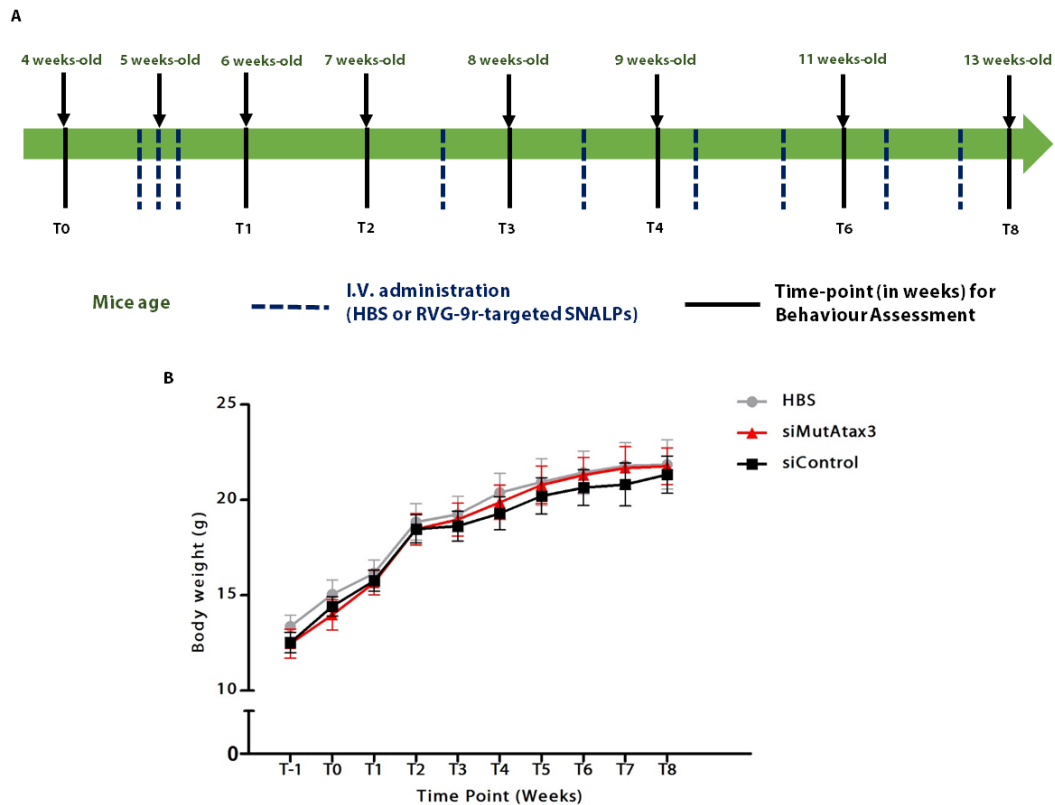


Figure 4.4. Timeline for behaviour assessment and body weight evolution with time. (A) Timeline used to intravenously inject and to assess the behaviour of treated animals. Mice were intravenously injected with HBS, RVG-9r-targeted liposomes encapsulating siCTR or siMutAtax3, according to the schematic representation. Behavioural assessment was performed every one week until the 4th week after starting the treatment and then on week 6th and 8th. Mice were sacrificed eight weeks after starting the treatment. **(B)** Body weight evolution with time.

Note that to guarantee that mice performance was not different *ab anteriori* between the groups of treatment, mice were trained and differences assessed for all the motor behaviour tests before starting the treatment (T0, Fig. 4.5). For clarity, data is presented for transgenic animals treated with RVG-9r-targeted liposomes encapsulating siCTR *versus* siMutAtax3 (Fig. 4.5 and 4.6).

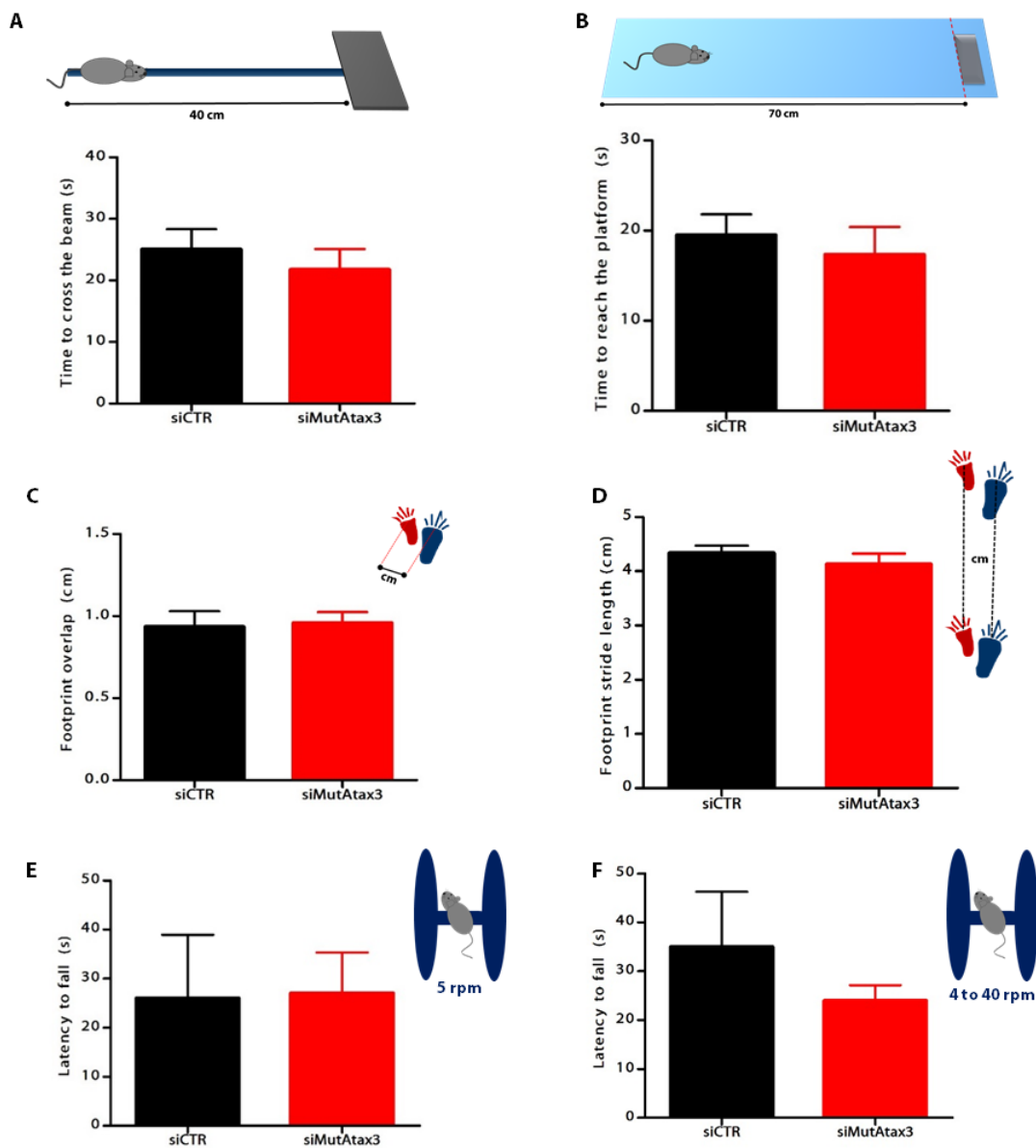


Figure 4.5. Behavioural assessment before starting the treatment (T0). (A) Beam walking: balance and motor coordination were measured by the mean time that mice took to cross the tested beams in seconds, at T0. (B) Swim test: motor coordination was evaluated by swimming performance, measuring the time that mice take to swim and reach a safe platform in seconds, at T0. (C, D) Footprint test: gait was analyzed by measuring the footprint overlap in cm (C, mean distance between forepaw and hindpaw placement) and footprint stride length (D, average distance of forward movement between each stride), at T0. (E, F) Rotarod performance: motor coordination was analyzed by measuring the mean latency time to fall in seconds at constant (E) and accelerated (F) velocity, at T0. Values are presented as mean±SEM of n=6. Student's t-test was used to compare animals injected with siMutAtax3 to siCTR (n.s. $p>0.05$).

To perform the beam walking test, we used two beams of increasing difficulty and measured the mean time each mouse spent to cross these in order to reach an enclosed safety platform. When compared to a control formulation (RVG-9r-targeted liposomes encapsulating siCTR), intravenous administration of RVG-9r-targeted liposomes encapsulating siMutAtax3 decreased significantly the time that mice spent to cross the elevated beams (Fig. 4.6A), over the time-course of the experiment.

We also evaluated swimming performance by recording the latency time each animal spent to swim across the pool and climb the platform. Although we did not observe a statistically significant difference between animals injected with siMutAtax3 and siCTR, during the time course of our experiment there was a clear tendency for mice treated with siMutAtax3 to take less time to swim and climb the platform (Fig. 4.6B).

The gait of the animals was analyzed by measuring footprint patterns: overlap and stride length. The footprint overlap was measured as the mean distance between forepaw and hindpaw placement. Healthy animals should perfectly superimpose forepaws and hindpaws as they walk, presenting values of footprint overlap close to zero, which increase with the severity of the motor behaviour defect. From the fourth week after starting the treatment until the end of the experiment, mice treated with siMutAtax3 revealed a significantly decreased (improved) footprint overlap compared to animals injected with siCTR (Fig. 4.6C). The footprint stride length was measured as the average distance of forward movement between each stride. When compared to wild type animals, transgenic mice present lower values of stride length. Although statistically non-significant, mice treated with siMutAtax3 revealed a tendency for an increased stride length compared to animals injected with siCTR (Fig. 4.6D).

The rotarod performance data did not show the same results, probably because of the higher variability verified in this test (Fig. 4.5E, F and Fig. 4.6E, F). Note that we only used 3 males and 3 females for each group, and the gender strongly influences rotarod performance.

Overall, our results indicate that non-invasive silencing of mutant ataxin-3 is able to alleviate motor impairments in this severely impaired Machado-Joseph disease transgenic mouse model.

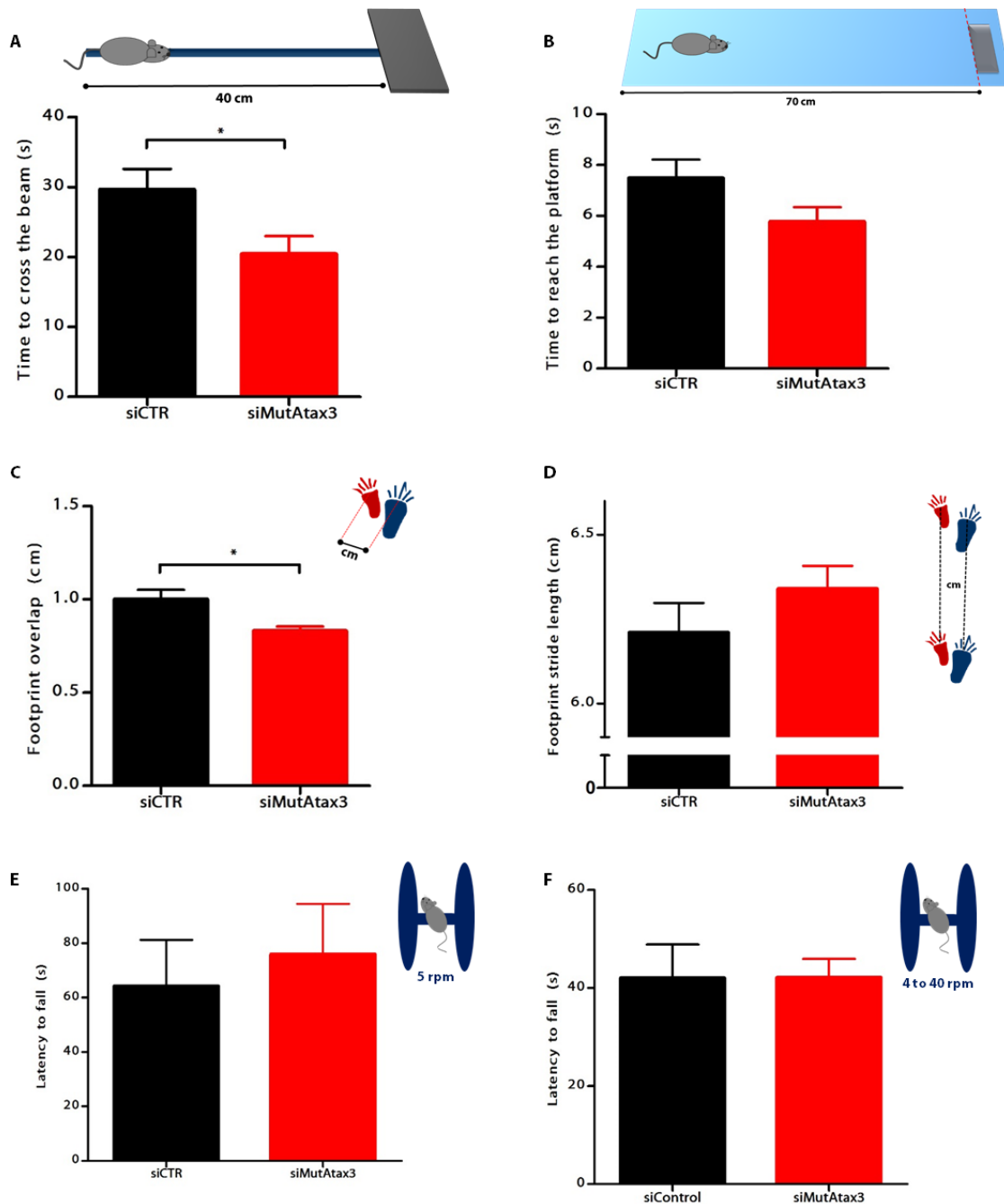


Figure 4.6. Intravenous administration of RVG-9r-targeted liposomes encapsulating siMutAtax3 alleviates motor behaviour disabilities of MJD transgenic mice. (A) Beam walking: balance and motor coordination were measured by the mean time that mice took to cross the tested beams in seconds, for all the time-points studied. **(B) Swim test:** motor coordination was evaluated by swimming performance, measuring the time that mice take to swim and reach a safe platform in seconds, for all the time-points studied. **(C, D) Footprint test:** gait was analyzed by measuring the footprint overlap in cm (C, mean distance between forepaw and hindpaw placement) and footprint stride length (D, average distance of forward movement between each stride) for 4th, 6th and 8th weeks time-points. **(E, F) Rotarod performance:** motor coordination was analyzed by measuring the mean latency time to fall in seconds at constant (E) and accelerated (F) velocity, for all the time-points studied. Values are presented as mean±SEM of n=6. Student's t-test was used to compare animals injected with siMutAtax3 to siCTR (*p<0.05).

4.4.4. Non-invasive silencing of mutant ataxin-3 attenuates cerebellar-associated neuropathology

Finally, we evaluated the impact of non-viral silencing of mutant ataxin-3 in the cerebellar-associated neuropathology, 8 weeks after starting the treatment. For this purpose, we quantified within the cerebellar region: the number of Purkinje cells, the number of mutant ataxin-3 aggregates and the thickness of the cerebellar layers.

Because C57BL/6 ataxin-3 [Q69]-transgenic mice express mutant ataxin-3 predominantly in Purkinje cells, we assessed whether silencing of mutant ataxin-3 would prevent Purkinje cell loss that is usually observed in this model (Torashima *et al.*, 2008). Our results suggest that intravenous administration of RVG-9r-targeted liposomes encapsulating siMutAtax3 may preserve the Purkinje cell number, when compared to siCTR, as shown by a tendency for higher number of calbindin-positive Purkinje cells for those animals (Fig. 4.7A-C).

As stated before, the neuronal intranuclear inclusions containing aggregated mutant ataxin-3 are one of the hallmarks of Machado-Joseph disease, and they are present in the Purkinje cells of this transgenic mouse model. Therefore, we evaluated whether silencing of mutant ataxin-3 could clear the mutant ataxin-3 aggregates from Purkinje cells. We observed that after intravenous administration of RVG-9r-targeted liposomes encapsulating siMutAtax3, when compared to siCTR, there was an almost significant decrease in the number of aggregates (HA-tag) per one hundred Purkinje cells (Fig. 4.7D-F).

Next, we evaluated the thickness of the cerebellar layers because this transgenic mouse model presents markedly cerebellar atrophy. Granular and molecular layers thickness were measured in the intersections of all lobules of the cerebellum upon cresyl violet staining, and revealed that mutant ataxin-3 silencing was able to significantly attenuate the cerebellar granular layer atrophy (Fig. 4.7G-I). Moreover, intravenous administration of RVG-9r-targeted liposomes encapsulating siMutAtax3 slightly attenuated the cerebellar molecular layer atrophy (Fig. 4.7G, H, J).

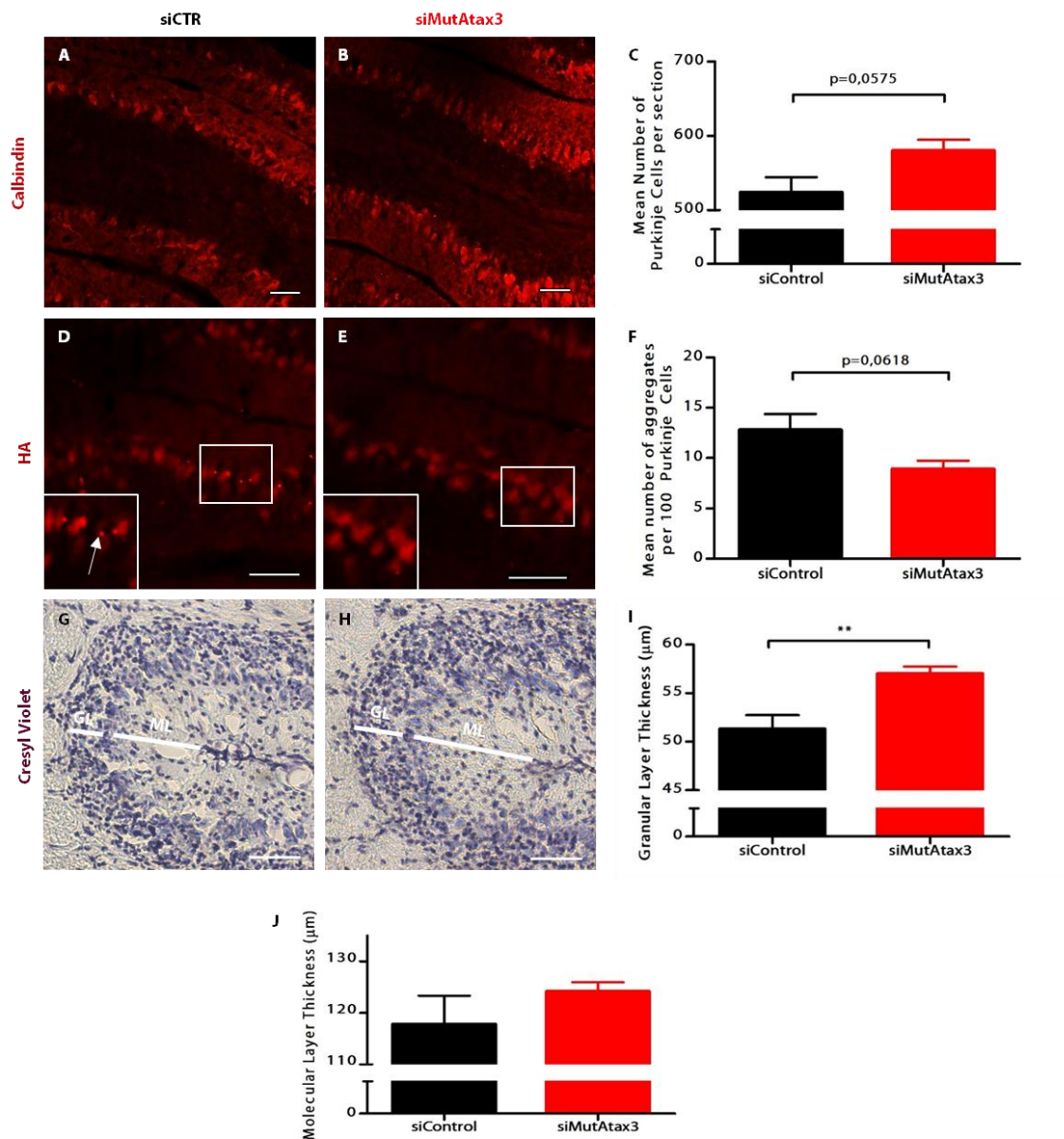


Figure 4.7. Intravenous administration of RVG-9r-targeted liposomes encapsulating siMutAtax3 attenuates cerebellar-associated neuropathology. 8 weeks after starting the treatment, mice were sacrificed and neuropathological features were evaluated by immunohistochemistry. (A, B) Fluorescence microscopy images of Purkinje cells stained with calbindin antibody (red) (C) Quantification of the mean number of Purkinje cells per section. (D, E) Fluorescence microscopy images of mutant ataxin-3 aggregates labeled with haemagglutinin (white arrow, HA). (F) Quantification of the mean number of aggregates per 100 Purkinje cells. (G, H) Visible microscopy images revealing granular layer thickness after cresyl violet staining. (I, J) Quantification of the mean granular (I) and molecular (J) layer thickness (μm) in the intersection of all lobules of the cerebellum. Scale bars, 50 μm. Values are presented as mean±SEM of n=5/6. Student's t-test was used to compare animals injected with siMutAtax3 to siCTR (**p<0.01 and n.s. p>0.05).

4.4.5. Intravenous administration of RVG-9r-targeted SNALPs stimulates IL-6 acute secretion

Given that a previous study suggested that intravenous administration of RVG-9r/siRNA complexes increased the levels of the IL-6 pro-inflammatory cytokine, we evaluated if RVG-9r-targeted SNALPs could result in a transient increase of IL-6 levels. We observed that, four hours after intravenous administration of RVG-9r-targeted SNALPs, we could detect increased levels of IL-6 (40 ± 12.5 pg/mL, Table 4.2).

Animal	Wild Type	
	Non-injected	RVG-9r-Liposomes siMutAtax3
IL-6 levels (pg/mL)	0	39.75 ± 12.5

Table 4.2. Intravenous administration of RVG-9r-targeted SNALPs increase IL-6 serum levels. The levels of IL-6 for non-injected wild-type mice or mice intravenously injected with RVG-9r-targeted liposomes encapsulating siMutAtax3 (siMutAtax3) were measured by ELISA, 4 hours after tail-vein injection. Values are presented as mean \pm SEM of n=4.

4.4.6. Repeated intravenous administration of RVG-9r-targeted SNALPs is well tolerated

Lastly, to assess the safety of repeated intravenous administration of RVG-9r-targeted SNALPs, we evaluated microglia activation by measuring Iba-1 immunoreactivity in the cerebellum. No significant increase in Iba-1 immunoreactivity was detected for the animals injected with RVG-9r-targeted SNALPs (siCTR or siMutAtx3), when compared to HBS-injected animals (Fig. 4.8).

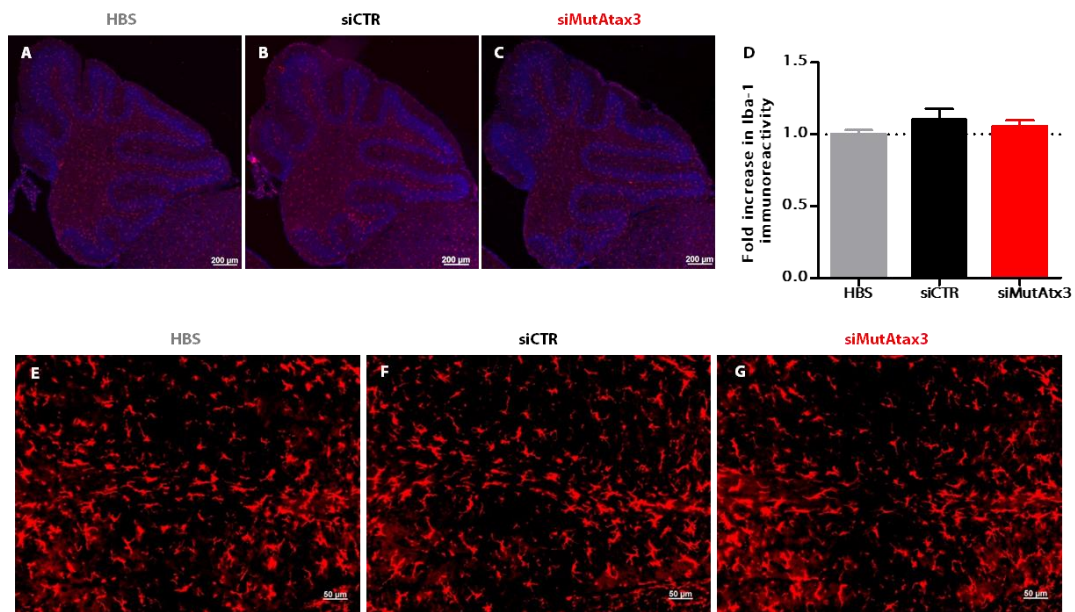


Figure 4.8. Repeated intravenous administration of RVG-9r-targeted SNALPs does not elicit local microglial activation. 8 weeks after starting the treatment, mice were sacrificed and Iba-1 staining was evaluated by fluorescence immunohistochemistry. **(A-C)** Fluorescence microscopy images of microglia stained with Iba-1 antibody, with a 5x objective. **(D)** Quantification of the Iba-1 immunoreactivity. Values are presented as mean±SEM of n=5/6. Student's t-test was used to compare animals injected with HBS versus siMutAtax3 and siCTR (n.s. p>0.05). **(E-G)** Fluorescence microscopy images of microglia stained with Iba-1 antibody, with a 20x objective.

Furthermore, we also evaluated serum levels of IL-6, to assess the safety of repeated intravenous administration of RVG-9r-targeted SNALPs. We observed that chronic intravenous administration of RVG-9r-targeted SNALPs did not increase the levels of IL-6, when compared to animals injected with a saline solution (Table 4.3).

Animal	Transgenic			Wild Type
	HBS-injected	siCTR	siMutAtax3	LPS
IL-6 levels (pg/mL)	1.53±1.25	2.9±1.03	0.85±0.85	+500

Table 4.3. Repeated intravenous administration of RVG-9r-targeted SNALPs does not increase serum levels of IL-6. The levels of IL-6 for transgenic mice that were intravenously injected with a saline solution (HBS), RVG-9r-targeted liposomes encapsulating siCTR (siCTR) and RVG-9r-targeted liposomes encapsulating siMutAtax3 (siMutAtax3) were evaluated by ELISA. Values are presented as mean±SEM of n=4. A wild-type animal injected with lipopolysaccharide was used as a positive control.

4.5. Discussion

One of the mostly affected brain regions in MJD patients, that has an essential role in motor coordination, is the cerebellum (Dürr A, 1996; Scherzed *et al.*, 2012; Sudarsky and Coutinho, 1995). Therefore, we tested the therapeutic potential of RVG-9r-targeted SNALPs in a cerebellar transgenic mouse model of MJD. We provide evidence that RVG-9r-targeted SNALPs a) internalize in the cerebellar parenchyma, where b) the carried siRNAs reduce mutant ataxin-3 levels, c) alleviate motor performance defects and d) rescue neuropathology constituting a promising therapy for MJD, and a proof-of-principle for many other brain disorders.

Most of the transgenic mice expressing the full-length ataxin-3 that have been developed during the last years, present a late and mild phenotype (Boy *et al.*, 2010; Cemal *et al.*, 2002; Silva-Fernandes *et al.*, 2010). In contrast, the transgenic mouse model used in this study expresses a truncated form of human mutant ataxin-3 with 69 CAG repeats that results in an early and severe MJD phenotype, being particularly suitable for pre-clinical studies (Torashima *et al.*, 2008).

This transgenic mouse model exhibits an extensive atrophy and reduced vascularization in the cerebellum, which we anticipated that could impair the delivery of the siRNAs, as previously reported for AAV9 (Konno *et al.*, 2014). Importantly, flow cytometry analysis of cerebellum homogenates provided evidence that tail-vein injection of RVG-9r-targeted liposomes encapsulating FAM-labeled siRNAs promoted accumulation of siRNAs in the cerebellum, despite the reduced vascularization of these transgenic animals (Fig. 4.1).

Furthermore, this MJD transgenic mouse model enables testing allele-specific strategies, as the truncated human ataxin-3 carries the C variant that can be found in 70% of the MJD patients (Gaspar *et al.*, 2001). Here, we addressed if intravenous administration of RVG-9r targeted liposomes encapsulating silencing sequences targeted to this single nucleotide polymorphism (Alves *et al.*, 2008a; Nóbrega *et al.*, 2014; Nóbrega *et al.*, 2013b), would be a promising therapeutic approach. Importantly, our results showed that this strategy was able to downregulate mutant ataxin-3 mRNA and aggregate levels in the cerebellum of MJD transgenic animals (Fig. 4.2), somehow innocuously because it did not increase the

mRNA levels of pro-inflammatory mediators and a microglia-related gene locally (Fig. 4.3). These results confirmed the *in vivo* potential of RVG-9r-targeted SNALPs to decrease the levels of the target gene in the cerebellum, which is relevant to MJD but also to other cerebellar-associated disorders. However, in the region targeted by the silencing sequence, there is no homology between mouse and human ataxin-3, which does not allow to further infer about the selectivity of the approach (Nóbrega *et al.*, 2013b).

Notably, non-invasive silencing of mutant ataxin-3 after the onset of disease-symptoms (started with 5-weeks-old mice) reduced motor behaviour deficits in this severely impaired transgenic mouse model of MJD (Fig. 4.6). Furthermore, the therapeutic effects on behaviour correlated with an alleviation of the cerebellar-associated neuropathology, which was particularly significant in terms of preservation of the granular layer thickness (Fig. 4.7). Thus, we conclude that intravenous delivery of nanoencapsulated siRNAs was able to preserve cerebellar integrity and function.

In a clinical setting, where multiple administrations of the therapeutic agent are usually required for improved therapeutic outcome, it is crucial to study the immunogenicity of the administered nanoparticles. In this regard, Kumar and colleagues concluded that repeated intravenous administration of naked RVG-9r/siRNA complexes did not induce inflammatory cytokines or anti-peptide antibody response (Kumar *et al.*, 2007), but a few years later it was reported that these complexes strongly stimulated IL-6 secretion (Alvarez-Erviti *et al.*, 2011). The reported differences may be due to the different protocols that these studies used to assess the immune stimulatory properties of the treatment. Indeed, we did not detect IL-6 secretion in the serum of the animals that were repeatedly intravenously injected over a 2-months period (the total duration of the behavioural assessment study, Table 4.3), but 4 hours after a single intravenous administration of RVG-9r-targeted SNALPs to wild-type animals, we were able to detect an increase in IL-6 levels (Table 4.2). An explanation for these differences is certainly the rapid and transient nature of cytokines induction, as reviewed by Robbins (Robbins *et al.*, 2009). In fact, for the first time-point, the levels of serum IL-6 were measured 5 days after the last injection, which probably missed the transient nature of cytokines activation. Nevertheless, Alvarez-Erviti and colleagues still detected increased levels of IL-6 secretion, three days after intravenous administration, which possibly means that naked RVG-9r/siRNA complexes

induce chronic stimulation of IL-6, while IL-6 stimulation by RVG-9r-targeted SNALPs is only acute and seems to be solved some time after treatment.

Our studies are in accordance with previous papers that demonstrated the substantial benefits of RNAi on polyglutamine disorders using either viral vectors on MJD animal models (Alves *et al.*, 2008a; Alves *et al.*, 2010; Costa Mdo *et al.*, 2013; Nóbrega *et al.*, 2014; Nóbrega *et al.*, 2013b; Rodriguez-Lebron *et al.*, 2013) or non-viral strategies for the related-Huntington's disease (DiFiglia *et al.*, 2007; Kordasiewicz *et al.*, 2012). However, several advantages make our non-viral strategy easier to translate into the clinic. While the aforementioned experiments involved craniotomy to inject the vectors into the brain, our nanoparticles enabled the use of a non-invasive procedure to administer the siRNA-based treatment. Moreover, the intravenous administration of RVG-9r-targeted SNALPs might overcome the challenge of transducing large areas of the human brain, which may be necessary given the diffuse regional neuropathology of MJD. In fact, as the brain is a highly vascularized organ, the delivery throughout the brain is possible with our strategy. Importantly, the transient nature of expression mediated by non-viral vectors allows an interruption of administration if at any moment there is a development of side-effects.

To our knowledge, this is the first report showing the positive impact of a non-viral strategy in Machado-Joseph disease and the first time that a non-invasive systemic administration proved to be beneficial on a polyglutamine disorder. Our studies open new avenues towards MJD therapy that can also be applied to other neurodegenerative diseases linked to the production of pathogenic proteins.

CHAPTER 5

Final conclusions and future perspectives

5. Final Conclusions and Future Perspectives

This thesis focused on the development of a non-viral strategy to deliver silencing sequences to the brain by a non-invasive administration, and the evaluation of its therapeutic potential in two genetically-modified mouse models of MJD.

In the first part of this work, we synthesized brain-targeted stable nucleic acid lipid particles (SNALPs) by covalent coupling of a short peptide derived from rabies virus glycoprotein (RVG-9r). The developed formulation displayed important features that make it adequate for systemic administration such as high encapsulation efficiency for siRNAs, ability to protect the encapsulated siRNAs, appropriate and homogeneous particle size distribution. Flow cytometry studies revealed that the attachment of RVG-9r to the liposomal surface enhanced the uptake of the liposomes by neuronal cells but not non-neuronal cells. In addition, the mechanism of entry of RVG-9r-targeted liposomes into neuronal cells was most likely receptor-mediated endocytosis which, together with the fact that the nanoparticles associated more with neuronal cells, may reduce undesired side effects that result from targeting of other tissues. Furthermore, RVG-9r-targeted SNALPs efficiently delivered siRNAs to cultured neuronal cells, significantly decreasing the mRNA and protein levels of mutant ataxin-3, the MJD-causing protein (Kawaguchi *et al.*, 1994). Importantly, *in vivo* experiments revealed that RVG-9r-conjugation to the nanoparticles enhanced the ability to cross the blood-brain barrier (BBB) and promoted de-targeting of heart and lungs, upon intravenous administration.

In the second part of this project, we evaluated whether intravenous administration of brain-targeted SNALPs could alleviate the striatal neuropathology in a lentiviral-based mouse model of MJD (Simões *et al.*, 2012). This MJD mouse model is a versatile research tool that replicates late stages of neurodegenerative diseases, providing precise quantitative neuropathological data and enabling to test therapeutic hypothesis in a time- and cost-effective manner. As genotyping of MJD patients could allow the initiation of the treatment before the first symptoms appear, these experiments were conducted initiating the treatment at an early time-point. We found that intravenous administration

of RVG-9r-targeted SNALPs promoted a significant reduction in the number of ubiquitin-positive inclusions in the mouse striatum, the pathological hallmark of MJD (Paulson *et al.*, 1997). Importantly, our strategy reduced the striatal neuronal dysfunction and degeneration induced by mutant ataxin-3 expression in this lentiviral-based mouse model of MJD.

In the third and final part of this work, we evaluated the therapeutic potential of RVG-9r-targeted SNALPs in a severely impaired cerebellar-transgenic mouse model of MJD (Torashima *et al.*, 2008), when initiated after disease onset. The transgenic mouse model used in this study expresses a truncated form of human mutant ataxin-3 with 69 CAG repeats that results in an early and severe MJD phenotype, being particularly suitable for pre-clinical studies. RVG-9r-targeted SNALPs internalized in the cerebellar parenchyma, where the carried siRNAs reduced mutant ataxin-3 levels, alleviated motor performance defects, rescued neuropathology and did not induce a strong immune response, constituting a promising therapy for MJD.

Overall, our results demonstrate that intravenous administration of brain-targeted SNALPs alleviate motor performance defects in a severely impaired transgenic mouse model of MJD and rescue striatal and cerebellar MJD-associated neuropathology in two different genetically-modified mouse models of MJD (Fig. 5.1). Notably, to our best knowledge, our study represents the first report showing the positive impact of a non-viral strategy in MJD and the first time that a non-invasive systemic administration proved to be beneficial on a polyglutamine disorder. Importantly, the silencing sequences used in our study targeted a single nucleotide polymorphism that we previously showed to enable allele-specific silencing of mutant ataxin-3, while preserving wild-type ataxin-3 (Alves *et al.*, 2008a; Nóbrega *et al.*, 2014; Nóbrega *et al.*, 2013b). Because ataxin-3 protein is ubiquitously expressed in neuronal and non-neuronal tissues and its function has been linked to several essential cell pathways, selective inhibition of the mutant allele has a higher probability to translate into a successful treatment for humans.

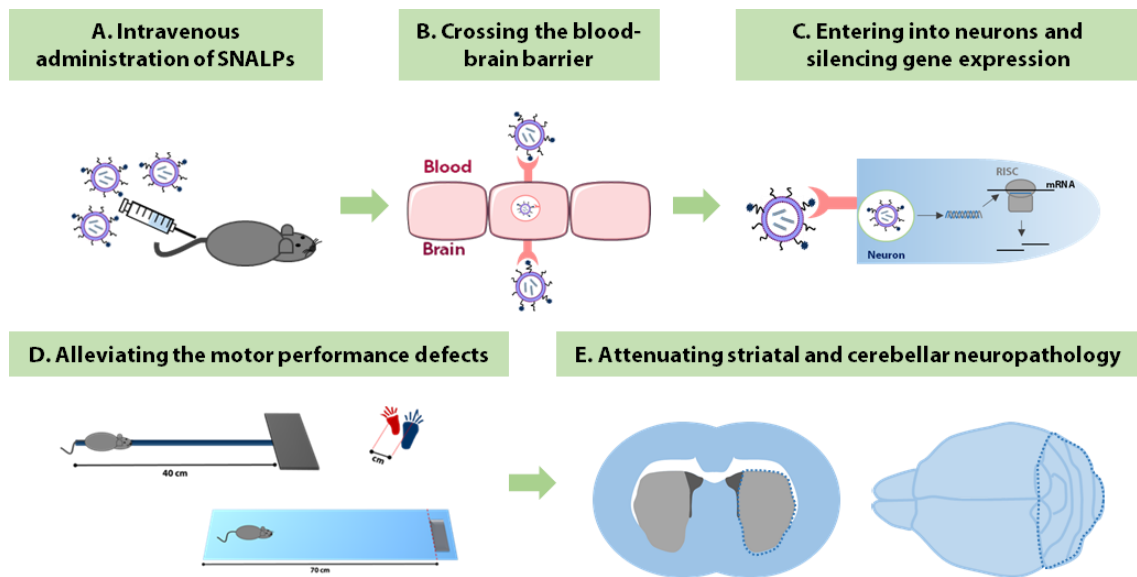


Figure 5.1. Schematic representation of our findings. (A) Intravenous administration of brain-targeted SNALPs, through tail-vein injection. (B) Brain-targeted SNALPs cross the blood-brain barrier, presumably through receptor-mediated transcytosis. (C) These nanoparticles silence mutant ataxin-3 expression in neurons of the affected brain-regions. (D) Alleviate motor performance defects. (E) Rescue striatal and cerebellar-associated neuropathology, constituting a promising therapy for Machado-Joseph disease and a proof-of-principle for many other neurodegenerative disorders.

Despite promising, additional studies are needed to have a best knowledge of the possible impact of this strategy on MJD patients. Namely, the therapeutic potential of RVG-9r-targeted SNALPs should be tested in an animal model that closely reflects the human disease environment, preferentially in an animal model with widespread pathology in the brain regions that are known to be affected in MJD patients. Although none of the developed transgenic mice of MJD until now, completely recapitulate human disease, there are several mouse models expressing the full-length human ataxin-3 disease gene that better reproduce human phenotype (Bichelmeier *et al.*, 2007; Boy *et al.*, 2010; Boy *et al.*, 2009; Cemal *et al.*, 2002; Chou *et al.*, 2008; Goti *et al.*, 2004; Silva-Fernandes *et al.*, 2010). Furthermore, as MJD is a chronic neurodegenerative disease which will require long-term RNAi administration, it is extremely important to study how long the silencing effect mediated by RVG-9r-targeted SNALPs is sustained *in vivo* during the time-course of the chronic treatment. Also, a wider and deeper study of the safety of the chronic

intravenous administration of RVG-9r-targeted SNALPs is extremely needed. Specifically, the levels of hepatic transaminases and other pro-inflammatory cytokines beyond IL-6 should be studied.

Finally, some aspects of our strategy could be refined to enhance therapeutic benefits for MJD, namely: 1) improvement of the delivery to the brain using for instance a dual-ligand approach, 2) testing other sequences that could more efficiently silence mutant ataxin-3 or 3) co-encapsulating a drug to obtain synergistic therapeutic effects. In the last case, SNALPs could provide a good platform to deliver simultaneously siRNAs to block mutant ataxin-3 production and an autophagy-activator (Silva-Fernandes *et al.*, 2014) or a calpain-inhibitor drug (Simões *et al.*, 2014) to decrease the toxicity of the pre-existing mutant ataxin-3 protein on neuronal cells.

In summary, the present thesis provides evidence that a clinically-relevant nanoparticle formulation is a promising therapeutic strategy for MJD patients and therefore deserves to be further explored in additional preclinical studies. Our study opens new avenues towards MJD treatment and can also be easily adapted for the treatment of several neurodegenerative diseases known to be linked to the production of pathogenic proteins.

References

References

- Abbott, N.J., Ronnback, L., and Hansson, E. (2006). Astrocyte-endothelial interactions at the blood-brain barrier. *Nature Reviews Neuroscience* 7, 41-53.
- Aiba, Y., Hu, J., Liu, J., Xiang, Q., Martinez, C., and Corey, D.R. (2013). Allele-Selective Inhibition of Expression of Huntingtin and Ataxin-3 by RNA Duplexes Containing Unlocked Nucleic Acid Substitutions. *Biochemistry* 52, 9329-9338.
- Akinc, A., Querbes, W., De, S., Qin, J., Frank-Kamenetsky, M., Jayaprakash, K.N., Jayaraman, M., Rajeev, K.G., Cantley, W.L., Dorkin, J.R., *et al.* (2010). Targeted Delivery of RNAi Therapeutics With Endogenous and Exogenous Ligand-Based Mechanisms. *Molecular Therapy* 18, 1357-1364.
- Allen, T.M., and Cullis, P.R. (2013). Liposomal drug delivery systems: From concept to clinical applications. *Advanced Drug Delivery Reviews* 65, 36-48.
- Allen, T.M., Hansen, C., Martin, F., Redemann, C., and Yau-Young, A. (1991). Liposomes containing synthetic lipid derivatives of poly(ethylene glycol) show prolonged circulation half-lives in vivo. *Biochimica et Biophysica Acta* 1066, 29-36.
- Alvarez-Erviti, L., Seow, Y., Yin, H., Betts, C., Lakhai, S., and Wood, M.J. (2011). Delivery of siRNA to the mouse brain by systemic injection of targeted exosomes. *Nature biotechnology* 29, 341-345.
- Alves, S., Nascimento-Ferreira, I., Auregan, G., Hassig, R., Dufour, N., Brouillet, E., Pedroso de Lima, M.C., Hantraye, P., Pereira de Almeida, L., and Deglon, N. (2008a). Allele-specific RNA silencing of mutant ataxin-3 mediates neuroprotection in a rat model of Machado-Joseph disease. *PloS one* 3, e3341.
- Alves, S., Nascimento-Ferreira, I., Dufour, N., Hassig, R., Auregan, G., Nobrega, C., Brouillet, E., Hantraye, P., Pedroso de Lima, M.C., Deglon, N., *et al.* (2010). Silencing ataxin-3 mitigates degeneration in a rat model of Machado-Joseph disease: no role for wild-type ataxin-3? *Human molecular genetics* 19, 2380-2394.
- Alves, S., Regulier, E., Nascimento-Ferreira, I., Hassig, R., Dufour, N., Koeppen, A., Carvalho, A.L., Simoes, S., de Lima, M.C., Brouillet, E., *et al.* (2008b). Striatal and nigral pathology in a lentiviral rat model of Machado-Joseph disease. *Human molecular genetics* 17, 2071-2083.
- Araujo, J., Breuer, P., Dieringer, S., Krauss, S., Dorn, S., Zimmermann, K., Pfeifer, A., Klockgether, T., Wuellner, U., and Evert, B.O. (2011). FOXO4-dependent upregulation of superoxide dismutase-2 in response to oxidative stress is impaired in spinocerebellar ataxia type 3. *Human molecular genetics* 20, 2928-2941.
- Bagga, S., Bracht, J., Hunter, S., Massirer, K., Holtz, J., Eachus, R., and Pasquinelli, A.E. (2005). Regulation by let-7 and lin-4 miRNAs Results in Target mRNA Degradation. *Cell* 122, 553-563.
- Benke, D., Honer, M., Michel, C., Bettler, B., and Mohler, H. (1999). γ -Aminobutyric Acid Type B Receptor Splice Variant Proteins GBR1a and GBR1b Are Both Associated with GBR2 in Situ and Display Differential Regional and Subcellular Distribution. *Journal of Biological Chemistry* 274, 27323-27330.
- Berke, S., Chai, Y., Marrs, G., Wen, H., and Paulson, H. (2005). Defining the role of ubiquitin-interacting motifs in the polyglutamine disease protein, ataxin-3. *Journal of Biological Chemistry* 280, 32026-32034.

- Bettencourt, C., Santos, C., Kay, T., Vasconcelos, J., and Lima, M. (2008). Analysis of segregation patterns in Machado-Joseph disease pedigrees. *Journal of Human Genetics* 53, 920-923.
- Bichelmeier, U., Schmidt, T., Hübener, J., Boy, J., Rüttiger, L., Häbig, K., Poths, S., Bonin, M., Knipper, M., Schmidt, W.J., *et al.* (2007). Nuclear Localization of Ataxin-3 Is Required for the Manifestation of Symptoms in SCA3: In Vivo Evidence. *The Journal of Neuroscience* 27, 7418-7428.
- Bird, T. (1998). Hereditary Ataxia Overview (GeneReviews® [Internet]).
- Biswas, S., Deshpande, P.P., Perche, F., Dodwadkar, N.S., Sane, S.D., and Torchilin, V.P. (2013). Octa-arginine-modified pegylated liposomal doxorubicin: an effective treatment strategy for non-small cell lung cancer. *Cancer letters* 335, 191-200.
- Boado, R. (2007). Blood–brain Barrier Transport of Non-viral Gene and RNAi Therapeutics. *Pharmaceutical research* 24, 1772-1787.
- Boado, R.J. (2005). RNA Interference and Nonviral Targeted Gene Therapy of Experimental Brain Cancer. *NeuroRx* 2, 139-150.
- Bohnsack, M.T., Czaplinski, K., and GÖRlich, D. (2004). Exportin 5 is a RanGTP-dependent dsRNA-binding protein that mediates nuclear export of pre-miRNAs. *RNA* 10, 185-191.
- Boudreau, R.L., McBride, J.L., Martins, I., Shen, S., Xing, Y., Carter, B.J., and Davidson, B.L. (2009). Nonallele-specific Silencing of Mutant and Wild-type Huntingtin Demonstrates Therapeutic Efficacy in Huntington's Disease Mice. *Molecular Therapy* 17, 1053-1063.
- Boudreau, R.L., Rodríguez-Lebrón, E., and Davidson, B.L. (2011). RNAi medicine for the brain: progresses and challenges. *Human molecular genetics* 20, 21-27.
- Boussif, O., Lezoualc'h, F., Zanta, M.A., Mergny, M.D., Scherman, D., Demeneix, B., and Behr, J.P. (1995). A versatile vector for gene and oligonucleotide transfer into cells in culture and in vivo: polyethylenimine. *Proceedings of the National Academy of Sciences of the United States of America* 92, 7297-7301.
- Boy, J., Schmidt, T., Schumann, U., Grasshoff, U., Unser, S., Holzmann, C., Schmitt, I., Karl, T., Laccone, F., Wolburg, H., *et al.* (2010). A transgenic mouse model of spinocerebellar ataxia type 3 resembling late disease onset and gender-specific instability of CAG repeats. *Neurobiology of Disease* 37, 284-293.
- Boy, J., Schmidt, T., Wolburg, H., Mack, A., Nuber, S., Böttcher, M., Schmitt, I., Holzmann, C., Zimmermann, F., Servadio, A., *et al.* (2009). Reversibility of symptoms in a conditional mouse model of spinocerebellar ataxia type 3. *Human molecular genetics* 18, 4282-4295.
- Buhmann, C., Bussopulos, A., and Oechsner, M. (2003). Dopaminergic response in Parkinsonian phenotype of Machado-Joseph disease. *Movement Disorders* 18, 219-221.
- Burnett, B., Li, F., and Pittman, R.N. (2003). The polyglutamine neurodegenerative protein ataxin-3 binds polyubiquitylated proteins and has ubiquitin protease activity. *Human molecular genetics* 12, 3195-3205.
- Burnett, B.G., and Pittman, R.N. (2005). The polyglutamine neurodegenerative protein ataxin 3 regulates aggresome formation. *Proceedings of the National Academy of Sciences of the United States of America* 102, 4330-4335.

- Cancel G, A.N., Stevanin G, Dürr A, Chneiweiss H, Néri C, Duyckaerts C, Penet C, Cann HM, Agid Y, et al. (1995). Marked phenotypic heterogeneity associated with expansion of a CAG repeat sequence at the spinocerebellar ataxia 3/Machado-Joseph disease locus. *The American Journal of Human Genetics* 57, 809-816.
- Carroll, J.B., Warby, S.C., Southwell, A.L., Doty, C.N., Greenlee, S., Skotte, N., Hung, G., Bennett, C.F., Freier, S.M., and Hayden, M.R. (2011). Potent and Selective Antisense Oligonucleotides Targeting Single-Nucleotide Polymorphisms in the Huntington Disease Gene / Allele-Specific Silencing of Mutant Huntingtin. *Molecular Therapy* 19, 2178-2185.
- Cemal, C.K., Carroll, C.J., Lawrence, L., Lowrie, M.B., Ruddle, P., Al-Mahdawi, S., King, R.H.M., Pook, M.A., Huxley, C., and Chamberlain, S. (2002). YAC transgenic mice carrying pathological alleles of the MJD1 locus exhibit a mild and slowly progressive cerebellar deficit. *Human molecular genetics* 11, 1075-1094.
- Chai Y, B.S., Cohen RE, Paulson HL (2004). Poly-ubiquitin binding by the polyglutamine disease protein ataxin-3 links its normal function to protein surveillance pathways. *The Journal of biological chemistry* 279, 3605-3611.
- Chai, Y., Koppenhafer, S., Bonini, N., and Paulson, H. (1999b). Analysis of the Role of Heat Shock Protein (Hsp) Molecular Chaperones in Polyglutamine Disease. *The Journal of Neuroscience* 19, 10338-10347.
- Chai, Y., Koppenhafer, S.L., Shoemith, S.J., Perez, M.K., and Paulson, H.L. (1999a). Evidence for Proteasome Involvement in Polyglutamine Disease: Localization to Nuclear Inclusions in SCA3/MJD and Suppression of Polyglutamine Aggregation in vitro. *Human molecular genetics* 8, 673-682.
- Chai, Y., Shao, J., Miller, V.M., Williams, A., and Paulson, H.L. (2002). Live-cell imaging reveals divergent intracellular dynamics of polyglutamine disease proteins and supports a sequestration model of pathogenesis. *Proceedings of the National Academy of Sciences of the United States of America* 99, 9310-9315.
- Chen, W., Zhan, C., Gu, B., Meng, Q., Wang, H., Lu, W., and Hou, H. (2010). Targeted brain delivery of itraconazole via RVG29 anchored nanoparticles. *Journal of Drug Targeting* 19, 228-234.
- Chen, Y., and Liu, L. (2012). Modern methods for delivery of drugs across the blood–brain barrier. *Advanced Drug Delivery Reviews* 64, 640-665.
- Chou, A.-H., Yeh, T.-H., Ouyang, P., Chen, Y.-L., Chen, S.-Y., and Wang, H.-L. (2008). Polyglutamine-expanded ataxin-3 causes cerebellar dysfunction of SCA3 transgenic mice by inducing transcriptional dysregulation. *Neurobiology of Disease* 31, 89-101.
- ClinicalTrials.gov (<https://clinicaltrials.gov/ct2/results?term=RNA+interference&recr=Open>).
- Cooper, J.M., Wiklander, P.B., Nordin, J.Z., Al-Shawi, R., Wood, M.J., Vithlani, M., Schapira, A.H., Simons, J.P., El-Andaloussi, S., and Alvarez-Erviti, L. (2014). Systemic exosomal siRNA delivery reduced alpha-synuclein aggregates in brains of transgenic mice. *Movement Disorders* 29, 1476-1485.
- Costa, M.d.C., Bajanca, F., Rodrigues, A.-J., Tomé, R.J., Corthals, G., Macedo-Ribeiro, S., Paulson, H.L., Logarinho, E., and Maciel, P. (2010). Ataxin-3 Plays a Role in Mouse Myogenic Differentiation through Regulation of Integrin Subunit Levels. *PloS one* 5, e11728.

- Costa Mdo, C., Luna-Cancelon, K., Fischer, S., Ashraf, N.S., Ouyang, M., Dharia, R.M., Martin-Fishman, L., Yang, Y., Shakkottai, V.G., Davidson, B.L., *et al.* (2013). Toward RNAi therapy for the polyglutamine disease Machado-Joseph disease. *Molecular Therapy* 21, 1898-1908.
- Costa Mdo, C., and Paulson, H.L. (2012). Toward understanding Machado-Joseph disease. *Progress in Neurobiology* 97, 239-257.
- Costa, P.M., Cardoso, A.L., Mendonca, L.S., Serani, A., Custodia, C., Conceicao, M., Simoes, S., Moreira, J.N., Pereira de Almeida, L., and Pedrosa de Lima, M.C. (2013). Tumor-targeted Chlorotoxin-coupled Nanoparticles for Nucleic Acid Delivery to Glioblastoma Cells: A Promising System for Glioblastoma Treatment. *Molecular Therapy - Nucleic Acids* 2, e100.
- D'Abreu, A., França, M.C., Paulson, H.L., and Lopes-Cendes, I. (2010). Caring for Machado-Joseph Disease: current understanding and how to help patients. *Parkinsonism & related disorders* 16, 2.
- Davidson, B.L., and McCray, P.B. (2011). Current prospects for RNA interference-based therapies. *Nature Reviews Genetics* 12, 329-340.
- Davis, M.E., Zuckerman, J.E., Choi, C.H.J., Seligson, D., Tolcher, A., Alabi, C.A., Yen, Y., Heidel, J.D., and Ribas, A. (2010). Evidence of RNAi in humans from systemically administered siRNA via targeted nanoparticles. *Nature* 464, 1067-1070.
- de Almeida, L.P., Ross, C.A., Zala, D., Aebischer, P., and Deglon, N. (2002). Lentiviral-mediated delivery of mutant huntingtin in the striatum of rats induces a selective neuropathology modulated by polyglutamine repeat size, huntingtin expression levels, and protein length. *Journal of Neuroscience* 22, 3473-3483.
- de Almeida, L.P., Zala, D., Aebischer, P., and Deglon, N. (2001). Neuroprotective effect of a CNTF-expressing lentiviral vector in the quinolinic acid rat model of Huntington's disease. *Neurobiology of Disease* 8, 433-446.
- Dehousse, V., Garbacki, N., Colige, A., and Evrard, B. (2010). Development of pH-responsive nanocarriers using trimethylchitosans and methacrylic acid copolymer for siRNA delivery. *Biomaterials* 31, 1839-1849.
- Di Martino, M.T., Campani, V., Misso, G., Gallo Cantafio, M.E., Gulla, A., Foresta, U., Guzzi, P.H., Castellano, M., Grimaldi, A., Gigantino, V., *et al.* (2014). In vivo activity of miR-34a mimics delivered by stable nucleic acid lipid particles (SNALPs) against multiple myeloma. *PloS one* 9, e90005.
- DiFiglia, M., Sena-Esteves, M., Chase, K., Sapp, E., Pfister, E., Sass, M., Yoder, J., Reeves, P., Pandey, R.K., Rajeev, K.G., *et al.* (2007). Therapeutic silencing of mutant huntingtin with siRNA attenuates striatal and cortical neuropathology and behavioral deficits. *Proceedings of the National Academy of Sciences* 104, 17204-17209.
- do Carmo Costa, M., Gomes-da-Silva, J., Miranda, C.J., Sequeiros, J., Santos, M.M., and Maciel, P.c. (2004). Genomic structure, promoter activity, and developmental expression of the mouse homologue of the Machado-Joseph disease (MJD) gene. *Genomics* 84, 361-373.
- Doench, J.G., Petersen, C.P., and Sharp, P.A. (2003). siRNAs can function as miRNAs. *Genes & Development* 17, 438-442.
- Donaldson, K.M., Li, W., Ching, K.A., Batalov, S., Tsai, C.-C., and Joazeiro, C.A.P. (2003). Ubiquitin-mediated sequestration of normal cellular proteins into

- polyglutamine aggregates. *Proceedings of the National Academy of Sciences* 100, 8892-8897.
- Doss-Pepe, E.W., Stenroos, E.S., Johnson, W.G., and Madura, K. (2003). Ataxin-3 Interactions with Rad23 and Valosin-Containing Protein and Its Associations with Ubiquitin Chains and the Proteasome Are Consistent with a Role in Ubiquitin-Mediated Proteolysis. *Molecular and Cellular Biology* 23, 6469-6483.
 - Drouet, V., Perrin, V., Hassig, R., Dufour, N., Auregan, G., Alves, S., Bonvento, G., Brouillet, E., Luthi-Carter, R., Hantraye, P., *et al.* (2009). Sustained effects of nonallele-specific Huntingtin silencing. *Annals of Neurology* 65, 276-285.
 - Duarte-Neves, J., Gonçalves, N., Cunha-Santos, J., Simões, A.T., den Dunnen, W.F.A., Hirai, H., Kügler, S., Cavadas, C., and Pereira de Almeida, L. (2015). Neuropeptide Y mitigates neuropathology and motor deficits in mouse models of Machado–Joseph disease. *Human molecular genetics* 24, 5451-5463.
 - Duncan, R., and Izzo, L. (2005). Dendrimer biocompatibility and toxicity. *Advanced Drug Delivery Reviews* 57, 2215-2237.
 - Dunlap, D.D., Maggi, A., Soria, M.R., and Monaco, L. (1997). Nanoscopic structure of DNA condensed for gene delivery. *Nucleic Acids Research* 25, 3095-3101.
 - Durcan, T.M., Kontogiannea, M., Thorarinsdottir, T., Fallon, L., Williams, A.J., Djarmati, A., Fantaneanu, T., Paulson, H.L., and Fon, E.A. (2011). The Machado–Joseph disease-associated mutant form of ataxin-3 regulates parkin ubiquitination and stability. *Human molecular genetics* 20, 141-154.
 - Dürr A, S.G., Cancel G, Duyckaerts C, Abbas N, Didierjean O, Chneiweiss H, Benomar A, Lyon-Caen O, Julien J, Serdaru M, Penet C, Agid Y, Brice A. (1996). Spinocerebellar ataxia 3 and Machado-Joseph disease: clinical, molecular, and neuropathological features. *Annals of Neurology* 39, 490-499.
 - El-Sayed, A., Khalil, I.A., Kogure, K., Futaki, S., and Harashima, H. (2008). Octarginine- and octalysine-modified nanoparticles have different modes of endosomal escape. *Journal of Biological Chemistry* 283, 23450-23461.
 - Elbashir, S.M., Harborth, J., Lendeckel, W., Yalcin, A., Weber, K., and Tuschl, T. (2001a). Duplexes of 21-nucleotide RNAs mediate RNA interference in cultured mammalian cells. *Nature* 411, 494-498.
 - Elbashir, S.M., Lendeckel, W., and Tuschl, T. (2001b). RNA interference is mediated by 21- and 22-nucleotide RNAs. *Genes & Development* 15, 188-200.
 - Evers, M., Toonen, L.A., and van Roon-Mom, W.C. (2014). Ataxin-3 Protein and RNA Toxicity in Spinocerebellar Ataxia Type 3: Current Insights and Emerging Therapeutic Strategies. *Mol Neurobiol* 49, 1513-1531.
 - Evert, B., Schelhaas, J., Fleischer, H., de Vos, R., Brunt, E., Stenzel, W., Klockgether, T., and Wüllner, U. (2006a). Neuronal intranuclear inclusions, dysregulation of cytokine expression and cell death in spinocerebellar ataxia type 3. *Clinical Neuropathology* 25, 272-281.
 - Evert, B.O., Araujo, J., Vieira-Saecker, A.M., de Vos, R.A.I., Harendza, S., Klockgether, T., and Wüllner, U. (2006b). Ataxin-3 Represses Transcription via Chromatin Binding, Interaction with Histone Deacetylase 3, and Histone Deacetylation. *The Journal of Neuroscience* 26, 11474-11486.
 - Fire, A., Xu, S., Montgomery, M.K., Kostas, S.A., Driver, S.E., and Mello, C.C. (1998). Potent and specific genetic interference by double-stranded RNA in *Caenorhabditis elegans*. *Nature* 391, 806-811.

- Freeman, W., and Wszolek, Z. (2005). Botulinum toxin type A for treatment of spasticity in spinocerebellar ataxia type 3 (Machado–Joseph disease). *Movement Disorders* 20, 644-644.
- Fritschy, J.-M., Sidler, C., Parpan, F., Gassmann, M., Kaupmann, K., Bettler, B., and Benke, D. (2004). Independent maturation of the GABAB receptor subunits GABAB1 and GABAB2 during postnatal development in rodent brain. *The Journal of Comparative Neurology* 477, 235-252.
- Fu, A., Wang, Y., Zhan, L., and Zhou, R. (2012). Targeted Delivery of Proteins into the Central Nervous System Mediated by Rabies Virus Glycoprotein-Derived Peptide. *Pharmaceutical research* 29, 1562-1569.
- Gao, Y., Wang, Z.Y., Zhang, J., Zhang, Y., Huo, H., Wang, T., Jiang, T., and Wang, S. (2014). RVG-peptide-linked trimethylated chitosan for delivery of siRNA to the brain. *Biomacromolecules* 15, 1010-1018.
- Gaspar, C., Lopes-Cendes, I., Hayes, S., Goto, J., Arvidsson, K., Dias, A., Silveira, I., Maciel, P., Coutinho, P., Lima, M., *et al.* (2001). Ancestral Origins of the Machado-Joseph Disease Mutation: A Worldwide Haplotype Study. *American journal of human genetics* 68, 523-528.
- Geisbert, T.W., Hensley, L.E., Kagan, E., Yu, E.Z., Geisbert, J.B., Daddario-DiCaprio, K., Fritz, E.A., Jahrling, P.B., McClintock, K., Phelps, J.R., *et al.* (2006). Postexposure protection of guinea pigs against a lethal ebola virus challenge is conferred by RNA interference. *Journal of Infectious Diseases* 193, 1650-1657.
- Geisbert, T.W., Lee, A.C., Robbins, M., Geisbert, J.B., Honko, A.N., Sood, V., Johnson, J.C., de Jong, S., Tavakoli, I., Judge, A., *et al.* (2010). Postexposure protection of non-human primates against a lethal Ebola virus challenge with RNA interference: a proof-of-concept study. *Lancet* 375, 1896-1905.
- Gonçalves, N., Simões, A.T., Cunha, R.A., and de Almeida, L.P. (2013). Caffeine and adenosine A2A receptor inactivation decrease striatal neuropathology in a lentiviral-based model of Machado–Joseph disease. *Annals of Neurology* 73, 655-666.
- Gong, C., Li, X., Xu, L., and Zhang, Y.H. (2012). Target delivery of a gene into the brain using the RVG29-oligoarginine peptide. *Biomaterials* 33, 3456-3463.
- Gorbatyuk, O.S., Li, S., Nash, K., Gorbatyuk, M., Lewin, A.S., Sullivan, L.F., Mandel, R.J., Chen, W., Meyers, C., Manfredsson, F.P., *et al.* (2010). In Vivo RNAi-Mediated [alpha]-Synuclein Silencing Induces Nigrostriatal Degeneration. *Molecular Therapy* 18, 1450-1457.
- Goti, D., Katzen, S.M., Mez, J., Kurtis, N., Kiluk, J., Ben-Haïem, L., Jenkins, N.A., Copeland, N.G., Kakizuka, A., Sharp, A.H., *et al.* (2004). A Mutant Ataxin-3 Putative-Cleavage Fragment in Brains of Machado-Joseph Disease Patients and Transgenic Mice Is Cytotoxic above a Critical Concentration. *The Journal of Neuroscience* 24, 10266-10279.
- Gotti, C., and Clementi, F. (2004). Neuronal nicotinic receptors: from structure to pathology. *Progress in Neurobiology* 74, 363-396.
- Greengard, P., Allen, P.B., and Nairn, A.C. (1999). Beyond the Dopamine Receptor: the DARPP-32/Protein Phosphatase-1 Cascade. *Neuron* 23, 435-447.
- Gregory, R.I., Yan, K.-p., Amuthan, G., Chendrimada, T., Doratotaj, B., Cooch, N., and Shiekhattar, R. (2004). The Microprocessor complex mediates the genesis of microRNAs. *Nature* 432, 235-240.

- Grondin, R., Kaytor, M.D., Ai, Y., Nelson, P.T., Thakker, D.R., Heisel, J., Weatherspoon, M.R., Blum, J.L., Burrig, E.N., Zhang, Z., *et al.* (2012). Six-month partial suppression of Huntingtin is well tolerated in the adult rhesus striatum. *Brain : a journal of neurology* *135*, 1197-1209.
- Gunawardena, S., Her, L.-S., Bruscia, R.G., Layman, R.A., Niesman, I.R., Gordesky-Gold, B., Sintasath, L., Bonini, N.M., and Goldstein, L.S.B. (2003). Disruption of Axonal Transport by Loss of Huntingtin or Expression of Pathogenic PolyQ Proteins in *Drosophila*. *Neuron* *40*, 25-40.
- Gwinn-Hardy, K., Singleton, A., O'Suilleabhain, P., and *et al.* (2001). Spinocerebellar ataxia type 3 phenotypically resembling parkinson disease in a black family. *Archives of Neurology* *58*, 296-299.
- Haacke, A., Hartl, F.U., and Breuer, P. (2007). Calpain Inhibition Is Sufficient to Suppress Aggregation of Polyglutamine-expanded Ataxin-3. *Journal of Biological Chemistry* *282*, 18851-18856.
- Hafez, I.M., Maurer, N., and Cullis, P.R. (2001). On the mechanism whereby cationic lipids promote intracellular delivery of polynucleic acids. *Gene therapy* *8*, 1188-1196.
- Harper, S.Q., Staber, P.D., He, X., Eliason, S.L., Martins, I.H., Mao, Q., Yang, L., Kotin, R.M., Paulson, H.L., and Davidson, B.L. (2005). RNA interference improves motor and neuropathological abnormalities in a Huntington's disease mouse model. *Proceedings of the National Academy of Sciences of the United States of America* *102*, 5820-5825.
- Haussecker, D. (2012). The Business of RNAi Therapeutics in 2012. *Molecular therapy - Nucleic acids* *1*, e8.
- Haussecker, D., and Kay, M.A. (2015). Drugging RNAi. *Science* *347*, 1069-1070.
- Heitz, F., Morris, M.C., and Divita, G. (2009). Twenty years of cell-penetrating peptides: from molecular mechanisms to therapeutics. *British Journal of Pharmacology* *157*, 195-206.
- Hsu, R.-J., Hsiao, K.-M., Lin, M.-J., Li, C.-Y., Wang, L.-C., Chen, L.-K., and Pan, H. (2011). Long Tract of Untranslated CAG Repeats Is Deleterious in Transgenic Mice. *PloS one* *6*, e16417.
- Hu, J., Gagnon, K.T., Liu, J., Watts, J.K., Syeda-Nawaz, J., Bennett, C.F., Swayze, E.E., Randolph, J., Chattopadhyaya, J., and Corey, D.R. (2011). Allele-selective inhibition of ataxin-3 (ATX3) expression by antisense oligomers and duplex RNAs. *Biological chemistry* *392*, 315-325.
- Hu, J., Matsui, M., Gagnon, K.T., Schwartz, J.C., Gabillet, S., Arar, K., Wu, J., Bezprozvanny, I., and Corey, D.R. (2009). Allele-specific silencing of mutant huntingtin and ataxin-3 genes by targeting expanded CAG repeats in mRNAs. *Nature biotechnology* *27*, 478-484.
- Huang, B., Schiefer, J., Sass, C., Landwehrmeyer, G.B., Kosinski, C.M., and Kochanek, S. (2007a). High-Capacity Adenoviral Vector-Mediated Reduction of Huntingtin Aggregate Load In Vitro and In Vivo. *Human Gene Therapy* *18*, 303-311.
- Huang, R.-Q., Qu, Y.-H., Ke, W.-L., Zhu, J.-H., Pei, Y.-Y., and Jiang, C. (2007b). Efficient gene delivery targeted to the brain using a transferrin-conjugated polyethyleneglycol-modified polyamidoamine dendrimer. *The FASEB Journal* *21*, 1117-1125.

- Huang, R., Ke, W., Liu, Y., Jiang, C., and Pei, Y. (2008). The use of lactoferrin as a ligand for targeting the polyamidoamine-based gene delivery system to the brain. *Biomaterials* 29, 238-246.
- Hübener, J., and Riess, O. (2010). Polyglutamine-induced neurodegeneration in SCA3 is not mitigated by non-expanded ataxin-3: Conclusions from double-transgenic mouse models. *Neurobiology of Disease* 38, 116-124.
- Hwang do, W., Son, S., Jang, J., Youn, H., Lee, S., Lee, D., Lee, Y.S., Jeong, J.M., Kim, W.J., and Lee, D.S. (2011). A brain-targeted rabies virus glycoprotein-disulfide linked PEI nanocarrier for delivery of neurogenic microRNA. *Biomaterials* 32, 4968-4975.
- Ichikawa, Y., Goto, J., Hattori, M., Toyoda, A., Ishii, K., Jeong, S.-Y., Hashida, H., Masuda, N., Ogata, K., Kasai, F., *et al.* (2001). The genomic structure and expression of MJD, the Machado-Joseph disease gene. *Journal of Human Genetics* 46, 413-422.
- Ikeda, H., Yamaguchi, M., Sugai, S., Aze, Y., Narumiya, S., and Kakizuka, A. (1996). Expanded polyglutamine in the Machado-Joseph disease protein induces cell death in vitro and in vivo. *Nat Genet* 13, 196-202.
- Jacobi, H., Hauser, T.-K., Giunti, P., Globas, C., Bauer, P., Schmitz-Hübsch, T., Baliko, L., Filla, A., Mariotti, C., Rakowicz, M., *et al.* (2012). Spinocerebellar Ataxia Types 1, 2, 3 and 6: the Clinical Spectrum of Ataxia and Morphometric Brainstem and Cerebellar Findings. *Cerebellum* 11, 155-166.
- Judge, A.D., Robbins, M., Tavakoli, I., Levi, J., Hu, L., Fronda, A., Ambegia, E., McClintock, K., and MacLachlan, I. (2009). Confirming the RNAi-mediated mechanism of action of siRNA-based cancer therapeutics in mice. *Journal of Clinical Investigation* 119, 661-673.
- Jung, J., Xu, K., Lessing, D., and Bonini, N.M. (2009). Preventing Ataxin-3 protein cleavage mitigates degeneration in a *Drosophila* model of SCA3. *Human molecular genetics* 18, 4843-4852.
- Kanasty, R., Dorkin, J.R., Vegas, A., and Anderson, D. (2013). Delivery materials for siRNA therapeutics. *Nature Materials* 12, 967-977.
- Kawaguchi, Y., Okamoto, T., Taniwaki, M., Aizawa, M., Inoue, M., Katayama, S., Kawakami, H., Nakamura, S., Nishimura, M., Akiguchi, I., *et al.* (1994). CAG expansions in a novel gene for Machado-Joseph disease at chromosome 14q32.1. *Nat Genet* 8, 221-228.
- Ke, W., Shao, K., Huang, R., Han, L., Liu, Y., Li, J., Kuang, Y., Ye, L., Lou, J., and Jiang, C. (2009). Gene delivery targeted to the brain using an Angiopep-conjugated polyethyleneglycol-modified polyamidoamine dendrimer. *Biomaterials* 30, 6976-6985.
- Kedmi, R., Ben-Arie, N., and Peer, D. (2010). The systemic toxicity of positively charged lipid nanoparticles and the role of Toll-like receptor 4 in immune activation. *Biomaterials* 31, 6867-6875.
- Keiser, M.S., Boudreau, R.L., and Davidson, B.L. (2014). Broad Therapeutic Benefit After RNAi Expression Vector Delivery to Deep Cerebellar Nuclei: Implications for Spinocerebellar Ataxia Type 1 Therapy. *Molecular Therapy* 22, 588-595.
- Keiser, M.S., Geoghegan, J.C., Boudreau, R.L., Lennox, K.A., and Davidson, B.L. (2013). RNAi or overexpression: Alternative therapies for Spinocerebellar Ataxia Type 1. *Neurobiology of disease* 56, 6-13.

- Khodr, C.E., Sapru, M.K., Pedapati, J., Han, Y., West, N.C., Kells, A.P., Bankiewicz, K.S., and Bohn, M.C. (2011). An alpha-synuclein AAV gene silencing vector ameliorates a behavioral deficit in a rat model of Parkinson's disease, but displays toxicity in dopamine neurons. *Brain research* 1395, 94-107.
- Khvorova, A., Reynolds, A., and Jayasena, S.D. (2003). Functional siRNAs and miRNAs Exhibit Strand Bias. *Cell* 115, 209-216.
- Kieling, C., Prestes, P.R., Saraiva-Pereira, M.L., and Jardim, L.B. (2007). Survival estimates for patients with Machado–Joseph disease (SCA3). *Clinical Genetics* 72, 543-545.
- Kim, J.Y., Choi, W.I., Kim, Y.H., and Tae, G. (2013). Brain-targeted delivery of protein using chitosan- and RVG peptide-conjugated, pluronic-based nano-carrier. *Biomaterials* 34, 1170-1178.
- Kim, S.I., Shin, D., Choi, T.H., Lee, J.C., Cheon, G.-J., Kim, K.-Y., Park, M., and Kim, M. (2007). Systemic and Specific Delivery of Small Interfering RNAs to the Liver Mediated by Apolipoprotein A-I. *Molecular Therapy* 15, 1145-1152.
- Kim, V.N. (2005). MicroRNA biogenesis: coordinated cropping and dicing. *Nature Reviews Molecular Cell Biology* 6, 376-385.
- Klockgether, T., Skalej, M., Wedekind, D., Luft, A.R., Welte, D., Schulz, J.B., Abele, M., Bürk, K., Laccone, F., Brice, A., *et al.* (1998). Autosomal dominant cerebellar ataxia type I. MRI-based volumetry of posterior fossa structures and basal ganglia in spinocerebellar ataxia types 1, 2 and 3. *Brain : a journal of neurology* 121, 1687-1693.
- Konno, A., Shuvaev, A.N., Miyake, N., Miyake, K., Iizuka, A., Matsuura, S., Huda, F., Nakamura, K., Yanagi, S., Shimada, T., *et al.* (2014). Mutant ataxin-3 with an abnormally expanded polyglutamine chain disrupts dendritic development and metabotropic glutamate receptor signaling in mouse cerebellar Purkinje cells. *Cerebellum* 13, 29-41.
- Kordasiewicz, H.B., Stanek, L.M., Wancewicz, E.V., Mazur, C., McAlonis, M.M., Pytel, K.A., Artates, J.W., Weiss, A., Cheng, S.H., Shihabuddin, L.S., *et al.* (2012). Sustained therapeutic reversal of Huntington's disease by transient repression of huntingtin synthesis. *Neuron* 74, 1031-1044.
- Kostarelos, K., and Miller, A.D. (2005). Synthetic, self-assembly ABCD nanoparticles; a structural paradigm for viable synthetic non-viral vectors. *Chemical Society Reviews* 34, 970-994.
- Kraft, J.C., and Ho, R.J. (2014). Interactions of indocyanine green and lipid in enhancing near-infrared fluorescence properties: the basis for near-infrared imaging in vivo. *Biochemistry* 53, 1275-1283.
- Kubowicz, P., Żelazczyk, D., and Pękala, E. (2013). RNAi in clinical studies. *Current Medicinal Chemistry* 20, 1801-1816.
- Kuhlbrodt, K., Janiesch, P.C., Kevei, E., Segref, A., Barikbin, R., and Hoppe, T. (2011). The Machado-Joseph disease deubiquitylase ATX-3 couples longevity and proteostasis. *Nature Cell Biology* 13, 273-281.
- Kumar, P., Wu, H., McBride, J.L., Jung, K.E., Kim, M.H., Davidson, B.L., Lee, S.K., Shankar, P., and Manjunath, N. (2007). Transvascular delivery of small interfering RNA to the central nervous system. *Nature* 448, 39-43.

- Lee, Y., Ahn, C., Han, J., Choi, H., Kim, J., Yim, J., Lee, J., Provost, P., Radmark, O., Kim, S., *et al.* (2003). The nuclear RNase III Drosha initiates microRNA processing. *Nature* 425, 415-419.
- Lee, Y., Jeon, K., Lee, J.-T., Kim, S., and Kim, V. (2002). MicroRNA maturation: stepwise processing and subcellular localization. *The EMBO Journal* 21, 4663-4670.
- Lentz, T.L., Burrage, T.G., Smith, A.L., Crick, J., and Tignor, G.H. (1982). Is the acetylcholine receptor a rabies virus receptor? *Science* 215, 182-184.
- Lewis, D.L., Hagstrom, J.E., Loomis, A.G., Wolff, J.A., and Herweijer, H. (2002). Efficient delivery of siRNA for inhibition of gene expression in postnatal mice. *Nat Genet* 32, 107-108.
- Li, F., Macfarlan, T., Pittman, R.N., and Chakravarti, D. (2002). Ataxin-3 Is a Histone-binding Protein with Two Independent Transcriptional Corepressor Activities. *Journal of Biological Chemistry* 277, 45004-45012.
- Li, L.-B., Yu, Z., Teng, X., and Bonini, N.M. (2008). RNA toxicity is a component of ataxin-3 degeneration in *Drosophila*. *Nature* 453, 1107-1111.
- Li, Y., Yokota, T., Matsumura, R., Taira, K., and Mizusawa, H. (2004). Sequence-dependent and independent inhibition specific for mutant ataxin-3 by small interfering RNA. *Annals of Neurology* 56, 124-129.
- Lima, L., and Coutinho, P. (1980). Clinical criteria for diagnosis of Machado-Joseph disease: report of a non-Azorena Portuguese family. *Neurology* 30, 319-322.
- Lima, W., Prakash, T., Murray, H., Kinberger, G., Li, W., Chappell, A., Li, C., Murray, S., Gaus, H., Seth, P., *et al.* (2012). Single-stranded siRNAs activate RNAi in animals. *Cell* 150, 883-894.
- Lin, Q., Chen, J., Zhang, Z., and Zheng, G. (2013). Lipid-based nanoparticles in the systemic delivery of siRNA. *Nanomedicine* 9, 105-120.
- Liu, J., Pendergraff, H., Narayanannair, K.J., Lackey, J.G., Kuchimanchi, S., Rajeev, K.G., Manoharan, M., Hu, J., and Corey, D.R. (2013a). RNA duplexes with abasic substitutions are potent and allele-selective inhibitors of huntingtin and ataxin-3 expression. *Nucleic Acids Research* 41, 8788-8801.
- Liu, J., Yu, D., Aiba, Y., Pendergraff, H., Swayze, E.E., Lima, W.F., Hu, J., Prakash, T.P., and Corey, D.R. (2013b). ss-siRNAs allele selectively inhibit ataxin-3 expression: multiple mechanisms for an alternative gene silencing strategy. *Nucleic Acids Research* 41, 9570-9583.
- Liu, Y., Guo, Y., An, S., Kuang, Y., He, X., Ma, H., Li, J., Lv, J., Zhang, N., and Jiang, C. (2013c). Targeting Caspase-3 as Dual Therapeutic Benefits by RNAi Facilitating Brain-Targeted Nanoparticles in a Rat Model of Parkinson's Disease. *PloS one* 8, e62905.
- Liu, Y., Huang, R., Han, L., Ke, W., Shao, K., Ye, L., Lou, J., and Jiang, C. (2009). Brain-targeting gene delivery and cellular internalization mechanisms for modified rabies virus glycoprotein RVG29 nanoparticles. *Biomaterials* 30, 4195-4202.
- Machida, Y., Okada, T., Kurosawa, M., Oyama, F., Ozawa, K., and Nukina, N. (2006). rAAV-mediated shRNA ameliorated neuropathology in Huntington disease model mouse. *Biochemical and Biophysical Research Communications* 343, 190-197.
- Maciel, P., Gaspar, C., DeStefano, A.L., Silveira, I., Coutinho, P., Radvany, J., Dawson, D.M., Sudarsky, L., Guimarães, J., Loureiro, J.E.L., *et al.* (1995). Correlation

between CAG Repeat Length and Clinical Features in Machado-Joseph Disease. *American Journal of Human Genetics* 57, 54-61.

- Mao, S., Sun, W., and Kissel, T. (2010). Chitosan-based formulations for delivery of DNA and siRNA. *Advanced Drug Delivery Reviews* 62, 12-27.
- Mao, Y., Senic-Matuglia, F., Di Fiore, P.P., Polo, S., Hodsdon, M.E., and De Camilli, P. (2005). Deubiquitinating function of ataxin-3: Insights from the solution structure of the Josephin domain. *Proceedings of the National Academy of Sciences of the United States of America* 102, 12700-12705.
- Maruyama, H.N., Shigenobu; Matsuyama, Zenjiro Sakai, Tetsuo; Doyu, Manabu; Sobue, Gen; Seto, Makiko; Tsujihata, Mitsuhiro; Oh-i, Takekazu; Nishio, Takeshi; Sunohara, Nobuhiko; Takahashi, Ryosuke; Hayashi, Michiyuki; Nishino, Ichizo; Ohtake, Toshiyuki; Oda, Tatsuro; Nishimura, Masataka; Saida, Takahiko; Matsumoto, Hiroyuki; Baba, Masayuki; Kawaguchi, Yoshiya; Kakizuka, Akira; Kawakami, Hideshi (1995). Molecular features of the CAG repeats and clinical manifestation of Machado-Joseph disease. *Human molecular genetics* 4, 807-812.
- Matilla, T., McCall, A., Subramony, S., and HY, Z. (1995). Molecular and clinical correlations in spinocerebellar ataxia type 3 and Machado-Joseph disease. *Annals of Neurology* 38, 68-72.
- Matos, C.A., de Macedo-Ribeiro, S., and Carvalho, A.L. (2011). Polyglutamine diseases: The special case of ataxin-3 and Machado-Joseph disease. *Progress in Neurobiology* 95, 26-48.
- Matsumura, R., Takayanagi, T., Murata, K., Futamura, N., Hirano, M., and Ueno, S. (1996). Relationship of (CAG)_nC configuration to repeat instability of the Machado-Joseph disease gene. *Human Genetics* 98, 643-645.
- Mazzucchelli, S., De Palma, A., Riva, M., D'Urzo, A., Pozzi, C., Pastori, V., Comelli, F., Fusì, P., Vanoni, M., Tortora, P., *et al.* (2009). Proteomic and biochemical analyses unveil tight interaction of ataxin-3 with tubulin. *The International Journal of Biochemistry & Cell Biology* 41, 2485-2492.
- McBride, J.L., Pitzer, M.R., Boudreau, R.L., Dufour, B., Hobbs, T., Ojeda, S.R., and Davidson, B.L. (2011). Preclinical Safety of RNAi-Mediated HTT Suppression in the Rhesus Macaque as a Potential Therapy for Huntington's Disease. *Molecular Therapy* 19, 2152-2162.
- McCaffrey, A.P., Meuse, L., Pham, T.-T.T., Conklin, D.S., Hannon, G.J., and Kay, M.A. (2002). Gene expression: RNA interference in adult mice. *Nature* 418, 38-39.
- Mendonca, L.S., Firmino, F., Moreira, J.N., Pedrosa de Lima, M.C., and Simoes, S. (2010a). Transferrin receptor-targeted liposomes encapsulating anti-BCR-ABL siRNA or asODN for chronic myeloid leukemia treatment. *Bioconjugate chemistry* 21, 157-168.
- Mendonca, L.S., Moreira, J.N., de Lima, M.C., and Simoes, S. (2010b). Co-encapsulation of anti-BCR-ABL siRNA and imatinib mesylate in transferrin receptor-targeted sterically stabilized liposomes for chronic myeloid leukemia treatment. *Biotechnology and Bioengineering* 107, 884-893.
- Mendonça, L.S., Nobrega, C., Hirai, H., Kaspar, B.K., and Pereira de Almeida, L. (2015). Transplantation of cerebellar neural stem cells improves motor coordination and neuropathology in Machado-Joseph disease mice. *Brain : a journal of neurology* 138, 320-335.

- Miller, V.M., Xia, H., Marrs, G.L., Gouvion, C.M., Lee, G., Davidson, B.L., and Paulson, H.L. (2003). Allele-specific silencing of dominant disease genes. *Proceedings of the National Academy of Sciences* *100*, 7195-7200.
- Moreira, J.N., Ishida, T., Gaspar, R., and Allen, T.M. (2002). Use of the post-insertion technique to insert peptide ligands into pre-formed stealth liposomes with retention of binding activity and cytotoxicity. *Pharmaceutical research* *19*, 265-269.
- Morrissey, D.V., Lockridge, J.A., Shaw, L., Blanchard, K., Jensen, K., Breen, W., Hartsough, K., Machemer, L., Radka, S., Jadhav, V., *et al.* (2005). Potent and persistent in vivo anti-HBV activity of chemically modified siRNAs. *Nature biotechnology* *23*, 1002-1007.
- Muñoz, E., Rey, M.J., Milà, M., Cardozo, A., Ribalta, T., Tolosa, E., and Ferrer, I. (2002). Intranuclear inclusions, neuronal loss and CAG mosaicism in two patients with Machado–Joseph disease. *Journal of the neurological sciences* *200*, 19-25.
- Nakano, K., Dawson, D., and Spence, A. (1972). Machado disease. A hereditary ataxia in Portuguese emigrants to Massachusetts. *Neurology* *22*, 49-55.
- Nascimento-Ferreira, I., Nóbrega, C., Vasconcelos-Ferreira, A., Onofre, I., Albuquerque, D., Aveleira, C., Hirai, H., Déglon, N., and Pereira de Almeida, L. (2013). Beclin 1 mitigates motor and neuropathological deficits in genetic mouse models of Machado–Joseph disease. *Brain : a journal of neurology* *136*, 2173-2188.
- Nascimento-Ferreira, I., Santos-Ferreira, T., Sousa-Ferreira, L., Auregan, G., Onofre, I., Alves, S., Dufour, N., Colomer Gould, V.F., Koeppen, A., Deglon, N., *et al.* (2011). Overexpression of the autophagic beclin-1 protein clears mutant ataxin-3 and alleviates Machado-Joseph disease. *Brain : a journal of neurology* *134*, 1400-1415.
- Nicastro, G., Masino, L., Esposito, V., Menon, R.P., De Simone, A., Fraternali, F., and Pastore, A. (2009). Josephin domain of ataxin-3 contains two distinct ubiquitin-binding sites. *Biopolymers* *91*, 1203-1214.
- Nicastro, G., Menon, R.P., Masino, L., Knowles, P.P., McDonald, N.Q., and Pastore, A. (2005). The solution structure of the Josephin domain of ataxin-3: Structural determinants for molecular recognition. *Proceedings of the National Academy of Sciences of the United States of America* *102*, 10493-10498.
- Nicastro, G., Todi, S.V., Karaca, E., Bonvin, A.M.J.J., Paulson, H.L., and Pastore, A. (2010). Understanding the Role of the Josephin Domain in the PolyUb Binding and Cleavage Properties of Ataxin-3. *PLoS one* *5*, e12430.
- Nishina, K., Mizusawa, H., and Yokota, T. (2013). Short interfering RNA and the central nervous system: development of nonviral delivery systems. *Expert Opinion on Drug Delivery* *10*, 289-292.
- Nishiyama, K., Murayama, S., Goto, J., Watanabe, M., Hashida, H., Katayama, S., Nomura, Y., Nakamura, S., and Kanazawa, I. (1996). Regional and cellular expression of the Machado-Joseph disease gene in brains of normal and affected individuals. *Annals of Neurology* *40*, 776-781.
- Nóbrega, C., Nascimento-Ferreira, I., Onofre, I., Albuquerque, D., Conceição, M., Déglon, N., and de Almeida, L. (2013a). Overexpression of Mutant Ataxin-3 in Mouse Cerebellum Induces Ataxia and Cerebellar Neuropathology. *Cerebellum* *12*, 441-455.

- Nóbrega, C., Nascimento-Ferreira, I., Onofre, I., Albuquerque, D., Deglon, N., and de Almeida, L.P. (2014). RNA interference mitigates motor and neuropathological deficits in a cerebellar mouse model of Machado-Joseph disease. *PloS one* 9, e100086.
- Nóbrega, C., Nascimento-Ferreira, I., Onofre, I., Albuquerque, D., Hirai, H., Deglon, N., and de Almeida, L.P. (2013b). Silencing mutant ataxin-3 rescues motor deficits and neuropathology in Machado-Joseph disease transgenic mice. *PloS one* 8, e52396.
- Nóbrega, C., and Pereira de Almeida, L. (2012). Machado-Joseph Disease / Spinocerebellar Ataxia Type 3. In *Spinocerebellar Ataxia*, D.J. Gazulla, ed. (<http://www.intechopen.com/books/spinocerebellar-ataxia/machado-joseph-disease-or-spinocerebellar-ataxia-type-3-sca3>: InTech), pp. 103-138.
- O'Mahony, A.M., Godinho, B.M.D.C., Cryan, J.F., and O'Driscoll, C.M. (2013). Non-Viral Nanosystems for Gene and Small Interfering RNA Delivery to the Central Nervous System: Formulating the Solution. *Journal of Pharmaceutical Sciences* 102, 3469-3484.
- Ohno, M., Cole, S.L., Yasvoina, M., Zhao, J., Citron, M., Berry, R., Disterhoft, J.F., and Vassar, R. (2007). BACE1 gene deletion prevents neuron loss and memory deficits in 5XFAD APP/PS1 transgenic mic. *Neurobiology of disease* 26, 134-145.
- Østergaard, M.E., Southwell, A.L., Kordasiewicz, H., Watt, A.T., Skotte, N.H., Doty, C.N., Vaid, K., Villanueva, E.B., Swayze, E.E., Frank Bennett, C., *et al.* (2013). Rational design of antisense oligonucleotides targeting single nucleotide polymorphisms for potent and allele selective suppression of mutant Huntingtin in the CNS. *Nucleic Acids Research* 41, 9634-9650.
- Ozcan, G., Ozpolat, B., Coleman, R.L., Sood, A.K., and Lopez-Berestein, G. (2015). Preclinical and clinical development of siRNA-based therapeutics. *Advanced Drug Delivery Reviews* 87, 108-119.
- Padiath, Q.S., Srivastava, A.K., Roy, S., Jain, S., and Brahmachari, S.K. (2005). Identification of a novel 45 repeat unstable allele associated with a disease phenotype at the MJD1/SCA3 locus. *American Journal of Medical Genetics Part B: Neuropsychiatric Genetics* 133B, 124-126.
- Pardridge, W.M. (2002). Drug and Gene Delivery to the Brain: The Vascular Route. *Neuron* 36, 555-558.
- Park, T.E., Singh, B., Li, H., Lee, J.Y., Kang, S.K., Choi, Y.J., and Cho, C.S. (2015). Enhanced BBB permeability of osmotically active poly(mannitol-co-PEI) modified with rabies virus glycoprotein via selective stimulation of caveolar endocytosis for RNAi therapeutics in Alzheimer's disease. *Biomaterials* 38, 61-71.
- Paul, C.P., Good, P.D., Winer, I., and Engelke, D.R. (2002). Effective expression of small interfering RNA in human cells. *Nat Biotech* 20, 505-508.
- Paulson, H. (2012). Machado-Joseph disease/spinocerebellar ataxia type 3. *Handbook of clinical neurology* 103, 437-449.
- Paulson, H., Das, S., Crino, P., Perez, M., Patel, S., Gotsdiner, D., Fischbeck, K., and Pittman, R. (1997a). Machado-Joseph disease gene product is a cytoplasmic protein widely expressed in brain. *Annals of Neurology* 41, 453-462.
- Paulson, H.L., Perez, M.K., Trotter, Y., Trojanowski, J.Q., Subramony, S.H., Das, S.S., Vig, P., Mandel, J.L., Fischbeck, K.H., and Pittman, R.N. (1997). Intranuclear

inclusions of expanded polyglutamine protein in spinocerebellar ataxia type 3. *Neuron* *19*, 333-344.

- Pecot, C.V., Calin, G.A., Coleman, R.L., Lopez-Berestein, G., and Sood, A.K. (2011). RNA interference in the clinic: challenges and future directions. *Nature Reviews Cancer* *11*, 59-67.
- Peer, D., and Lieberman, J. (2011). Special delivery: targeted therapy with small RNAs. *Gene therapy* *18*, 1127-1133.
- Pérez-Martínez, F., Carrión, B., and Ceña, V. (2012). The use of nanoparticles for gene therapy in the nervous system. *Journal of Alzheimer's Disease* *31*, 697-710.
- Pérez-Martínez, F.C., Guerra, J., Posadas, I., and Ceña, V. (2011). Barriers to Non-Viral Vector-Mediated Gene Delivery in the Nervous System. *Pharmaceutical research* *28*, 1843-1858.
- Piedrahita, D., Hernández, I., López-Tobón, A., Fedorov, D., Obara, B., Manjunath, B.S., Boudreau, R.L., Davidson, B., LaFerla, F., Gallego-Gómez, J.C., *et al.* (2010). Silencing of CDK5 Reduces Neurofibrillary Tangles in Transgenic Alzheimer's Mice. *The Journal of neuroscience : the official journal of the Society for Neuroscience* *30*, 13966-13976.
- Posadas, I., Guerra, F.J., and Ceña, V. (2010). Nonviral vectors for the delivery of small interfering RNAs to the CNS. *Nanomedicine* *5*, 1219-1236.
- Provost, P., Dishart, D., Doucet, J., Frenthewey, D., Samuelsson, B., and Rådmark, O. (2002). Ribonuclease activity and RNA binding of recombinant human Dicer. *The EMBO Journal* *21*, 5864-5874.
- Pulford, B., Reim, N., Bell, A., Veatch, J., Forster, G., Bender, H., Meyerett, C., Hafeman, S., Michel, B., Johnson, T., *et al.* (2010). Liposome-siRNA-peptide complexes cross the blood-brain barrier and significantly decrease PrP on neuronal cells and PrP in infected cell cultures. *PLoS one* *5*, e11085.
- Ramachandran, P., Boudreau, R., Schaefer, K., La Spada, A., and Davidson, B. (2014). Nonallele specific silencing of ataxin-7 improves disease phenotypes in a mouse model of SCA7. *Molecular Therapy* *22*, 1635-1642.
- Rana, T.M. (2007). Illuminating the silence: understanding the structure and function of small RNAs. *Nature Reviews Molecular Cell Biology* *8*, 23-36.
- Ranum, L.P., Lundgren, J.K., Schut, L.J., Ahrens, M.J., Perlman, S., Aita, J., Bird, T.D., Gomez, C., and Orr, H.T. (1995). Spinocerebellar ataxia type 1 and Machado-Joseph disease: incidence of CAG expansions among adult-onset ataxia patients from 311 families with dominant, recessive, or sporadic ataxia. *American Journal of Human Genetics* *57*, 603-608.
- Reina, C.P., Zhong, X., and Pittman, R.N. (2010). Proteotoxic stress increases nuclear localization of ataxin-3. *Human molecular genetics* *19*, 235-249.
- Riess, O.R., Udo; Pastore, Annalisa; Bauer, Peter; Schols, Ludger (2008). SCA3: Neurological features, pathogenesis and animal models. *Cerebellum* *7*, 125-137.
- Robbins, M., Judge, A., and MacLachlan, I. (2009). siRNA and innate immunity. *Oligonucleotides* *19*, 89-102.
- Rodrigues, A.-J., Coppola, G., Santos, C., Costa, M.d.C., Ailion, M., Sequeiros, J., Geschwind, D.H., and Maciel, P. (2007). Functional genomics and biochemical characterization of the *C. elegans* orthologue of the Machado-Joseph disease protein ataxin-3. *The FASEB Journal* *21*, 1126-1136.

- Rodrigues, A.-J., do Carmo Costa, M., Silva, T.-L., Ferreira, D., Bajanca, F., Logarinho, E., and Maciel, P. (2010). Absence of ataxin-3 leads to cytoskeletal disorganization and increased cell death. *Biochimica et Biophysica Acta (BBA) - Molecular Cell Research* 1803, 1154-1163.
- Rodrigues, A.J., Neves-Carvalho, A., Teixeira-Castro, A., Rokka, A., Corthals, G., Logarinho, E., and Maciel, P. (2011). Absence of Ataxin-3 Leads to Enhanced Stress Response in *C. elegans*. *PLoS one* 6, e18512.
- Rodriguez-Lebron, E., Costa Mdo, C., Luna-Cancelon, K., Peron, T.M., Fischer, S., Boudreau, R.L., Davidson, B.L., and Paulson, H.L. (2013). Silencing mutant ATXN3 expression resolves molecular phenotypes in SCA3 transgenic mice. *Molecular Therapy* 21, 1909-1918.
- Rodriguez-Lebron, E., Denovan-Wright, E.M., Nash, K., Lewin, A.S., and Mandel, R.J. (2005). Intrastratial rAAV-Mediated Delivery of Anti-huntingtin shRNAs Induces Partial Reversal of Disease Progression in R6/1 Huntington's Disease Transgenic Mice. *Molecular therapy* 12, 618-633.
- Rodriguez-Lebron, E., Gouvion, C.M., Moore, S.A., Davidson, B.L., and Paulson, H.L. (2009). Allele-specific RNAi Mitigates Phenotypic Progression in a Transgenic Model of Alzheimer's Disease. *Molecular Therapy* 17, 1563-1573.
- Rosenberg, R., Nyhan, W., Bay, C., and Shore, P. (1976). Autosomal dominant striatonigral degeneration. A clinical, pathologic, and biochemical study of a new genetic disorder. *Neurology* 26, 703-714.
- Ross, C.A., and Poirier, M.A. (2005). What is the role of protein aggregation in neurodegeneration? *Nature Reviews Molecular Cell Biology* 6, 891-898.
- Rüb, U., Brunt, E.R., and Deller, T. (2008). New insights into the pathoanatomy of spinocerebellar ataxia type 3 (Machado-Joseph disease). *Current Opinion in Neurology* 21, 111-116.
- Rüb, U., Schöls, L., Paulson, H., Auburger, G., Kermer, P., Jen, J.C., Seidel, K., Korf, H.-W., and Deller, T. (2013). Clinical features, neurogenetics and neuropathology of the polyglutamine spinocerebellar ataxias type 1, 2, 3, 6 and 7. *Progress in Neurobiology* 104, 38-66.
- Sakurai, H., Kawabata, K., Sakurai, F., Nakagawa, S., and Mizuguchi, H. (2008). Innate immune response induced by gene delivery vectors. *International Journal of Pharmaceutics* 354, 9-15.
- Sapru, M.K., Yates, J.W., Hogan, S., Jiang, L., Halter, J., and Bohn, M.C. (2006). Silencing of human α -synuclein in vitro and in rat brain using lentiviral-mediated RNAi. *Experimental Neurology* 198, 382-390.
- Sasaki, H., Wakisaka, A., Fukazawa, T., Iwabuchi, K., Hamada, T., Takada, A., Mukai, E., Matsuura, T., Yoshiki, T., and Tashiro, K. (1995). CAG repeat expansion of Machado-Joseph disease in the Japanese: analysis of the repeat instability for parental transmission, and correlation with disease phenotype. *Journal of the neurological sciences* 133, 128-133.
- Saute, J.A.M., and Jardim, L.B. (2015). Machado Joseph disease: clinical and genetic aspects, and current treatment. *Expert Opinion on Orphan Drugs* 3, 517-535.
- Scaglione, K.M., Zavodszky, E., Todi, S.V., Patury, S., Xu, P., Rodríguez-Lebrón, E., Fischer, S., Konen, J., Djarmati, A., Peng, J., *et al.* (2011). Ube2w and ataxin-3 coordinately regulate the ubiquitin ligase CHIP. *Molecular cell* 43, 599-612.

- Scherzed, W., Brunt, E.R., Heinsen, H., de Vos, R.A., Seidel, K., Bürk, K., Schöls, L., Auburger, G., Del Turco, D., Deller, T., *et al.* (2012). Pathoanatomy of Cerebellar Degeneration in Spinocerebellar Ataxia Type 2 (SCA2) and Type 3 (SCA3). *Cerebellum* 11, 749-760.
- Schlachetzki, F., Zhang, Y., Boado, R., and Pardridge, W. (2004). Gene therapy of the brain: the trans-vascular approach. *Neurology* 62, 1275-1281.
- Schmidt T, L.G., Schmitt I, Trottier Y, Auburger G, Laccone F, Klockgether T, Völpel M, Epplen JT, Schöls L, Riess O (1998). An isoform of ataxin-3 accumulates in the nucleus of neuronal cells in affected brain regions of SCA3 patients. *Brain Pathology* 8, 669-679.
- Schmidt, T., Lindenberg, K., Krebs, A., Schöls, L., Laccone, F., Herms, J., Rechsteiner, M., Riess, O., and Landwehrmeyer, G. (2002). Protein surveillance machinery in brains with spinocerebellar ataxia type 3: redistribution and differential recruitment of 26S proteasome subunits and chaperones to neuronal intranuclear inclusions. *Annals of Neurology* 51, 302-310.
- Schmitt, I., Linden, M., Khazneh, H., Evert, B.O., Breuer, P., Klockgether, T., and Wuellner, U. (2007). Inactivation of the mouse *Atxn3* (ataxin-3) gene increases protein ubiquitination. *Biochemical and Biophysical Research Communications* 362, 734-739.
- Schnell, M.J., McGettigan, J.P., Wirblich, C., and Papaneri, A. (2010). The cell biology of rabies virus: using stealth to reach the brain. *Nat Rev Microbiol* 8, 51-61.
- Schöls L, A.G., Büttner T, Przuntek H, Epplen JT, Riess O (1997). Autosomal dominant cerebellar ataxia: phenotypic differences in genetically defined subtypes? . *Annals of Neurology* 42, 924-932.
- Schols, L., Bauer, P., Schmidt, T., Schulte, T., and Riess, O. (2004). Autosomal dominant cerebellar ataxias: clinical features, genetics, and pathogenesis. *Lancet Neurology* 3, 291-304.
- Schöls, L., Haan, J., Riess, O., Amoiridis, G., and Przuntek, H. (1998). Sleep disturbance in spinocerebellar ataxias: is the SCA3 mutation a cause of restless legs syndrome? *Neurology* 51, 1603-1607.
- Schulz, J.B., Borkert, J., Wolf, S., Schmitz-Hübsch, T., Rakowicz, M., Mariotti, C., Schoels, L., Timmann, D., van de Warrenburg, B., Dürr, A., *et al.* (2010). Visualization, quantification and correlation of brain atrophy with clinical symptoms in spinocerebellar ataxia types 1, 3 and 6. *NeuroImage* 49, 158-168.
- Schwarz, D.S., Hutvágner, G., Du, T., Xu, Z., Aronin, N., and Zamore, P.D. (2003). Asymmetry in the Assembly of the RNAi Enzyme Complex. *Cell* 115, 199-208.
- Seidel, K., Siswanto, S., Brunt, E.P., den Dunnen, W., Korf, H.-W., and Rüb, U. (2012). Brain pathology of spinocerebellar ataxias. *Acta Neuropathol* 124, 1-21.
- Semple, S.C., Klimuk, S.K., Harasym, T.O., Dos Santos, N., Ansell, S.M., Wong, K.F., Maurer, N., Stark, H., Cullis, P.R., Hope, M.J., *et al.* (2001). Efficient encapsulation of antisense oligonucleotides in lipid vesicles using ionizable aminolipids: formation of novel small multilamellar vesicle structures. *Biochimica et Biophysica Acta (BBA) - Biomembranes* 1510, 152-166.
- Shi, N., and Pardridge, W.M. (2000). Noninvasive gene targeting to the brain. *Proceedings of the National Academy of Sciences* 97, 7567-7572.

- Shim, M.S., and Kwon, Y.J. (2010). Efficient and targeted delivery of siRNA in vivo. *The FEBS journal* 277, 4814-4827.
- Shimohata, T., Nakajima, T., Yamada, M., Uchida, C., Onodera, O., Naruse, S., Kimura, T., Koide, R., Nozaki, K., Sano, Y., *et al.* (2000). Expanded polyglutamine stretches interact with TAFII130, interfering with CREB-dependent transcription *Nat Genet* 26, 29-36.
- Silva-Fernandes, A., Costa, M.d.C., Duarte-Silva, S., Oliveira, P., Botelho, C.M., Martins, L., Mariz, J.A., Ferreira, T., Ribeiro, F., Correia-Neves, M., *et al.* (2010). Motor uncoordination and neuropathology in a transgenic mouse model of Machado–Joseph disease lacking intranuclear inclusions and ataxin-3 cleavage products. *Neurobiology of Disease* 40, 163-176.
- Silva-Fernandes, A., Duarte-Silva, S., Neves-Carvalho, A., Amorim, M., Soares-Cunha, C., Oliveira, P., Thirstrup, K., Teixeira-Castro, A., and Maciel, P. (2014). Chronic treatment with 17-DMAG improves balance and coordination in a new mouse model of Machado-Joseph disease. *Neurotherapeutics* 11, 433-449.
- Simões, A.T., Gonçalves, N., Koeppen, A., Déglon, N., Kügler, S., Duarte, C.B., and Pereira de Almeida, L. (2012). Calpastatin-mediated inhibition of calpains in the mouse brain prevents mutant ataxin 3 proteolysis, nuclear localization and aggregation, relieving Machado–Joseph disease. *Brain : a journal of neurology* 135, 2428-2439.
- Simões, A.T., Goncalves, N., Nobre, R.J., Duarte, C.B., and Pereira de Almeida, L. (2014). Calpain inhibition reduces ataxin-3 cleavage alleviating neuropathology and motor impairments in mouse models of Machado-Joseph disease. *Human molecular genetics* 23, 4932-4944.
- Singer, O., Marr, R.A., Rockenstein, E., Crews, L., Coufal, N.G., Gage, F.H., Verma, I.M., and Masliah, E. (2005). Targeting BACE1 with siRNAs ameliorates Alzheimer disease neuropathology in a transgenic model. *Nature Neuroscience* 8, 1343-1349.
- Son, S., Hwang do, W., Singha, K., Jeong, J.H., Park, T.G., Lee, D.S., and Kim, W.J. (2011). RVG peptide tethered bio-reducible polyethylenimine for gene delivery to brain. *Journal of Controlled Release* 155, 18-25.
- Song, E., Lee, S.-K., Wang, J., Ince, N., Ouyang, N., Min, J., Chen, J., Shankar, P., and Lieberman, J. (2003). RNA interference targeting Fas protects mice from fulminant hepatitis. *Nature Medicine* 9, 347-351.
- Stiles, D.K., Zhang, Z., Ge, P., Nelson, B., Grondin, R., Ai, Y., Hardy, P., Nelson, P.T., Guzaev, A.P., Butt, M.T., *et al.* (2012). Widespread suppression of huntingtin with convection-enhanced delivery of siRNA. *Experimental Neurology* 233, 463-471.
- Sudarsky, L., and Coutinho, P. (1995). Machado-Joseph disease. *Clinical neuroscience* 3, 17-22.
- Takahashi, T., Katada, S., and Onodera, O. (2010). Polyglutamine Diseases: Where does Toxicity Come from? What is Toxicity? Where are We Going? *Journal of Molecular Cell Biology* 2, 180-191.
- Takahashi, T., Kikuchi, S., Katada, S., Nagai, Y., Nishizawa, M., and Onodera, O. (2008). Soluble polyglutamine oligomers formed prior to inclusion body formation are cytotoxic. *Human molecular genetics* 17, 345-356.
- Takiyama, Y., Nishizawa, M., Tanaka, H., Kawashima, S., Sakamoto, H., Karube, Y., Shimazaki, H., Soutome, M., Endo, K., Ohta, S., *et al.* (1993). The gene for Machado-Joseph disease maps to human chromosome 14q. *Nat Genet* 4, 300-304.

- Taniwaki, T., Sakai, T., Kobayashi, T., Kuwabara, Y., Otsuka, M., Ichiya, Y., Masuda, K., and Goto, I. (1997). Positron emission tomography (PET) in Machado-Joseph disease. *Journal of the neurological sciences* 145, 63-67.
- Tao, Y.H., Han, J.F., and Dou, H.Y. (2012). Brain-targeting gene delivery using a rabies virus glycoprotein peptide modulated hollow liposome: bio-behavioral study. *Journal of Materials Chemistry* 22, 11808-11815.
- Taroni, F.D., Stefano (2004). Pathways to motor incoordination: the inherited ataxias. *Nature Reviews Neuroscience* 5, 641-655.
- Thomas, C.E., Ehrhardt, A., and Kay, M.A. (2003). Progress and problems with the use of viral vectors for gene therapy. *Nature Reviews Genetics* 4, 346-358.
- Thoulouze, M.-I., Lafage, M., Schachner, M., Hartmann, U., Cremer, H., and Lafon, M. (1998). The Neural Cell Adhesion Molecule Is a Receptor for Rabies Virus. *Journal of Virology* 72, 7181-7190.
- Todi, S.V., Winborn, B.J., Scaglione, K.M., Blount, J.R., Travis, S.M., and Paulson, H.L. (2009). Ubiquitination directly enhances activity of the deubiquitinating enzyme ataxin-3. *The EMBO Journal* 28, 372-382.
- Tomalia, D.A., Baker, H., Dewald, J., Hall, M., Kallos, G., Martin, S., Roeck, J., Ryder, J., and Smith, P. (1985). A New Class of Polymers: Starburst-Dendritic Macromolecules. *Polymer Journal* 17, 117-132.
- Torashima, T., Koyama, C., Iizuka, A., Mitsumura, K., Takayama, K., Yanagi, S., Oue, M., Yamaguchi, H., and Hirai, H. (2008). Lentivector-mediated rescue from cerebellar ataxia in a mouse model of spinocerebellar ataxia. *EMBO reports* 9, 393-399.
- Trottier, Y., Cancel, G., An-Gourfinkel, I., Lutz, Y., Weber, C., Brice, A., Hirsch, E., and Mandel, J.-L. (1998). Heterogeneous Intracellular Localization and Expression of Ataxin-3. *Neurobiology of Disease* 5, 335-347.
- Tuffereau, C., Bénéjean, J., Blondel, D., Kieffer, B., and Flamand, A. (1998). Low-affinity nerve-growth factor receptor (P75NTR) can serve as a receptor for rabies virus. *The EMBO Journal* 17, 7250-7259.
- Tuite, P., Rogaeva, E., St George-Hyslop, P., and Lang, A. (1995). Dopa-responsive parkinsonism phenotype of Machado-Joseph disease: confirmation of 14q CAG expansion. *Annals of Neurology* 38, 684-687.
- Uchihara, T., Iwabuchi, K., Funata, N., and Yagishita, S. (2002). Attenuated Nuclear Shrinkage in Neurons with Nuclear Aggregates— A Morphometric Study on Pontine Neurons of Machado–Joseph Disease Brains. *Experimental Neurology* 178, 124-128.
- Valadi, H., Ekstrom, K., Bossios, A., Sjostrand, M., Lee, J.J., and Lotvall, J.O. (2007). Exosome-mediated transfer of mRNAs and microRNAs is a novel mechanism of genetic exchange between cells. *Nature Cell Biology* 9, 654-659.
- van Rooy, I., Mastrobattista, E., Storm, G., Hennink, W.E., and Schiffelers, R.M. (2011). Comparison of five different targeting ligands to enhance accumulation of liposomes into the brain. *Journal of Controlled Release* 150, 30-36.
- Wan, C., Allen, T.M., and Cullis, P.R. (2014). Lipid nanoparticle delivery systems for siRNA-based therapeutics. *Drug Deliv and Transl Res* 4, 74-83.
- Wang, G., Ide, K., Nukina, N., Goto, J., Ichikawa, Y., Uchida, K., Sakamoto, T., and Kanazawa, I. (1997). Machado–Joseph Disease Gene Product Identified in

Lymphocytes and Brain. *Biochemical and Biophysical Research Communications* 233, 476-479.

- Wang, J.J., Zeng, Z.W., Xiao, R.Z., Xie, T., Zhou, G.L., Zhan, X.R., and Wang, S.L. (2011a). Recent advances of chitosan nanoparticles as drug carriers. *International Journal of Nanomedicine* 6, 765-774.
- Wang, L.-C., Chen, K.-Y., Pan, H., Wu, C.-C., Chen, P.-H., Liao, Y.-T., Li, C., Huang, M.-L., and Hsiao, K.-M. (2011b). Muscleblind participates in RNA toxicity of expanded CAG and CUG repeats in *Caenorhabditis elegans*. *Cell Mol Life Sci* 68, 1255-1267.
- Wang, Y.-L., Liu, W., Wada, E., Murata, M., Wada, K., and Kanazawa, I. (2005). Clinico-pathological rescue of a model mouse of Huntington's disease by siRNA. *Neuroscience Research* 53, 241-249.
- Weksler, B.B., Subileau, E.A., Perrière, N., Charneau, P., Holloway, K., Leveque, M., Tricoire-Leignel, H., Nicotra, A., Bourdoulous, S., Turowski, P., *et al.* (2005). Blood-brain barrier-specific properties of a human adult brain endothelial cell line. *The FASEB Journal* 19, 1872-1874.
- Wender, P.A., Mitchell, D.J., Pattabiraman, K., Pelkey, E.T., Steinman, L., and Rothbard, J.B. (2000). The design, synthesis, and evaluation of molecules that enable or enhance cellular uptake: peptoid molecular transporters. *Proceedings of the National Academy of Sciences* 97, 13003-13008.
- Winborn, B.J., Travis, S.M., Todi, S.V., Scaglione, K.M., Xu, P., Williams, A.J., Cohen, R.E., Peng, J., and Paulson, H.L. (2008). The Deubiquitinating Enzyme Ataxin-3, a Polyglutamine Disease Protein, Edits Lys(63) Linkages in Mixed Linkage Ubiquitin Chains. *The Journal of biological chemistry* 283, 26436-26443.
- Wong, H.L., Wu, X.Y., and Bendayan, R. (2012). Nanotechnological advances for the delivery of CNS therapeutics. *Advanced Drug Delivery Reviews* 64, 686-700.
- Wu, S.Y., and McMillan, N.A. (2009). Lipidic systems for in vivo siRNA delivery. *AAPS J* 11, 639-652.
- Wullner, U., Reimold, M., Abele, M., Burk, K., Minnerop, M., Dohmen, B.M., Machulla, H.J., Bares, R., and Klockgether, T. (2005). Dopamine transporter positron emission tomography in spinocerebellar ataxias type 1, 2, 3, and 6. *Archives of Neurology* 62, 1280-1285.
- Xia, C.-F., Zhang, Y., Zhang, Y., Boado, R., and Pardridge, W. (2007). Intravenous siRNA of Brain Cancer with Receptor Targeting and Avidin-Biotin Technology. *Pharmaceutical research* 24, 2309-2316.
- Xia, H., Mao, Q., Eliason, S.L., Harper, S.Q., Martins, I.H., Orr, H.T., Paulson, H.L., Yang, L., Kotin, R.M., and Davidson, B.L. (2004). RNAi suppresses polyglutamine-induced neurodegeneration in a model of spinocerebellar ataxia. *Nature Medicine* 10, 816-820.
- Xia, H., Mao, Q., Paulson, H.L., and Davidson, B.L. (2002). siRNA-mediated gene silencing in vitro and in vivo. *Nature biotechnology* 20, 1006-1010.
- Xiang, L., Zhou, R., Fu, A., Xu, X., Huang, Y., and Hu, C. (2010). Targeted delivery of large fusion protein into hippocampal neurons by systemic administration. *Journal of Drug Targeting* 19, 632-636.
- Xiong, Q., Wilson, W.K., and Pang, J. (2007). The Liebermann-Burchard reaction: sulfonation, desaturation, and rearrangement of cholesterol in acid. *Lipids* 42, 87-96.

- Yamada, M., Hayashi, S., Tsuji, S., and Takahashi, H. (2001). Involvement of the cerebral cortex and autonomic ganglia in Machado-Joseph disease. *Acta Neuropathol* 101, 140–144.
- Yi, R., Qin, Y., Macara, I.G., and Cullen, B.R. (2003). Exportin-5 mediates the nuclear export of pre-microRNAs and short hairpin RNAs. *Genes & Development* 17, 3011-3016.
- Yu, D., Pendergraff, H., Liu, J., Kordasiewicz, H.B., Cleveland, D.W., Swayze, E.E., Lima, W.F., Crooke, S.T., Prakash, T.P., and Corey, D.R. (2012). Single-Stranded RNAs Use RNAi to Potently and Allele-Selectively Inhibit Mutant Huntingtin Expression. *Cell* 150, 895-908.
- Zadran, S., Akopian, G., Zadran, H., Walsh, J., and Baudry, M. (2013). RVG-mediated calpain2 gene silencing in the brain impairs learning and memory. *Neuromolecular medicine* 15, 74-81.
- Zamore, P.D., Tuschl, T., Sharp, P.A., and Bartel, D.P. (2000). RNAi: Double-Stranded RNA Directs the ATP-Dependent Cleavage of mRNA at 21 to 23 Nucleotide Intervals. *Cell* 101, 25-33.
- Zeller, S., Choi, C.S., Uchil, P.D., Ban, H.S., Siefert, A., Fahmy, T.M., Mothes, W., Lee, S.K., and Kumar, P. (2015). Attachment of cell-binding ligands to arginine-rich cell-penetrating peptides enables cytosolic translocation of complexed siRNA. *Chemistry and Biology* 22, 50-62.
- Zeng, Y., Wagner, E., and Cullen, B. (2002). Both natural and designed micro RNAs can inhibit the expression of cognate mRNAs when expressed in human cells. *Molecular cell* 9, 1327-1333.
- Zeng, Y., Yi, R., and Cullen, B.R. (2003). MicroRNAs and small interfering RNAs can inhibit mRNA expression by similar mechanisms. *Proceedings of the National Academy of Sciences of the United States of America* 100, 9779-9784.
- Zhan, C., Yan, Z., Xie, C., and Lu, W. (2010). Loop 2 of Ophiophagus hannah Toxin b Binds with Neuronal Nicotinic Acetylcholine Receptors and Enhances Intracranial Drug Delivery. *Molecular Pharmaceutics* 7, 1940-1947.
- Zhang, Y., Boado, R., and Pardridge, W. (2003a). Absence of toxicity of chronic weekly intravenous gene therapy with pegylated immunoliposomes. *Pharmaceutical research* 20, 1779-1785.
- Zhang, Y., Boado, R.J., and Pardridge, W.M. (2003b). In vivo knockdown of gene expression in brain cancer with intravenous RNAi in adult rats. *The Journal of Gene Medicine* 5, 1039-1045.
- Zhang, Y., Calon, F., Zhu, C., Boado, R., and Pardridge, W. (2003c). Intravenous nonviral gene therapy causes normalization of striatal tyrosine hydroxylase and reversal of motor impairment in experimental parkinsonism. *Human Gene Therapy* 14, 1-12.
- Zhang, Y., Peng, L., Mumper, R.J., and Huang, L. (2013). Combinational delivery of c-myc siRNA and nucleoside analogs in a single, synthetic nanocarrier for targeted cancer therapy. *Biomaterials* 34, 8459-8468.
- Zhang, Y., Schlachetzki, F., and Pardridge, W.M. (2003d). Global Non-Viral Gene Transfer to the Primate Brain Following Intravenous Administration. *Molecular Therapy* 7, 11-18.

- Zhang, Y., Wang, Y., Boado, R., and Pardridge, W. (2008). Lysosomal Enzyme Replacement of the Brain with Intravenous Non-Viral Gene Transfer. *Pharmaceutical research* 25, 400-406.
- Zhang, Y., Zhang, Y.-f., Bryant, J., Charles, A., Boado, R.J., and Pardridge, W.M. (2004). Intravenous RNA Interference Gene Therapy Targeting the Human Epidermal Growth Factor Receptor Prolongs Survival in Intracranial Brain Cancer. *Clinical Cancer Research* 10, 3667-3677.
- Zhang, Y., Zhu, C., and Pardridge, W. (2002). Antisense gene therapy of brain cancer with an artificial virus gene delivery system. *Molecular Therapy* 6, 67-72.
- Zimmermann, T.S., Lee, A.C., Akinc, A., Bramlage, B., Bumcrot, D., Fedoruk, M.N., Harborth, J., Heyes, J.A., Jeffs, L.B., John, M., *et al.* (2006). RNAi-mediated gene silencing in non-human primates. *Nature* 441, 111-114.